UNIVERSITÉ CATHOLIQUE DE LOUVAIN
École Polytechnique de Louvain
Institut de la Matière Condensée et des Nanosciences

Charge Transfer Processes in Atomic Collisions from First Principles

Dissertation présentée en vue de l'obtention du grade de
Docteur en Sciences de l'Ingénieur
par

Guillermo Avendaño-Franco

Membres du jury :
Prof. Xavier Gonze, promoteur
Prof. Pierre Defrance, président
Prof. Arnaud Delcorte
Prof. Miguel Marques
Prof. Bernard Piraux
Prof. Matthieu Verstraete

Août 2013

Dedicatoria:

A mi madre Martha Lucia
A mi padre Angel Guillermo
A mi hermano Marcelo
A minha esposa Viviane
A minha enteada Aline
A mi hijo Théo

Por la fortuna de tener una familia a la cual dedicar una tesis.

Contents

1

Introduction

Wer Wissenschaft und Kunst besitzt,
Hat auch Religion;
Wer jene beiden nicht besitzt,
Der habe Religion.

He who has Science and has Art,
Religion, too, has he;
Who has not Science, has not Art,
Let him religious be!

Johann Wolfgang von Goethe
Zahmen Xenien IX (Gedichte aus dem Nachlass).

Historically, the subject of collisions at atomic and subatomic levels developed as the backbone of Physics during the XXth century. The Rutherford model came out from experiments with α particles in collision with thin films of gold. All the theory of nuclei is the result of decades of experiments with particles impacting nucleus and observe how those nuclei decay. Cosmic rays, the higher energetic particles ever observed in nature, are detected due to the secondary cascades produced when they collision with the atoms in our atmosphere. Those particles, with energies between 10^9 eV to 10^{20} eV, are in most cases, higher in energy than anything that humans can produce today in particle accelerators. The research in physics is undoubtedly attached to the physics of collisions.

The XXth century was the century of quantum mechanics. Quantum mechanics was the language developed to formalize the understanding of a world with rules so particular that books are still written today trying to popularize the subject for the layman. During the first 30 years of the XXth century, humanity finally reached an effective understanding of the basic laws that govern our world at the atomic scale. The rest of the century is the bridge between those fundamental laws and the complex interplay of those laws, fields and particles to build up the macroscopic world at human scale.

At the atomic level, the pioneers in quantum mechanics discovered early the

central role played by electrons in the understanding of the microworld. Electronic structure is the key element to understand the behaviour of molecules and materials. Electrons are responsible for keeping nuclei together; they are responsible for declaring which molecules could be formed, why atoms crystallize in a certain way and not in another. Electronic structure of matter is of fundamental importance to understand the behaviour of the world not only at the atomic level but also in our scale.

When quantum mechanics search for description of systems in equilibrium, systems that do not change in time, it relies on the time-independent Schrödinger equation

$$E\Psi = \hat{\mathrm{H}}\Psi. \tag{1.1}$$

Words like static, equilibrium, ground state comes to mind when such equation or derivations of such equation are used. For systems changing, out of equilibrium, quantum mechanics relies on the time-dependent Schrödinger equation

$$i\hbar\frac{\partial}{\partial t}\Psi = \hat{\mathrm{H}}\Psi. \tag{1.2}$$

For systems in equilibrium or close to it, the time-independent Schrödinger equation is the way of choice. The equation is presented as the problem of finding the eigenvalues of the operator $\hat{\mathrm{H}}$. This kind of problems are typically solved using the techniques developed in linear algebra and by using self-consistent approaches.

Equilibrium is the exception rather than the rule in Nature. Quantum non-equilibrium phenomena have been growing in importance but their theoretical understanding is still at a very early stage. From the statistical point of view, we can distinguish two domains for systems out of equilibrium: Out of equilibrium dissipative quantum systems and the process of thermalisation of isolated quantum systems, evolving with unitary dynamics after an abrupt or slow change in a parameter. For the latter, the theoretical approach is usually determined by the strength of the perturbation. When deviation of equilibrium is small, the solution for the system can still be found by using response functions. However, for a strong external potential, such approach fails and non-linear effects are important. One way to account for non-linear effects is the explicit propagation of the time-dependent Schrödinger equation. The state of the system needs to be propagated in real time. This involves a different sort of tools compared with those used for solving the time-independent problem.

The kind of problems that requires the solution of a time-dependent Schrödinger equation are wide in scope. They include problems involving time-dependent electromagnetic fields, for example, intense and pulsed laser sources or intense magnetic pulses. Even without the presence of external fields, there are a whole set of phenomena that could be treated by a full solution of the time-dependent Schrödinger equation. Problems like atomic and molecular collisions, stopping or implantation of atoms in surfaces. In some cases, the intensity of those event prevents us of treat them using adiabatic procedures. The complete numerical solution of the time-dependent Schrödinger equation is the way to go.

For many years now, problems involving the movement of ions has been the domain of several branches of science. From one side, classical molecular dynamics, where effective force fields are used to determined the path that atoms follow when they interact with each other. In this case, all the complexity of the electronic structure remains hidden in phenomenological potentials. The other side is atomic physics where atomic collisions are an area by itself. In this case, the collisions are usually fast, not many atoms are involved and the electronic states of the atoms involved are very precisely described.

More recently, molecular dynamics was enriched when the description of electrons was included into the ionic movement. Those are the so-called ab-initio molecular dynamics methods. The electrons are described using quantum mechanical methods, such as Hartree-Fock or Density Functional Theory (DFT). The ions follow classical trajectories dictated by the forces computed by those electronic structure methods.

Among the methods in ab-initio molecular dynamics, only a subset is able to describe electronic excitations or charge transfer. This thesis will focus on one method in particular: time-dependent density functional theory (TDDFT).

Although classical molecular dynamics is able of modelling millions of particles, the entire electronic structure is missing and will never account for processes such as ionization or electronic scattering. In the other side of spectrum, there are methods such as those used in atomic physics, that describe correctly and accurately the electronic dynamics. Those methods, even if highly accurate are not able to overcome the exponential barrier that represents solving the time-dependent Schrödinger equation for many interacting electrons. In general, their scope remains limited to a very few atoms with no many electrons.

The goal of the thesis is to study the dynamics of electrons during atomic collisions using time-dependent density functional theory. New tools and techniques need to be developed in order to be able to understand those processes. Across the different chapters, the different tools will be presented as well as their applicability and limitations. Some applications will be presented on selected cases of interest.

The structure of this work is as follows: The first chapter will describe the fields of application that could be enriched by first principles studies in atomic collisions. The second chapter deals with the methods used in the determination of electronic structure of atomic systems, the dynamics of the atoms and the propagation of electrons coupled with the movement of those atoms. This chapter is intended to explore, not only the method used in this work but also its alternatives, presenting its advantages and limitations. The third chapter is dedicated to develop the tools that allow to extract useful information from the simulations. Special attention is put into explaining the different approaches to solve the problem of associating charges to atoms in dynamical circumstances like those that this work is focused into. One chapter is dedicated to show how for relatively simple atomic collisions, TDDFT is able to compute the single capture cross section with reasonable agreement with experiments. The fifth chapter describes the proper initialization of projectiles when some electronic state is attached to them. The concept of velocity phase

factor is introduced in this chapter. The following chapters are focused on specific applications. For the second application, the collision between a Li^+ion and a C_{60} molecule is studied. The last chapter presents the final conclusions, works in progress and perspectives for future exploration.

The different examples are chosen to cover a wide range of physical conditions. The simple cases with monoatomic projectile and target, are simple enough to compare with experiments and higher levels of theory. Such is the case with the proton - He collision and the carbon - Li in the sixth chapter. More challenging is the problem with molecular targets, not only because the configuration space is larger, there are more electrons involved and the availability of accurate experiments is more limited. Such is the case of the Li^+-C_{60} collision and the collision between Au and Butane presented in the chapter four. Finally we explore the interesting case of a collision between an atom of Helium and a piece of graphene with the purpose of including the case of collision with extended systems.

The specific goals of this work include the use of TDDFT to provide accurate values for of charge exchange and ionization probabilities in atom-atom, atom-molecule and atom-surface collisions. For atom-atom collisions, the typical measure is the capture, excitation or ionization cross sections. Impacting molecules and clusters increase the configuration space significantly, for that reason in this thesis only highly symmetric molecules are used as a target. They reduce the configuration space and allow for a direct comparison with experimental results to be still feasible. The ultimate goal is to compute charge transfer processes with large targets, far beyond the state of the art methods used until now. For most of simulations with large targets, the results are more qualitative than quantitative and they serve as a proof of concept for future exploration in the area.

2 Motivation and Context

> The universe is not required to be in perfect harmony with human ambition.
>
> Carl Sagan

2.1 Introduction

The movement of atoms is a natural phenomena at the micro-scale level. Even if artificially frozen close to the physical zero temperature, atoms are always moving [1]. In general, atoms move at very high speeds compared with the human experience. Take for example a carbon atom with a kinetic energy of 1 eV, a very typical energy for atomic systems, this atom is moving at 14436 km/hour. This speed is faster than any human machine [2] and faster than the speed of sound of around 1200 km/hour.

Since the Rutherford's experiments [Rutherford, 1911], it has become clear that most of the mass of an atom is concentrated in the nucleus. The electrons are light entities with a large difference in mass respect to the nucleus. This fact is a key element in all the methodologies that have been developed until now to describe the movement of atoms in matter.

The combined effect of the central nucleus and the surrounding electrons can be integrated to create an averaged potential that could be used to simulate the dynamics of an ensemble of atoms [Allen and Tildesley, 1989; van Gunsteren and Berendsen, 1990]. That is, indeed, the basis of one of the methods to simulate atoms in movement called classical molecular dynamics (CMD). CMD has been very successful to describe the dynamics of large ensembles of atoms and is still used today.

[1] Zero-point motion

[2] Except for space probes, like: New Horizons (57,600 km/h) Voyager 1 (59,760 km/h) or Helios 2 (252,792 km/h)

The nucleus is very heavy compared with the electrons, and the energies of nuclear photo excitation (typically MeV) are approximately six orders of magnitude higher than energies of electronic photo-excitation (typically a few eV). Those facts allow for methods that consider the nuclei as a point-like classical particle and allow to disentangle the role of nuclear and electronics positions. For the electrons, the natural theory is quantum mechanics. Methods to model the movement of atoms and describing the quantum nature of electrons are called ab-initio molecular dynamics (AIMD) [Kresse and Hafner, 1993; Marx and Hutter, 2000, 2009].

In the perspective of dynamical processes, those methods were developed historically from three sides. From one side are atomic physicists describing as accurately as possible the evolution of the wavefunction of electrons that interact with other atoms during atomic collisions. In experimental atomic physics, they are able to compute not only the final charge of the particle but also its state, the kinetic energies of the projectiles can be finely controlled and also the angle of scattering can be measured. From the theoretical point of view, the methods evolved to describe highly accurately the electronic structure. However, in practice, those methods become limited in the amount of electrons that can be present in the system under study. There are also studies with small molecules, but the expectations with larger systems are severely limited with our present computational capabilities.

From another side, chemistry developed methods to describe the movement of atoms during molecular reactions. Those are called quantum chemistry methods [Levine, 2000; Jensen, 2007] and specialize in the description of electrons attached to the nuclei. Compared with atomic physics the range of energies is in general lower, also the kinetic energy of the interacting entities has only statistical meaning. The focus in most cases is to determine reaction paths of chemical interest. For theoreticians, it becomes natural, in those cases, to expand the wavefunction in atom-centered basis sets. In many cases, only the valence electrons are active in the processes and pseudopotentials were developed to reduce the computational overload with larger molecules.

From a third side, solid-state physics developed alternatives to the explicit description of the electronic wavefunction. Instead of wavefunctions the main object of description is the electronic density [Martin, 2004]. Electrons are usually more delocalized in crystals and the electronic density has the practical advantage of being a real scalar field (in the mathematical sense). By contrast, the wavefunction has values in the complex domain and its structure is far more complex. The better known method belonging to this side is called Density Functional Theory (DFT).

Now, a selection of applications will be presented. The common denominator of all those applications is that collisions of atoms are important and the electronic structure description must be taken into account.

2.2 Applications

Lets us present four different areas of applied science and technology where the study of atoms in collision has a practical interest. First, secondary ion

mass spectrometry (SIMS), one of the most precise techniques to inquire the composition of a given surface. Second, biomedical sciences, where ion beam therapy has been developed as a promising alternative to radiotherapy in the treatment of certain kinds of cancer. This technique is aimed to replace the high energetic photons by accelerated atoms. The third area is in astrochemistry, our quest to understand the origins of life in the cosmos is deeply connected with the knowledge of the interstellar chemistry. In outer space atomic collisions are as important as interaction with light. Finally, we describe a domain of application where science is deeply connected with economics, geopolitics and general human welfare: the energetic challenge. Two promising alternatives for energy generation are being explored for medium and long term: Fourth generation nuclear fission reactors and nuclear fusion reactors. In both cases, atomic collisions has an important role, not only because the actual operation of those systems involves atoms at important speeds but also because atomic collision processes can be used to probe the state of those systems that typically work at very high temperatures.

With this wide landscape, I expect to convince the reader that the area of atomic collisions has a role to play in the development of future technologies and a better understanding of our origin and place in the cosmos.

2.2.1 Secondary Ion Mass Spectrometry

Secondary ion mass spectrometry (SIMS) is an experimental technique developed to analyze the composition of surfaces and thin films. The principle of operation is based on the idea that impacting with atoms or photons on a surface will eventually release some atoms or molecules from the surface that could be analysed by a mass spectrometer, and yield their composition [Gross, 2011].

SIMS is considered the most sensitive surface analysis tool and is able to detect the presence of elements in a surface from parts per million to parts per billion.

A SIMS instrument is composed of the following elements:

- A source of atoms (Ar, C, Cs, Ga, Au, Bi), molecules (C_{60}), clusters (Au_{400}) or photons (Laser). In the case of massive projectiles, those are typically ionized in order to be accelerated and impact on the sample.

- A target sample, such as a surface or a thin film. The sample must be solid and stable in vacuum conditions. [3]

- A system to transfer, redirect and collect the secondary ions. It is used to extract the secondary ions out of the collision chamber toward the mass analyzer.

[3] Liquid secondary ion mass spectrometry (LSIMS) is also an alternative. In such case, sample compounds are dissolved in a liquid matrix such as glycerin then spread on a metallic target plate. The plate is then bombarded by primary ions (Ar^+, Xe^+, Cs^+) accelerated to $2 \sim 30$ kV and with a current density of $2 \sim 3nA/cm^2$ or less.

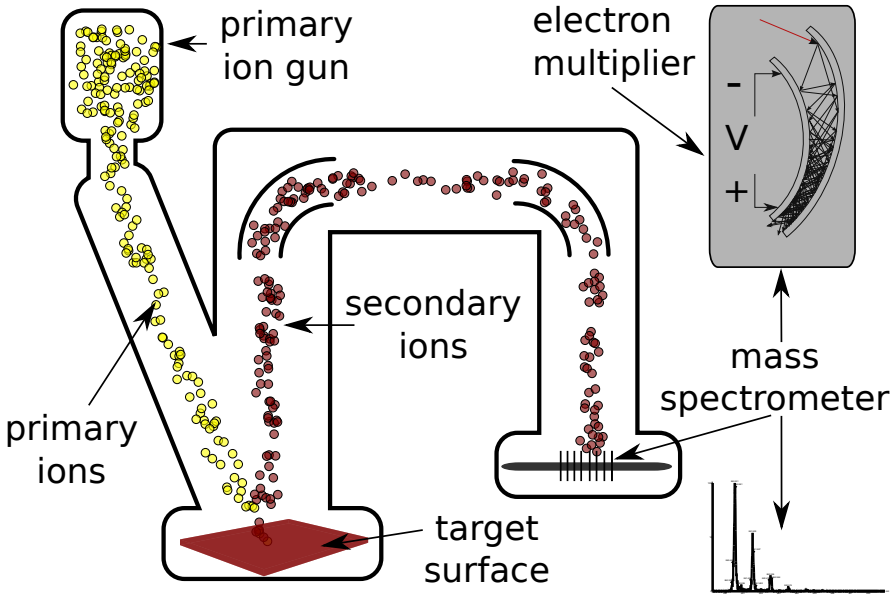

Figure 2.1: Simplified scheme of a SIMS device.

- A mass analyzer. It is used to differentiate the ionized secondary fragments emitted by the collisions. For example a Time-of-flight detector can be used to measure the mass-to-charge ratio of the fragments.

- An ion detection system to integrate the measures and provide the magnitude of the secondary ion signal.

A simplified scheme of a SIMS equipment can be observed on figure 2.1. The important point to stress here is that the particles ejected from the material must be ionized in order to be observed by the mass spectrometer. One of the methods used to obtain information about the composition of a surface is called *Time-of-flight mass spectrometry* (TOFMS). The concept behind TOFMS was called originally "Velocitron" by Cameron and Eggers in 1948 [Cameron and D. F. Eggers, 1948]. The idea is to measure the mass-to-charge ratio of an atom, molecule or cluster by measuring the time it takes this particle to travel a known path in space. The potential energy of a charge particle in the presence of an electric field is

$$E_p = qU, \tag{2.1}$$

where U is the potential difference, and q is the charge of the particle. If this potential energy is used to accelerate a particle until it reaches a certain velocity:

$$qU = \frac{mv^2}{2}, \tag{2.2}$$

the flight time can be expressed by computing the velocity of a particle that travels a distance d in a time t as $v = d/t$ and solving for t

$$t = \frac{d}{\sqrt{2U}}\sqrt{\frac{m}{q}}. \tag{2.3}$$

As soon as the different parameters d and U are known, particles with different mass-to-charge ratios can be separated by their time of arrival to the detector. The next step is to infer the mass by applying empirical assumptions on the charge state of the secondary ions. Otherwise, a single charge monoatomic ion will be indistinguishable from a double ionized dimer.

As soon as the fragment can be ionized, all the stable elements in the periodic table can be detected. As a SIMS system is designed to measure the charge to mass ratio with extreme precision, it is able to discriminate isotopic species to a precision between 0.5% to 0.05% [Gross, 2011]. Bi-dimensional reconstruction of a surface can be produced and even 3D imaging reconstruction by successive ablation of layers in the sample [Lamberti, 2005].

However, SIMS has some challenges, in particular the analysis of the yield material is particularly elaborate as it collects not only single atoms but also molecular fragments and clusters. The sputtering processes is not entirely understood. In some cases, to obtain quantitative results, empirical models are used to correct the findings from the machine. The sensitivity of a measure in SIMS depends on an effective release of ionized material. The amount of ionized material is a function of the kind of projectile, its kinetic energy, the properties of the unknown surface and eventually the preparation of the sample. Finally the sample must be compatible with high vacuum environment limiting its applicability.

Many studies have been performed to solve the limitations of SIMS. One of them is the sensitivity of the measure or limit of detection(LOD)[Gross, 2011]. Studies have shown that the amount of material ejected as ions can be enhanced if a metallic deposition occurs on top of the target sample. This procedure is called metal-assisted secondary ion mass spectrometry (MetA-SIMS) [Delcorte *et al.*, 2003] and has been object of research in the last years [Delcorte *et al.*, 2007; Restrepo *et al.*, 2010; Restrepo and Delcorte, 2011] The theoretical approaches until now have included classical molecular dynamics [Solomko *et al.*, 2004; Restrepo *et al.*, 2010; Restrepo and Delcorte, 2011] and using ground-state density functional theory to compute the ionization and fragmentation potentials [Solomko *et al.*, 2006]

A study of the time evolution of the electronic structure during a collisional process can improve the knowledge of this phenomena and eventually help improving the ionization in SIMS. In general, there are no general methods to predict the spectra of ionization; those ionization processes involve a large number of atoms in a wide range of energetic scales. The ultimate goal could be to be able to simulate the electronic dynamics of atomic impacts on surfaces. Compared with classical molecular dynamics it is unlikely that such simulations

can be done in the near future. However, in the long term it is more likely that such efforts can be achieved with methodologies such as TDDFT instead of wavefunction based methods.

2.2.2 Ion Beam Therapy

Ionizing radiation has been used for more than 100 years to treat cancerous tumours [Schwab, 2012; Slater, 2012]. This form of treatment works by destroying the ability of cancerous cells to reproduce, by damaging their DNA [Buffa, 2009]. In general, the DNA has several mechanisms of self correction, the double strand allows the cell to repair one of the strands from the undamaged one. Even a double strand break can be repaired with a low but non-zero probability of fidelity. However, if the damage is more intense, large sections of the DNA become destroyed, making the repair mechanisms less and less reliable. The DNA in general is a very robust system for storing information. However, when the cell is under heavy ionizing radiation, the functional capacities of the DNA could be damaged to a level that the replication of the cell is not longer possible. The damage is not only caused by the primary ionizing beam, but also by secondary ions and radicals emitted by the interaction of ionizing radiation with the biological molecules. As the body is composed of an important amount of water, the formation of hydroxyl radicals is one common source of secondary DNA damage.

The radiotherapy is in general non selective; it damages normal cells as much as the cancerous ones. For that reason, the usual procedure is having several beams acting on the same location inside the body but entering from different angles in order to concentrate the energy on the specific region where the tumour is located.

For therapy with ionizing radiation, the most common kind of beam used is electromagnetic radiation, typically x-rays. The problem with such kind of radiation is that an important amount of energy is deposited on healthy tissue, creating free radicals that damage cancerous cells as much as normal ones. The amount of energy deposited by different sources of ionizing radiation is shown on figure 2.2. As seen, soft x-rays deposit most of their energy on the first centimetres with an exponential decrease due to scattered Compton electrons. High energy photons have also a very wide profile crossing completely the body and depositing the energy all along the way.

As an alternative, instead of photons, the ionizing beam can be replaced by protons or heavier ions [Yajnik, 2013]. This kind of therapy is called *Ion Beam Therapy* (IBT) [Slater, 2012] or *Hadronic Beam Therapy* (HBT) and it is a promising alternative for certain kinds of cancerous tumours. The major advantage of IBT is that the zone of ionization can be better targeted. That is due to the fact that hadronic projectiles have a big peak of energy release at a specific distance known as a Bragg Peak [Kraft, 2000; Currell, 2003]. The main sources for hadronic beam therapy are protons, carbon and neon atoms [Schardt *et al.*, 2010].

In general, protons and heavier ions shown an increased depth-dose distribution compared with x-rays or other highly energetic photons. The mechanism

of ionization is rather different for massive particles compared with photons. They enter into the tissue with high speed, interact with the electrons with a small cross section and quasi-elastic scattering, releasing only a fraction of energy. With increasing depth, they start to release an increasing amount of energy. Finally, for a specific depth they release a maximum, the Bragg maximum and suddenly the flux of particles is sharply cut.

The first to measure the profile of penetration of hadrons in a medium was Sir William Henri Bragg. [Bragg and Kleeman, 1905] Forty years later, R. Wilson realized the possibilities that the Bragg-peak could offer for radiation therapy. His original paper deals with protons, but also discusses possibilities with heavier projectiles like alpha particles and carbon ions [Wilson, 1946]. Ten years later, the first patient was treated with protons at the Lawrence Berkeley National Laboratory in 1954. Studies with heavier ions took place in the following decade, Helium in 1957 and Argon in 1975.

The advantage of heavier atoms is that in general the heavier the particle the sharper the Bragg-peak is and better localization of the energy release can be achieved. Another advantage is a lower lateral scattering also contributing to a more focused area of irradiation. However the use of inert gases as source present also its limitations. A treatment with Neon is about 3.6 times more expensive than with protons, a factor that limits its applicability worldwide. With the years the evidence shows that the better compromise between effective ionization and collateral damage was offered by Helium ions [Slater, 2012] and carbon ions [Amaldi and Braccini, 2011]

With this brief survey about ion beam therapy, I expect to convince the reader about the role of a proper understanding of charge dynamics of ions impacting organic molecules. Charge transfer impact processes are directly or indirectly responsible for DNA damage. Those studies would benefit from a method that could deal with the electronic structure of larger molecules under atomic impact. Recent studies have been done in the ionization processes due to fast ion-atom collisions, see [Belkić, 2010] for an updated review of theories. In the case of ion-molecule collisions, the methods used until now are limited in most cases to very precise descriptions of atomic collisions with diatomic molecules [Rozsályi *et al.*, 2010, 2011; Rozsályi *et al.*, 2012].

2.2.3 Astrochemistry

The chemical processes taking place in interstellar medium (ISM) are particularly different from those in a planet like earth. The density is low, typically 10^6 molecules per cm^3. In some regions of ISM, matter is primarily ionized with densities as low as 10^{-4} ions per cm^3. The interstellar medium is composed of particles in gas phase (99% of mass) and dust.

From the gases in the ISM, 89% of the atoms are hydrogen, 9% are helium and the last 2% is represented dominantly by carbon, nitrogen and oxygen as seen on Fig. 2.3. The abundance of elements in the solar system has been measured [Cameron, 1973; Anders and Ebihara, 1982; Lodders, 2003] by analysis of C1 chondrites. Li, Be and B are rare because they are poorly synthesized during Big Bang nucleosynthesis and poorly created by stars. As a general

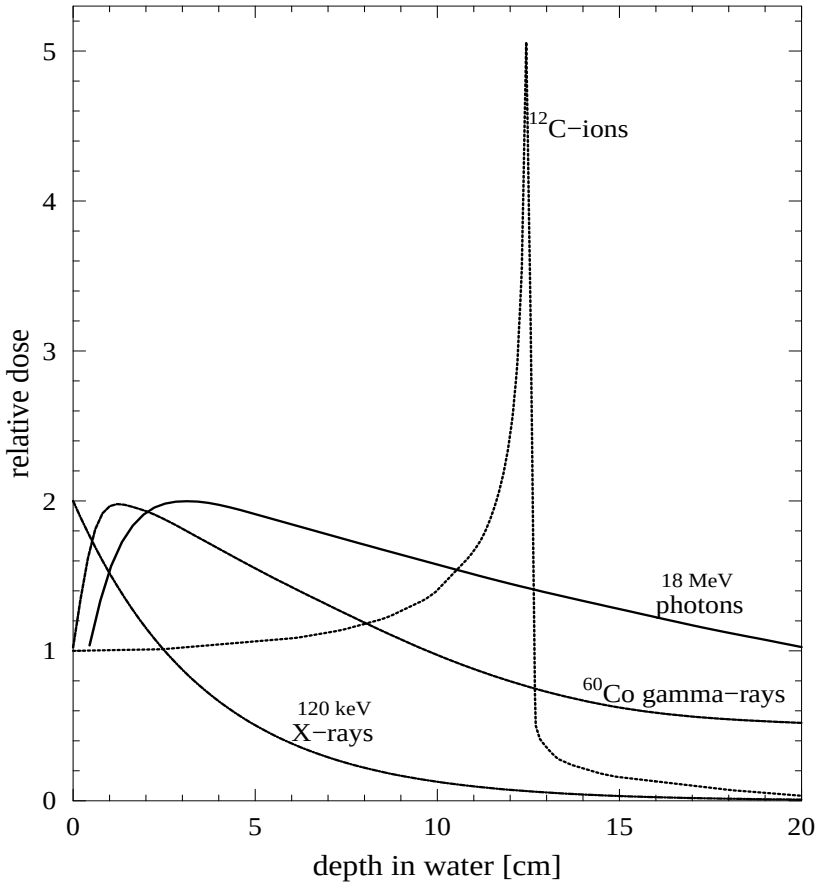

Figure 2.2: Depth-dose distribution for several forms of ionizing radiation Figure taken from [Kraft, 2000]. For photons, most of the energy is released superficially. For massive particles as shown here for a carbon beam, a sharp peak is created.

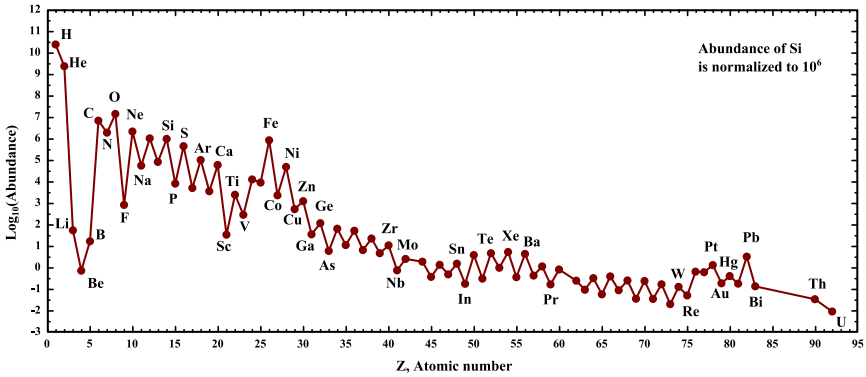

Figure 2.3: Estimated abundances of the chemical elements in the Solar system. Image taken from wikipedia with data taken from [Lodders, 2003] .

rule atoms with even atomic number are more abundant than their closest odd species because the nuclear spin shells are completed. Iron-56 is particularly common, since it is the most stable element that can easily be made by stars. Elements heavier than iron are made in endothermic processes in large stars, and their abundance in the universe (and on Earth) follows in general a decreasing tendency.

The temperatures of the ISM range from less than 300 K to 10^6 K produced by a supernovae. The classical model to explain this range of temperatures was proposed by Field, Goldsmith and Habing in 1969 [Field *et al.*, 1969] with the addition of a 10^6 K hot phase [McKee and Ostriker, 1977].

This combination of properties, low densities, low temperatures and atomic abundances, produces a very different physics and chemistry compared with planetary gases.

The study of the interstellar medium is relevant in astrophysics for basically two reasons [Maciel *et al.*, 2013]. First, the physical processes that lead to the creation of new stars are directly related to the behaviour of the clouds of dust and gas that condense to create them. Second, astrochemical processes taking place in those interstellar gases could have an influence in the emergence of organic molecules and ultimately the creation of life in planets. From a long futuristic view, the presence of those atoms in the space between stars could be the alternative solution to the "cargo dilemma" of interstellar travel, ie, most of the fuel needed to move an interstellar spacecraft is spent moving the fuel.

Focusing on the interstellar chemistry, it is important to stress here that space gases and dust are composed by a very limited variety of atoms: H, He, C, N and O. With He as an inert gas and H usually in molecular form, most of the interstellar chemistry is dominated by the molecules that can be produced from C, N and O [Winnewisser, 2011]. One typical molecule found in interstellar space is carbon monoxide CO. This molecule is very stable to dissociation and is so common that it is frequently used to trace the space for the presence of molecular dust. Other molecules have been found, for example the radical

OH [Wyrowski *et al.*, 2010], water [Ziurys, 2006; Ossenkopf *et al.*, 2010] and even large molecules like anthracene $C_{10}H_{14}$ [Iglesias-Groth *et al.*, 2010] or fullerenes [Foing and Ehrenfreund, 1994; Cami *et al.*, 2010; Cami, 2012; Berne *et al.*, 2012; García-Hernández *et al.*, 2011] and possibly graphene fragments [García-Hernández *et al.*, 2011]. In some cases molecules completely absent in the natural chemistry of the earth are particularly abundant in the interstellar space, such is the case of protonated molecular hydrogen H_3^+ [Dalgarno, 2006].

The particular conditions of the space, very low temperature, low density and processes taking place for long periods of time, opens challenges to researchers following the chemical reactions that this environment provides. From the physical point of view, one of the peculiarities of interstellar conditions is that atomic collisions are as important as radiation as sources of dissociation and ionization. In fact, molecules usually ionize due to interaction with cosmic rays, creating ions that slowly attract nearby molecules in a process that spans thousands of years.

Atomic collision processes in astrophysics has been studied for several decades [Dalgarno, 1967]. More recently molecular collisions have been investigated using first-principles approaches [Stahl *et al.*, 2001; Mada *et al.*, 2007]. Recent experiments with ions impacting polycyclic aromatic hydrocarbon (PAH) [Lawicki *et al.*, 2011] are waiting for a theoretical counterpart. For all of this, having the possibility to simulate those processes could be a complementary tool to the experiments that are done in laboratory.

2.2.4 Materials for Fusion and Generation IV Fission Reactors

Two promising alternatives for energy generation appear for the medium and long term; Gen-IV fission reactors and fusion reactors.

First, Gen-IV reactors are conceived to improve nuclear safety, reduce proliferation concerns, minimize nuclear waste or process the existing stocks of such waste, maximize the fuel utilization and reduce the building and operational costs of such plants. Most of reactors in operation around the world are generally considered second- or third-generation systems. Six technologies are under development for Gen-IV nuclear reactors. Nominally thermal are Very-high-temperature reactor (VHTR), Supercritical-water-cooled reactor (SCWR) and Molten-salt reactor (MSR) Considered in the fast regime are: Gas-cooled fast reactor (GFR), Sodium-cooled fast reactor (SFR) and Lead-cooled fast reactor (LFR) Those reactors works at more extreme conditions compared with the commercially used pressurized water reactors (PWR).

Fusion reactors are a second alternative, they reproduce the conditions of energy generation in stars. Fusion reactors are intended to produce a more cleaner energy, reduce the lifetimes of the activated material and avoid the problem of long life of actinides in fission reactors. Recently the Joint European Torus (JET) succeeded to produced more power than the input power for a very short time (0.5 s). The International Thermonuclear Experimental Reactor (ITER) is under construction and it is designed to produced ten times more power than the input put into the plasma. A production system is not expected

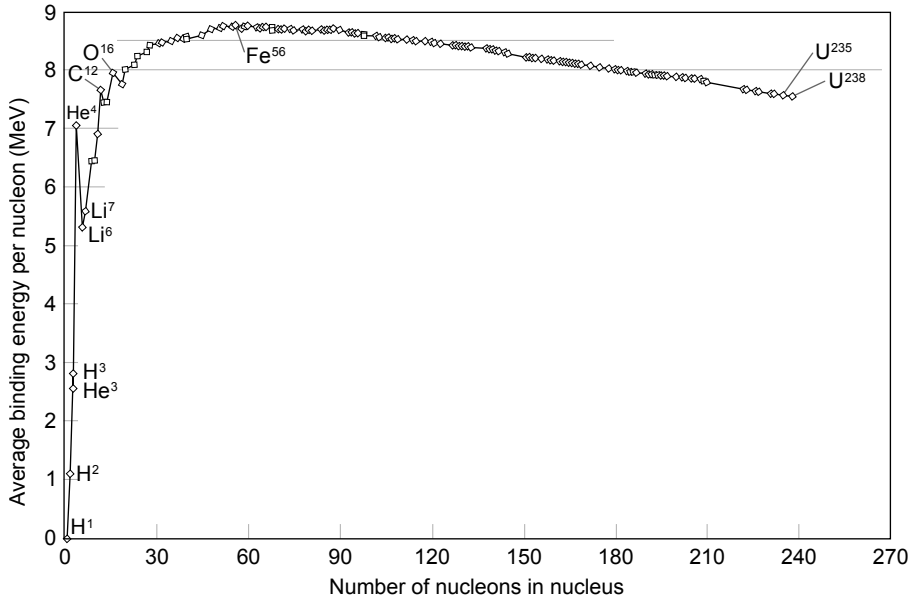

Figure 2.4: Binding energy curve for common isotopes

in less than 40 years.

From the physical point of view, the connection between a fission reactor and a fusion reactor is that the fission of a heavy nuclei or the fusion of a very light nuclei are exotermic reactions. This means that they produce more energy than the energy needed to induce the reaction. That can be understood from the binding energy curve shown in 2.4. A typical fission of uranium ^{235}U will produce around 211 MeV of energy. A fusion reaction of deuterium and tritium requires 3.5 MeV of input energy and releases 14.1 MeV, an exothermic process that releases 10.6 MeV of thermal energy.

One of the big challenges in both Gen-IV and fusion reactors is on the materials required to build such reactors. In the case of fusion, the temperatures are so high that the plasma needs to be confined magnetically. However, the structure of the reactor is still under heavy stress due to fast atomic collisions. For example the International Fusion Material Irradiation Facility (IFMIF), planned to be completed around 2017, will test materials under heavy neutron radiation. The high-energy neutrons will produce hydrogen and helium, in various nuclear reactions, that tends to form bubbles at grain boundaries and result in swelling, blistering or embrittlement of the materials used to confined the reactor. That effect is also critical in some of the Gen-IV fission reactors.

The study of materials and surfaces under fast atomic impact could help to design new materials that minimize those effects during the lifetime of the reactor. Studies at IFMIF will concentrate on testing the long-term behavior of materials under conditions similar to those expected at the inner wall of a fusion reactor. Even if the main concern is on the effect of neutrons, atomic impacts are also relevant when collisions on the surface induces atomic implantation

changing the properties of the target material.

More recently, ion irradiation has emerge an important tool in the development of materials for Gen IV reactor concepts [Was, 2007]. Some dynamical effects have been understood thanks to the use of ion-irradiation experiments. Among them we can mention, alloy stability under radiation and irradiation-assisted stress corrosion cracking (IASCC) processes. Ion irradiation is not meant to substitute neutron irradiation. Ions produce different initial recoil spectra compare with neutrons. Being charged particles, ions have a much larger cross sections for interaction with atoms. However, ion irradiation is able to reproduce almost the same radiation induced segregation (RIS) as was demonstrated for Cr in stainless steel [Was *et al.*, 2002]. Another example is heavy ion irradiation of a UMo-Al fuel clad couple. The experiment revealed the formation of a single intermetallic compound, in agreement with neutron-irradiation results [Palancher *et al.*, 2009].

In the case of fusion reactors, the presence of Hydrogen and Helium in the plasma edge is an important element to consider. The details of hydrogen diffusion in the solid wall are a complex subject. For both metals and non-metals the diffusing hydrogen and helium atoms can be trapped at lattice vacancies, interstitials or other imperfections, modifying the structural properties of the wall and limiting the lifetime of the entire structure. Another important effect is sputtering, in particular physical sputtering. Sputtering is the removal of atoms from the surface of a solid as a result of collisions with incident ions or atoms. Those impurities make ignition more difficult to achieve when interacting with the plasma. Among the atoms relevant in fusion reactor are beryllium, carbon and tungsten. Determine sputtering yield and probabilities of ionization are fundamental in the search for materials that reduce the sputtering yield.

Another important point with fusion reactors is that the plasma is at such high temperatures that no physical equipment can be used to probe the conditions of the plasma. The use of fast Lithium atoms has been proposed to measure the density of the plasma [Oliveira *et al.*, 2004]. The interaction of fast particles with the plasma helps to better understand the parameters that govern the behavior of the plasma.

2.3 Conclusions

In this chapter were presented a selection of applications for atomic impacts where the electronic structure plays a role. The key elements are the high kinetic energy of the collisions, the fact that the target is composed of an important number of atoms and that classical molecular dynamics is unable to describe properly charge transfer processes.

In the next chapter will be presented the theoretical tools developed that could be used to model such systems.

3

Theoretical Background

Dicebat Bernardus Carnotensis nos esse quasi nanos gigantium humeris insidentes, ut possimus plura eis et remotiora videre, non utique proprii visus acumine, aut eminentia corporis, sed quia in altum subvehimur et extollimur magnitudine gigantea.

Bernard of Chartres used to say that we are like dwarfs on the shoulders of giants, so that we can see more than they, and things at a greater distance, not by virtue of any sharpness of sight on our part, or any physical distinction, but because we are carried high and raised up by their giant size.

Ioannes Saresberiensis
Metalogicon

If I have seen further it is by standing on the shoulders of Giants

Isaac Newton
Letter to Robert Hooke

3.1 Introduction

As was presented in the previous chapter, the electronic structure in charge transfer processes is of prominent importance in several domains of applied and fundamental science. However, solving the Schrödinger equation for a system with many particles is a very challenging problem.

This chapter will present an overview of the different concepts normally used to describe electronic structure. The focus is biased towards the examination

of the evolution of electronic structure during atomic collisions. This thesis is focused on a very specific level of theory for electronic structure (DFT). However, this chapter will explore a broader set of concepts in higher and lower levels of theory to get a better landscape of the field and a better understanding of the advantages and limitations of the method of choice.

This chapter starts by describing the most emblematic methods to describe a system of electrons, from independent particles to density functional theory. After, some refined methods are presented that rely on orbital wavefunctions and used traditionally in quantum chemistry. In the next section, we present some methods and concepts used predominantly in the domain of atomic physics, where collisions and electronic structure are treated with outstanding accuracy. Next, the attention is concentrated on the methods used to describe the movement of atoms. Finally, time-dependent density functional theory is presented in the context of time-dependent Hamiltonians due to the movement of atoms.

3.2 Electronic Structure

In this section, we will focus the attention in the solution of the electronic structure problem. We start considering the time-independent problem. The time-dependent version will be treated in the context of the movement of atoms, the core of this work.

The fundamental equation to be solved is the Schrödinger equation

$$\hat{\mathrm{H}}\Psi = E\Psi, \tag{3.1}$$

where $\hat{\mathrm{H}}$ is the Hamiltonian of the system, an operator in the Hilbert space, whose eigenvalues provide the energy spectrum of a quantum system. The main issue with an equation like Eq. 3.1 is the wavefunction Ψ, an object defined in a very large and complex space. For a many-electron system the dimension of the Hilbert space increases to a point were even the computational storage of such object is unfeasible. This is the main challenge when Eq. 3.1 must to be solved for a realistic system composed by a significant amount of interacting particles.

There are traditionally three paradigms developed when quantum mechanics solve Eq. 3.1 for atomic systems. The first approach is to directly solve the Eq. 3.1 using the wavefunction as the main object, and reduce the large dimensionallity of the problem by assuming approximations to the wavefunction Ψ. Those are the methods that we group under the tag of wavefunction-based methods. A second paradigm was born almost at the same time as the quantum mechanics was created, it is based on the electronic density as the main object. The pioneers of this method are Thomas [Thomas, 1927] and Fermi [Fermi, 1927] their publication occur less than one year after the publication of Erwin Schrödinger [Schrödinger, 1926]. This shift in focus from the wavefunction to the density was extended a few years later by Dirac [Dirac, 1930] with contributions by Majorana [Guerra and Robotti, 2005; Esposito, 2005]. The most recent incarnation of the density-based method is the now widely used den-

sity functional theory (DFT). A third paradigm are the so-called semiclassical wavefunction methods. In this case, the idea of classical trajectory is preserved but for each trajectory is given a phase that has no classical correspondence and is responsible for the quantum effects. The WKB approximation and the Eikonal approximation inherit the ideas from semiclassical approaches.

In this section, an overview is presented of the most relevant concepts in electronic structure, with a particular bias towards the method of choice for this work, DFT.

3.2.1 Hartree Approximation

The first solution that can be proposed in the paradigm of wavefunctions is to completely factorize the wavefunction in terms of single-particle wavefunctions

$$\Psi(\{\mathbf{r}\}) = \psi(\mathbf{r}_1)\psi(\mathbf{r}_2)\cdots\psi(\mathbf{r}_N). \tag{3.2}$$

That factorization is justified if the Hamiltonian operator can be written as the sum of the Hamiltonians acting on each particle

$$\hat{\mathrm{H}} = \hat{\mathrm{H}}_1 + \hat{\mathrm{H}}_2 + \cdots + \hat{\mathrm{H}}_N. \tag{3.3}$$

Even if the factorization reduces the dimensionality of the Hilbert space, this naive solution is not respecting the basic symmetries of a set of identical quantum particles. In the factorization proposed, the interchange of two electrons produce the same quantum state, but in quantum mechanics the wavefunction changes sign.

The Hartree approximation comes from ignoring this effect and assume that the wavefunction is separable in products of single electron orbitals, each being different from all others

$$\Psi(\{\mathbf{r}\}) = \psi(\mathbf{r}_1)\psi(\mathbf{r}_2)\cdots\psi(\mathbf{r}_N). \tag{3.4}$$

The potential in the Hamiltonian is replaced by an effective potential, the so-called Hartree potential

$$\hat{\mathrm{V}}_{\mathrm{H}}(\mathbf{r}) = \int \frac{n(\mathbf{r}')}{|\mathbf{r}-\mathbf{r}'|} d\mathbf{r}', \tag{3.5}$$

where the density is defined as the sum of the densities of each orbital

$$n(\mathbf{r}) = \sum_j \psi_j^*(\mathbf{r})\psi_j(\mathbf{r}). \tag{3.6}$$

The wavefunctions are obtained from the solution of N Schrödinger equations time-independent

$$\left(-\frac{1}{2}\nabla^2 + \hat{\mathrm{V}}_{ext} + \hat{\mathrm{V}}_H\right)\psi_j(\mathbf{r}) = \epsilon_j\psi_j(\mathbf{r}), \tag{3.7}$$

or time dependent

$$\left(-\frac{1}{2}\nabla^2 + \hat{\mathrm{V}}_{ext}(\mathbf{r},t) + \hat{\mathrm{V}}_H(\mathbf{r})\right)\psi_j(\mathbf{r},t) = i\frac{d}{dt}\psi_j(\mathbf{r},t). \tag{3.8}$$

This method has important advantages compared with the solution of a fully interacting Schrödinger equation. The price to pay is that important physics is missing here. This basic idea, namely that we replace interacting particles by non-interacting particles with an effective potential, is in the core of the method of choice in this work (DFT) but solving its fundamental deficiencies.

3.2.2 Hartree-Fock Approximation

The problem with a simple factorization of the many-body wavefunction is that such scheme is not respecting the symmetries of the wavefunctions. For example, the interchange of two particles let the system unchanged, but the actual wavefunction should have opposite sign.

V. Fock [Fock, 1930] and Slater [Slater, 1951] showed that the Hartree formulation only respects the old version of the Pauli principle of exclusion, two fermions can not have all the same quantum numbers, but the antisymmetry of the wavefunctions of a system of fermions is not enforced. The solution to that was to use a single Slater determinant Eq. 3.9 and keep the potential proposed by Hartree.

$$\Psi(\{\mathbf{r}\}) = \frac{1}{\sqrt{N!}} \begin{vmatrix} \psi_1(\mathbf{r}_1) & \psi_2(\mathbf{r}_1) & \cdots & \psi_N(\mathbf{r}_1) \\ \psi_1(\mathbf{r}_2) & \psi_2(\mathbf{r}_2) & \cdots & \psi_N(\mathbf{r}_2) \\ \vdots & \vdots & \ddots & \vdots \\ \psi_1(\mathbf{r}_N) & \psi_2(\mathbf{r}_N) & \cdots & \psi_N(\mathbf{r}_N) \end{vmatrix}, \tag{3.9}$$

where the single electron orbitals ψ can be found as the solution of single electron Schrödinger equation

$$\left(\frac{1}{2}\nabla^2 + V\right)\psi_i(\mathbf{r}) = i\frac{d\psi_i(\mathbf{r})}{dt}. \tag{3.10}$$

The solution of the many-body wavefunction has been replaced by the solution of N single-electron Schrödinger equations. This is the basis of the so-called Hartree-Fock method (HF).

This method has been very successful and has been extended to include open shell systems by using the so-called Restricted open-shell HartreeFock (ROHF) [Roothaan, 1960] and unrestricted HartreeFock (UHF) [Pople and Nesbet, 1954].

In the case of ground-state calculations, HF uses the idea of self consistency between the wavefunctions and the electronic density as shown in 3.1. In fact, before DFT became popular, the Hartree-Fock method was called *Self-Consistent Field method (SCF)*. Such denomination is now ambiguous because DFT and other post-HF methods also rely on self consistency.

For many years, HF and the methods derived from it, called Post-HF have been instrumental in the development of quantum chemistry. Even immediately after the formulation of DFT, post-HF methods were in general far more accurate in molecules compared with DFT. Only when DFT used improved exchange-correlation functionals, such as the generalized gradient approximation (GGA), the precision was competitive enough and the computational cost

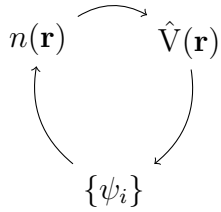

Figure 3.1: Diagram of the self consistent cycle in time-independent Hartree-Fock

much affordable to replace HF and Post-HF as the method of choice for large molecules and macromolecules.

The next section of this chapter will be dedicated to some of the most prominent post-HF methods some of them effectively used in atomic collisions.

3.2.3 Ground-State Density Functional Theory

The big limitations of the Hartree-Fock approach are the neglect of the electronic correlation. The properties computed without taking into account the correlation could largely deviate from experiments. Two-electron systems like Helium are the prototypical case in atomic physics [Kestner and Sinanaglu, 1962], where the lack of correlation is crucial. Correlated electron materials are the equivalent in condensed matter physics, those materials have exotic properties because the assumption of separability of the wavefunction is fundamentally wrong.

Density functional theory (DFT) adopts an intermediate vision in the correlation problem. The wavefunction is still separable as in the Hartree approximation but the Hamiltonian includes correlation effects via a model local or semilocal potential. In the next section we describe the foundations of DFT and its fundamental approximations or limitations. As this work is based on TDDFT, the ground state DFT is somehow the basement on top of which the time-dependent version is built in, even if the theorems that support each theory are different.

3.2.4 Hohenberg-Kohn Theorems

Hohenberg and Kohn published a paper in 1964 entitled "Inhomogeneous Electron Gas" [Hohenberg and Kohn, 1964], that offers a new vision in the problem of solving the Schrödinger equation for systems with many electrons. The idea, as usual, is to replace a problem with another. Substitute the complicated and fully interacting electronic problem by replacing it by a much more tractable one. The emphasis is displaced from the wavefunctions to the electronic density $n(\mathbf{r})$. This shift is indeed of an enormous advantage from the computational point of view as the density is mathematically a scalar field in space.

Two theorems support this shift to the density

Theorem 1. *The ground state electronic density $n(\mathbf{r})$ of a system of interacting electrons uniquely determines the external potential $V_{ext}(\mathbf{r})$ (up to a global constant) in which the electrons are confined.*

Theorem 2. *An universal functional for the energy $E[n(\mathbf{r})]$ can be defined in terms of the electronic density $n(\mathbf{r})$. The ground-state is obtained for the function $n(\mathbf{r})$ such that $E[n(\mathbf{r})]$ assumes a minimal value.*

We will follow here the pedagogical approach from Engel and Dreizler [Engel *et al.*, 2011]. These theorems could be better understood with two maps between three sets: the set $\mathcal{V}$ of all possible external potentials, excluding those that differ by a constant.

$$\begin{aligned}\mathcal{V} \quad = \quad & \{\nu_{ext} \mid \nu_{ext} \text{ is multiplicative}, |\Psi_0\rangle \text{ exists} \\ & \text{and different by more than a constant } \nu'_{ext} \neq \nu_{ext} + c\}\,,\end{aligned}$$

the set of ground state wavefunctions derivated from those potentials

$$\begin{aligned}\mathcal{G} \quad = \quad & \{\Psi_0 \mid \Psi_0 \text{ is the ground state from one element} \\ & \nu_{ext} \in \mathcal{V} \text{ excluding a global phase } \Psi'_0 \neq e^{i\phi}\Psi_0\}\end{aligned}$$

and the set of densities created from elements of $\mathcal{G}$

$$\begin{aligned}\mathcal{N} \quad = \quad & \{n(\mathbf{r}) \mid n(\mathbf{r}) = \langle\Psi_0|\,\hat{n}\,|\Psi_0\rangle \text{ is the density} \\ & \text{from one element } \Psi_0 \in \mathcal{G}\}\,.\end{aligned}$$

The functions that connects the sets $\mathcal{V}$, $\mathcal{G}$ and $\mathcal{N}$ are surjective by construction ($\mathcal{V} \twoheadrightarrow \mathcal{G}$ and $\mathcal{G} \twoheadrightarrow \mathcal{N}$), ie every element in the codomain has a corresponding element in the domain. Those three sets and two maps are sketched in the figure 3.2 The Hohenberg-Kohn theorem proves the bijective character of the maps that connect those three sets, demonstrating at the end, that there is a one-to-one relation between the potentials ν_{ext} and the densities $n(\mathbf{r})$.

There are several remarks to be done at this level. In a three dimensional space $\nu_{ext}(\mathbf{r}) \in F : \{\mathbb{R}^3 \to \mathbb{R}\}$, but the elements in $\mathcal{G}$ belong to a larger and different domain $\Psi \in \mathbb{C}^{3N}$ and finally the densities are again scalars defined on a 3D space $n(\mathbf{r}) \in N : \{\mathbb{R}^3 \to \mathbb{R}\}$. By construction the elements in $\mathcal{V}$ exists if the corresponding Ψ_0 exists. The theorem does not mention the existence of a potential for an arbitrary Ψ.

Another important remark is done on the local character of the potential ν_{ext}. This requirement excludes the important case of the standard type of pseudopotentials used currently in DFT. There is, nevertheless, the corresponding extension of the Hohenbert-Kohn theorem for non-local potentials [Gilbert, 1975; Berrondo and Goscinski, 1975]. In general, non-local pseudopotentials are used in the traditional approach once the HK theorem is justified for the all-electron case.

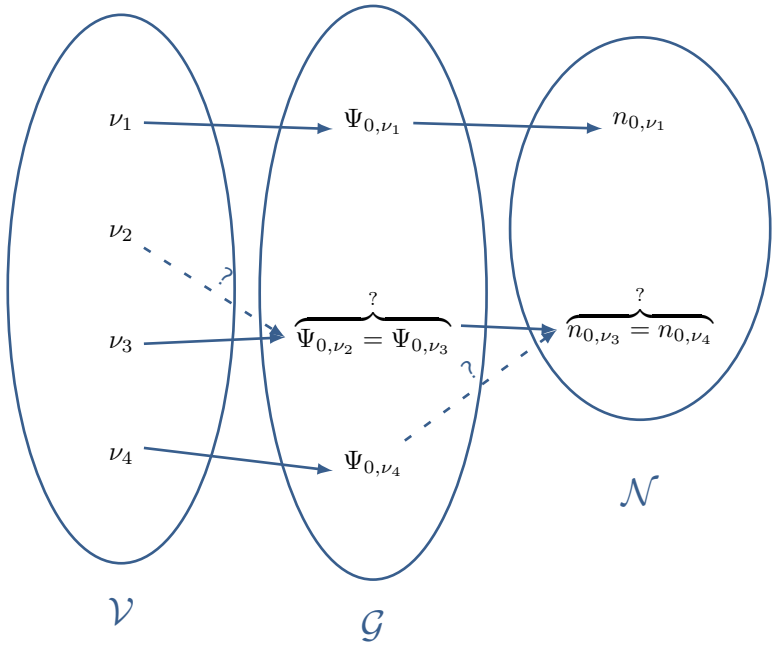

Figure 3.2: Relations between the three sets $\mathcal{V}$, $\mathcal{G}$ and $\mathcal{N}$ and the two maps that connect them. The dashed lines shows the relations that the Hohenberg-Kohn theorem removes in order to prove the character injective of the functions that connect the three sets.This presentation of the Hohenberg-Kohn theorem comes from [Engel *et al.*, 2011]

As the relation between Ψ_0 and $n(\mathbf{r})$ is bijective, there is also an inverse map that connects one element from $\mathcal{N}$ with one element of $\Psi[n] \in \mathcal{G}$. As all the observables from a quantum system are obtained from the information in the wavefunction Ψ, also those observables are formally functionals of the density $n(\mathbf{r})$.

The maps presented here and the outlined proof, relies strongly on the non-degeneracy of the states Ψ. A modified argument makes possible to prove the Hohenberg-Kohn theorem in the case of degenerate states. In this situation, two or more ground states $|\psi_{n,\nu_n}\rangle$ originate from the same potential ν_{ext}.

3.2.5 Kohn-Sham Scheme

Once the Hohenberg-Kohn Theorem (or Runge-Gross theorem in the case of TDDFT, see later) is proved, the natural step is to construct the auxiliary Kohn-Sham scheme.

The Hohenberg-Kohn theorem is formulated for wavefunctions in the set $\mathcal{G}$, those wavefunctions are in principle the interacting wavefunctions in the complete Hilbert space.

The basic idea of Kohn and Sham [Kohn and Sham, 1965] is to replace the interacting wavefunctions of N particles with a set of auxiliary equal number N functions that reproduce the same density as the original interacting system.

The construction of a KS scheme is supported on the construction of a auxiliary potential. The Kohn-Sham approach rewrite the energy functional in the form:

$$E_{KS} = T_s[n] + \int d\mathbf{r} V_{\text{ext}}(\mathbf{r}) n(\mathbf{r}) + E_{\text{Hartree}}[n] + E_{\text{II}} + E_{\text{XC}}[n] \tag{3.11}$$

where T_s is given as

$$T_s = -\frac{1}{2}\sum_{i=1}^{N} \langle \psi_i | \nabla^2 | \psi_i \rangle = \frac{1}{2}\sum_{i=1}^{N} \int \mathrm{d}^3 r |\nabla \psi_i(\mathbf{r})|^2 \tag{3.12}$$

and the Hartree energy as an explicit function of the density

$$E_{\text{Hartree}}[n] = \frac{1}{2}\int \mathrm{d}^3 r \, \mathrm{d}^3 r' \frac{n(\mathbf{r}) n(\mathbf{r}')}{|\mathbf{r} - \mathbf{r}'|} \tag{3.13}$$

the term E_{II} is the interaction between nuclei. All the many-body contributions to the energy are condensed in the last term, known as the exchange-correlation energy E_{XC}.

The results in DFT are as good as E_{XC}. As soon as E_{XC} is good enough to describe the true exchange-correlation, the physical properties obtained by using the Kohn-Sahm method are also close the ground-state properties of the full-interacting electron system. That is the reason why an important effort has been devoted since the beginning in providing reliable exchange-correlation functionals that are able to capture as much as possible the physics behind the exact functional.

3.2.6 Exchange-Correlation Functional

Once separated the independent-particle kinetic energy and the Hartree term, the remaining exchange-correlation functional is the next term to consider. The different flavors is given by the choice of functional form for the exchange-correlation energy. The functional is a unique functional, the only thing that is known is that such functional is not simple. The different versions of exchange-correlation functionals are ways to get a close approximation to the complete functional. There are, however, a series of properties that the exact functional must have, the approximate functionals only have a partial subset of properties. This is the reason why the different exchange-correlation functionals are more or less accurate depending of how important is each property for an specific property.

It many cases the exchange-correlation E_{xc} into two parts, the exchange E_x and the correlation E_c, even if only the combination of E_x and E_c. Both functionals, are described in mathematical form using parameters. The parameters are set by enforcing the properties of the exact E_{xc} or by fitting with experimental data, higher levels of theory or a mix of all of them. Each of the exchange and correlation energies are customary written as integrals of the energy densities ϵ_x and ϵ_c.

$$E_{xc}[n] = E_x[n] + E_c[n] \tag{3.14}$$

$$= \int \mathrm{d}\mathbf{r}\, n(\mathbf{r})\epsilon_{\mathrm{x}}([n],\mathbf{r}) + \int \mathrm{d}\mathbf{r}\, n(\mathbf{r})\epsilon_{\mathrm{c}}([n],\mathbf{r}) \tag{3.15}$$

If for wave function-based methods, the quality of the correlation defines the level of the theory, such hierarchy is not theoretically grounded for DFT methods. The exchange and correlation functionals are in many cases empirical in nature. J. P. Perdew suggest a certain ordering for the various E_{xc}. The DFT's "Jacob's ladder" classifies the E_{xc} based on the number and qualities of the variables used to define each functional. Only in principle, we can expect that a more elaborated functional be better, but in some cases lower steps in the ladder fulfill better the properties and could be a more reasonable choice than other higher level functionals.

In most of this work, the Local Density Approximation (LDA) is used. LDA assume that the E_{xc} could be computed assuming that the density is a slowly varying function, and the values of E_x and E_c could be integrated from contributions from locally uniform electron gas. The exchange energy is given by the Dirac formula:

$$E_x^{LDA}[n] = -C_x \int n^{4/3}(\mathbf{r}) d\mathbf{r} \tag{3.16}$$

$$\epsilon_x^{LDA} = -C_x n^{4/3} \tag{3.17}$$

In the case where both spins are not equal, it is the sum of the both contributions that should be raised to the 4/3 power. However, it is customary to

use the Local Spin Density Approximation (LSDA) where each contribution is independently raised to the 4/3 power.

$$E_x^{LSDA}[n] = -2^{1/3}C_x \int (n_\uparrow^{4/3} + n_\uparrow^{4/3})d\mathbf{r} \tag{3.18}$$

$$\epsilon_x^{LSDA} = -2^{1/3}C_x(n_\uparrow^{4/3} + n_\downarrow^{4/3}) \tag{3.19}$$

For the analytical form of the correlation energy the Perdew and Wang (PW) [Perdew and Wang, 1992] is one of several parametrizations. LDA is an exact method for an uniform electron gas. It is also a very good approximation for systems close to that uniform gas, such as metals where a slowly varying electron density is reasonably justified.

In the case of atomic and molecular systems is customary go one step up in the Jacob's ladder and consider the so called Generalized Gradient Approximation (GGA). In GGA the first derivative of the density is included as a new variable. Going further in the ladder, some functionals depend on higher order derivatives of the electron density or depend on the orbital kinetic density τ. There is an active research in the development of better functionals, for the context of this work most of the simulations are done at the LDA level.

3.2.7 Norm-conserving Pseudopotentials

There are basically three reasons to introduce pseudopotentials in an ab-initio calculation [Heine, 1970; Martin, 2004]: to reduce the number of electrons treated explicitly, smooth the oscillatory behavior of the wavefunctions when the distance to the nuclei is small and introduce partial relativistic corrections when necessary.

In the physics community uses the term Pseudopotential (PP) to describe the functions that model the core electrons. In the chemical community the equivalent functions are usually called Effective Core Potentials (ECP).

The theoretical justification for the use of pseudopotentials is that the electrons with lower principal quantum number are strongly localized and they are more strongly attached to the nuclei. This spatial and energetic separation is the main argument to consider the electrons in the core as frozen; not participating in any chemical reaction.

As the valence electrons are orthogonal to the core electrons, the core wavefunctions contain many nodes near the nucleus. The practical effect of the use of pseudopotentials is to avoid such behavior for the core electrons. This has as a consequence important savings in computational effort both in memory and in time. In the case of wavefunctions expanded in plane waves, the reduction is due to a decrease in the number of plane waves used as a basis for the expansion. In the case of real-space grid discretization, the smoothness in the wavefunction allows one to use a more spaced grid with the advantage in memory and computing time in a very similar way as the plane wave expansions.

A pseudopotential replaces the generic Coulomb potential $-Z/|\mathbf{r} - \mathbf{r}_\tau|$ felt by the N electrons in the system by some alternative operator that includes

the potential created by the nucleus and the Coulomb repulsion by those electrons considered in the core. Using this procedure, the core electrons are not described explicitly anymore and are effectively eliminated from the problem.

When a pseudopotential is created, a reference calculation is done considering all the electrons. Then, a pseudopotential is an analytic fit, created to reproduce the same spectrum and wavefunctions as the original all electron reference. A cut-off radius around each nuclei is chosen in such a way that bound states will reproduce the wavefunctions outside of the sphere defined by the cut-off radius. Inside the sphere the wavefunctions are smoothed.

Local and non-Local Pseudopotentials

The simplest approach for a pseudopotential, is a multiplicative function. The first constraint is that far from the nucleus the potential should be $Z_{ion}/|\mathbf{r}|$, Z_{ion} is the atomic number of the nucleus, minus the number of electrons considered in the core. The problem with this approach is that analytic fits are not flexible enough. That is even more important for pseudopotentials of heavy atoms, but, even for the first s and p atoms this multiplicative form is not sufficiently good.

The alternative is to add some non-locality using projector functions. The projectors are created to ensure orthogonality between the valence states and the core states. The usual form is

$$\hat{\mathrm{V}}_{NLps} = \hat{\mathrm{V}}_{local} + \sum_i \alpha_i \left|\psi_i\right\rangle \left\langle\psi_i\right| \tag{3.20}$$

where i spans in the core states. The wavefunctions ψ_i and the coefficients α_i can be chosen to fit the valence eigenstates. Another way to describe the projectors is using the spherical harmonics Y_l^m

$$\hat{\mathrm{V}}_{NLps} = \hat{\mathrm{V}}_{local} + \sum_i \alpha_i \left|Y_l^m\right\rangle \left\langle Y_l^m\right| \tag{3.21}$$

Kleinman and Bylander [Kleinman and Bylander, 1982] present a scheme where the pseudopotentials could be put in a "separable form", such that projections with basis functions could be calculated much easier. The drawback is that this scheme produces in some cases spurious or ghost states, that are lower in energy than physical states. This side-effect and the procedure for its elimination was studied [Gonze *et al.*, 1991].

Pseudopotential Parametrization

The most used type of norm-conserving pseudopotential was created by Troullier and Martins [Troullier and Martins, 1991a]. They proposed an analytical form for the projector functions following a method from Kerker [Kerker, 1980].

Another approach was proposed [Hartwigsen *et al.*, 1998]. In this case, a generalized form of pseudopotential is constructed with the advantage that the expression is separable by construction. All the element until Rn were fitted. Their method hast the advantage of being possible to use several projector functions for each angular momentum. Another parametrization with this property is [Teter, 1993]

Pseudopotentials in Atomic Collisions

Special remarks have to be done with respect to the use of pseudopotentials in the case of atomic collisions. First, with the kinetic energies explored in this work, there is enough energy to excite even the lowest orbitals in the atoms. Such effects of deep excitation are completely missing in our approach. The use of pseudopotentials with less or no electrons frozen in the core limits their applicability to larger systems.

Another important effect present in the context of collisions is related with the cutoff radius of the pseudopotentials. Norm-conserving pseudopotentials includes the condition that outside a certain radius r_c, the norm of each pseudo-wavefunction should be identical to the results of an all-electron calculation for the same level of theory. The figure 3.3 shows the pseudo potential and pseudo wavefunctions for carbon. In general, norm-conserving pseudopotentials has the tendency to have large r_c to reduce the basis-set or the size of the mesh. However, in the case of collisions, it is very often the case that atoms approach to each other to distances shorter than the sum of their cutoff radius. The spheres defined by those cutoff radius eventually overlap and this overlapping could eventually create spurious effects.

3.3 Quantum Chemistry Methods (post-HF)

Historically the electronic study of atoms and molecules was developed by refining the ideas from Hartree-Fock. The methods described in this section are traditionally used in quantum chemistry and are contructed on top of Hartree-Fock. For that reason, those methods are called Post-HF.

Those higher levels of theory has been developed in atomic physics or quantum chemistry to compute excited states with a very high accuracy, albeit at expense of being limited to systems with just a few electrons. This section will discuss some of those higher levels of theory to get a glimpse about what is beyond the method of choice for this work, TDDFT.

3.3.1 Configuration Interaction and Beyond

The Hatree-Fock method uses a single Slater determinant built from a complete set of orbitals to describe the ground state of a system [Jensen, 2007]. For excited states, a series of Slater determinants could be generated by replacing an increasing number of occupied orbitals by an equivalent number of unoccupied ones. Doing this and computing a linear combination of those Slater determinants we finish with a series like:

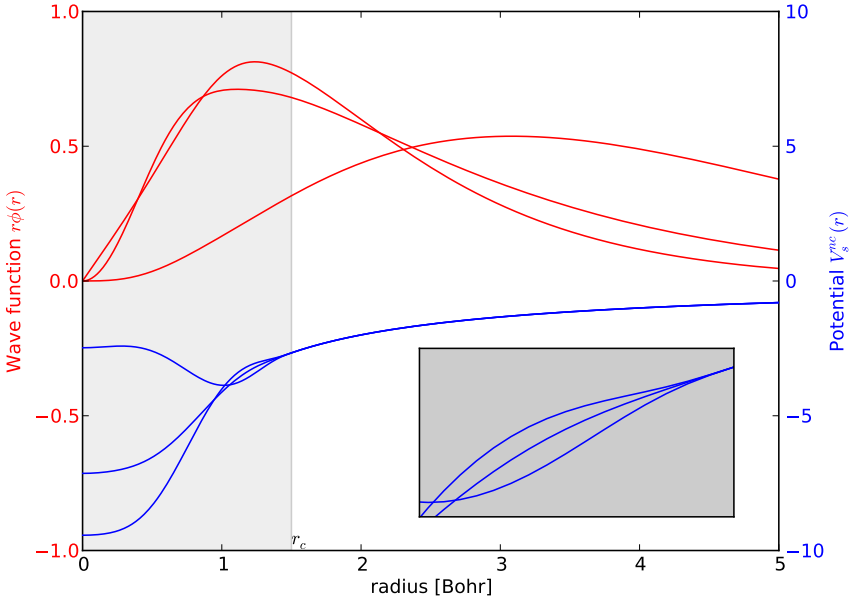

Figure 3.3: Norm-conserving pseudopotentials: Pseudo wavefunctions and pseudo potentials for the $1s$, $2s$ and $2p$ orbitals of carbon. The red lines shows the wavefunctions and the blue lines shows the pseudopotentials. The light gray region represent the sphere of radius r_c. Outside of a cutoff radius the three potentials converge and the wavefunctions becomes identical to an all electron calculation. A zoom into the region close to r_c shows as the potentials for the different states converge to the Coulomb potential of an ion, beyond r_c.

$$
\begin{aligned}
\Psi \;=\; & c_0\Phi_0 + \underbrace{\sum_{i=1}^{N}\sum_{a=N+1}^{K} c_i^a \Phi_i^a}_{\text{single excitations (S)}} \\
& + \underbrace{\sum_{i>j=1}^{N}\sum_{a>b=N+1}^{K} c_{ij}^{ab} \Phi_{ij}^{ab}}_{\text{double excitations (D)}} \\
& + \underbrace{\sum_{i>j>k=1}^{N}\sum_{a>b>c=N+1}^{K} c_{ijk}^{abc} \Phi_{ijk}^{abc}}_{\text{triple excitations (T)}} \\
& + \underbrace{\sum_{i>j>k>l=1}^{N}\sum_{a>b>c>d=N+1}^{K} c_{ijkl}^{abcd} \Phi_{ijkl}^{abcd}}_{\text{quadruple excitations (Q)}} \\
& + \cdots
\end{aligned}
\tag{3.22}
$$

This is the base of the so-called Configuration Interaction (CI) method. The first term $c_0\Phi_0$ is the Hartree-Fock wavefunction. The next term is a sum with Slater determinants Φ_i^a, it means that the i occupied orbital is replaced by the a unoccupied orbital. The next term involves terms like Φ_{ij}^{ab} where two orbitals are excited. Following sums involve triple and quadruple and more excitations.

In CI, the excited states are constructed from Hartree-Fock orbitals and they are also limited for the adequacy of such contruction.

An infinite summation like expressed in Eq. 3.22 is not possible to compute, the first element to truncate is the limit of the orbitals that will be considered. The order of the CI expression is done by the value of $K - N$. At zeroth-order we have Hartree-Fock and only the ground state. The second possibility is to truncate the number of excitations considered. The first double summation includes only single excitations, the next one, double excitation and so on. If the summation is not truncated, ie, we allow to excite the N electrons in the system, we say that a Full CI is done.

The number of Slater determinants needed to compute n excited orbitals for a system with N electrons and a total number of orbitals equal to K is

$$
\text{Number of determinants} = \binom{N}{n}\binom{K-N}{n}, \tag{3.23}
$$

except for a very few number of electrons and a very limited amount of excited states, the number of determinants to compute is cumbersome in most of cases.

Notice also that as usually formulated, CI is intended to be solved using a linear variational method, creating a matrix representation of the Hamiltonian expanded in a basis of N-electron wavefunctions and solving the resulting eigenvalue problem.

3.3.2 Multiconfiguration Self-Consistent Field Method

The internal coefficients of the orbital Φ_i in the base used to create them are fixed in CI. The Multiconfiguration Self-Consistent Field Method (MCSCF) not only optimizes c_i but also the coefficients for the one electron orbital ψ[Jensen, 2007].

The intention of MCSCF is to reduce the size of the basis that represent the one-electron orbitals. This method could be thought as a mix of the Hartree-Fock method that optimizes the basis and configuration interaction that optimizes the coefficients in the Slater determinants.

This method can be used to provide the alternative configurations needed for methods such as MRCI, using MCSCF results, a subset of the configurations are used, those with high value in the expansion. As the MCSCF configurations are already excited, the new configurations from MRCI contains elements with higher level of excitation.

3.4 Atomic Physics Concepts

Atomic collisions is a major branch in the domain of atomic physics [Bransden and Joachain, 2003]. Other areas could be the interaction of atoms with photons or electromagnetic fields. The methods have been used, for example, in the case of electron impact [Morrison, 1983; Burke, 1993; Brunger and Buckman, 2002] and ion impact [Fainstein *et al.*, 1988; Eichler, 1990; Bransden and McDowell, 1992].

It is useful to classify atomic collisions in three domains, low, medium and high energy. The classification is based on the comparison of the velocity of the projectile v_0 with the typical Bohr velocity v_e of the valence electron in the target or even projectile. The low, intermediate and high-energy regions are defined according to whether $v_0 \ll v_e$, $v_0 \approx v_e$ or $v_0 \gg v_e$ respectively. In the low-energy region the movement of the electrons is higher than the relative velocity of the nuclei. The adiabatic picture is appropriate, the electrons have enough time to follow the formation of a bond between the atoms. Charge transfer is the dominant process in this region. In the intermediate-energy region a competition is established between the movement of ions and the movement of electrons. We can imagine that when the relative movement of the ions is close to the velocity of the valence electrons there is a large probability for the electron to jump to another atom and follow its path. In most cases the maximum capture cross section occurs for a kinetic energy where the velocity of the nuclei is of the same order of magnitude as the velocity of the valence electron v_e in the target. In the high energy domain, but below the relativistic regime, the probabilities of charge-exchange decrease rapidly (typically like v_0^{-12} or v_0^{-11}). One characteristic of this region is that the time of interaction is small and the interaction between the atoms can be considered an small perturbation. Contrary to the low-energy region, the dominant process in the high-energy region is ionization and direct excitation [Bransden and McDowell, 1992].

As the focus of the area is to produce an accurate representation of the

quantum phenomena, most of the experiments and theoretical developments involve usually light atoms. Experimental studies had been done impacting atoms on gases. The projectiles are usually ions because charging the particles is the natural way to accelerate them by electrostatic fields.

The basic idea about how those experiments are done starts with ions extracted from ion sources. Those ions are accelerated using electrostatic fields and focused using magnetic fields. In the next step, the ions are separated by charge-to-mass ratio using for example a perpendicular uniform magnetic field. The ions that follows the path are again filtered to remove neutrals. After a sequence of manipulations, the ions enter in the chamber where the target atoms are located. Once they interact with the target the state of the projectile and/or target is measured.

One of the main purposes of those experiences is to determine the capture cross sections in a certain range of energies. Typically the energies of such experiments are in the order of keV.

As an example of the kind of experiences, it is worth to mention the work of Aumayr and Winter [Aumayr and Winter, 1985] impacting light atoms on Li and measuring single-capture cross section. In two papers DuBois [DuBois, 1985] and DuBois and Toburen [DuBois and Toburen, 1985] measure the capture cross section for H^+ and He^{2+} from Li, Na and Mg. In more recent years the attention has been concentrated in consider heavier interacting particles and more active electrons. It is worth to mention studies on fast ion-atom collisions with two actively participating electrons [Belkić *et al.*, 2008]. For fast collisions, ionization is a major process; cross sections for single, double ionization have been measured for C_{60} being impacted by C, F and Si ions at high energies [Kelkar *et al.*, 2010].

We will focus in this section to provide some of the theoretical elements used in the description of atomic collisions. Even if some of them will not be used for the purposes of this work, they are important to contextualize the theoretical efforts made in the past to understand atomic collision processes.

3.4.1 Cross Sections

The cross section is a very useful concept in scattering processes. We start with a classical picture of the scattering process.

Consider a beam of classical particles impacting a target The projectiles are monoenergetic and the target is in such low density gas or a thin film that single collisions between projectile and target occurs. The projectile enters with a well defined trajectory and it is scattered into a particlular direction (θ, ϕ).

Suppose the interaction between particles has a limited range, and becomes null beyond a distance a. The particles scattered are detected out of the range of interaction. If the detector subtends a solid angle $d\Omega$ centered in the target and with direction (θ, ϕ), a number of particles $Nd\Omega$ can be detected. This number is proportional to the flux of projectiles.

A flux of particles is defined as the number of projectiles crossing per unit time a unit surface that is perpendicular to the trajectory of the projectiles.

The differential scattering cross section is defined as ratio between the number of particles scattered into the direction (θ, ϕ) per unit of time, per unit solid angle, divided by the incident flux

$$\frac{d\sigma}{d\Omega} = \frac{N}{F} \tag{3.24}$$

The total scattering cross-section σ_{tot} is defined as the integral of the differential cross-section over the complete sphere

$$\sigma_{tot} = \int \frac{d\sigma}{d\Omega} d\Omega \tag{3.25}$$

$$= \int_0^{2\pi} d\phi \int_0^{\pi} d\theta \sin\theta \frac{d\sigma}{d\Omega} \tag{3.26}$$

A cross section has dimensions of area, in the limit case of macroscopic objects where the interaction of an object is negligible, the cross-section coincides with the area of the object perpendicular to the incident beam.

There are several kinds of scattering. In the elastic scattering, the internal energies of the incident and target particles do not change all across the interaction, and no further particles are created as a consequence. Many collisions, and in particular, those relevant in this work are not elastic, the electrons of both, projectile and target can be excited, electrons can escape or being transferred between atoms. In the case of collisions with molecules, those molecules could fragment or reconfigure, the kind of processes that could take place in non-elastic collisions is far more richer and complex.

In quantum mechanics the idea of a single classical trajectory is not longer valid an we must to replace the picture of a beam composed of single particles by a plane wave. We will describe briefly the scattering produced by a fixed central force field. We start with the non-relativistic Schrödinger equation:

$$\frac{\partial \Psi(\mathbf{r}, t)}{\partial t} = \left[-\nabla^2 + V(\mathbf{r})\right] \Psi(\mathbf{r}, t) \tag{3.27}$$

As mention before, the detector is located far away, so the scattered wavefunction must be represented for a certain radial flow.

$$\Psi_{scat}(\mathbf{r}) = f(k, \theta, \phi) \frac{e^{ikr}}{r} \tag{3.28}$$

The scattering amplitude f determines the number of particles scattered in a particular direction. The number of particles being detected per unit of time $N d\Omega$ is

$$N d\Omega = k |f(k, \theta, \phi)|^2 d\Omega \tag{3.29}$$

And the differential cross-section is given by

$$\frac{d\sigma}{d\Omega} = |f(k, \theta, \phi)|^2 \tag{3.30}$$

The problem of describe the scattering amplitude in a convenient way determine several of the methods developed in the theory of quantum scattering. In the case of a central potential, the scattering amplitude is no longer a function of the azimuthal angle ϕ and the function $f(k,\theta)$ can be expanded in series of Legendre polynomials.

$$f(k,\theta) = \sum_{l=0}^{\infty} f_l(k) P_l(cos\theta) \tag{3.31}$$

The wavefunction can be also expanded with Legendre polynomials and that give us the so called method of partial waves. In practical cases the number of those partial waves needed to well represent the scattering amplitude may be large. Assuming a weak potential, or a high energy perturbative methods can be used such as the scattering wavefunction can be expanded in the Born series.

$$\begin{aligned} \psi_0(\mathbf{r}) &= \phi_{\mathbf{k}}(\mathbf{r}) = e^{i\mathbf{k}\cdot\mathbf{r}}, \\ \psi_1(\mathbf{r}) &= \phi_{\mathbf{k}}(\mathbf{r}) + \int G_0(k,\mathbf{r},\mathbf{r}')U(\mathbf{r}')\psi(\mathbf{r}')d\mathbf{r}', \\ &\vdots \\ \psi_n(\mathbf{r}) &= \phi_{\mathbf{k}}(\mathbf{r}) + \int G_0(k,\mathbf{r},\mathbf{r}')U(\mathbf{r}')\psi_{n-1}(\mathbf{r}')d\mathbf{r}' \end{aligned} \tag{3.32}$$

where G_0 is the Green's function

$$G_0(k,\mathbf{r},\mathbf{r}') = -\frac{1}{4\pi}\frac{\exp(ik|\mathbf{r}-\mathbf{r}'|)}{|\mathbf{r}-\mathbf{r}'|} \tag{3.33}$$

We obtain the Born series for the scattering amplitude using eq. 3.33 to solve the integral representation for the scattering amplitude

$$f(k,\theta,\phi) = -\frac{1}{4\pi}\langle\phi_{\mathbf{k}}|\,U\,|\psi\rangle \tag{3.34}$$

where U is proportional to the potential $V(\mathbf{r})$

Both, the method of partial waves and the Born series are very classical methods in atomic collisions, in particular when the central potential condition is reasonable to assume.

3.4.2 Eikonal Approximation

The eikonal approximation has a very important place in scattering theory by its connections with classical optics and semiclassical physics. The idea comes from optics assuming that light travels in a straight line as a particle swarm. This approximation is valid in optics, as soon as the obstacle is large compared with the wavelength of the incident light. From the semi-classical point of view, the method is justified as soon as the Broglie wavelength $\lambda = 2\pi/k$ is small enough with respect to the size of the target, ie, the distance in which

the potential varies appreciable. Another condition is that the impact energies should be much larger than the typical strength of the potential.

The eikonal approximation was introduced in quantum scattering by Moliére [Moliére, 1947] and expanded by Glauber [Glauber *et al.*, 1959] in the context of nuclear physics [Glauber and Matthiae, 1970; Kabat, 1992] and has been ported to the domain of quantum field theory [Lévy and Sucher, 1969]

We will present the derivation from the Schrödinger equation, an alternative derivation is possible from the Lippmann-Schwinger equation by linearizing the Green's function in momentum space. In the context of atomic collisions we start by subtracting from the total Hamiltonian the kinetic energy of the projectile (Non relativistic)

$$\hat{\mathrm{H}}(\mathbf{r},\mathbf{R}) = -\frac{1}{2\mu}\nabla^2_{\mathbf{R}} + \hat{\mathrm{H}}_{int}(\mathbf{r},\mathbf{R}) \tag{3.35}$$

Since the potential varies slowly on the length scale of the incident wavelength, we can extract the free incident plane wave from the scattering wavefunction as a factor and expand the wavefunction in terms of the reduced mass of the projectile $\mu = \frac{M_p M_t}{M_p + M_t}$

$$\Psi(\mathbf{r},\mathbf{R}) = e^{(i\mathbf{K}\cdot\mathbf{R})}\left[\psi(\mathbf{r},\mathbf{R}) + \frac{1}{\mu}\psi^{(1)}(\mathbf{r},\mathbf{R}) + \frac{1}{\mu^2}\psi^{(2)}(\mathbf{r},\mathbf{R}) + \cdots\right] \tag{3.36}$$

Applying this expansion on the Hamiltonian Eq. 3.35 and defining the vector $\mathbf{K}$ such as $|\mathbf{K}|^2 = 2\mu E$ we obtain

$$i\mathbf{K}\cdot\nabla_{\mathbf{R}}\psi = \mu\hat{\mathrm{H}}_{int}\psi \tag{3.37}$$

Assuming now that the projectile follows a classical rectilinear trajectory; the equation for the trajectory can be expressed in terms of the vector of impact parameter $\mathbf{b}$ where the closest encounter with the target is produced at time $t = 0$

$$\mathbf{R} = \mathbf{b} + \mathbf{v}t, \mathbf{v}\cdot\mathbf{b} = 0 \tag{3.38}$$

Now we can recast the term $\nabla_{\mathbf{R}}$ as a time derivative as

$$\nabla_{\mathbf{R}} = \frac{\mathbf{v}}{|\mathbf{v}|^2}\frac{\partial}{\partial t}, \tag{3.39}$$

The Schrödinger equation Eq. 3.37 can be written

$$\left[\hat{\mathrm{H}}_{int} - i\frac{\partial}{\partial t}_{\mathbf{r}}\right]\psi(\mathbf{r},\mathbf{R}) = 0 \tag{3.40}$$

This is the expression produced by the eikonal approximation. The eikonal approximation has been used in the case of electron atom collisions, but also is important in high energy ion-atom collisions [Belkić *et al.*, 1979]. The eikonal approximation can be also coupled to other levels of electronic structure. One example was shown by Micha et al [Micha and Runge, 1994] with Time-dependent Hartree-Fock.

3.5 Movement of Nuclei

In the previous sections we see how the electronic structure can be computed with different levels of refinement. In this chapter we explore the methods that allow to describe the movement of the nuclei and the electronic structure dynamics created by this movement.

There are several options to deal with this problem. The first one could be to completely ignore it and assume that the nuclei follows a rectilinear path. That is the assumption done very often in atomic physics for high energy collisions, the idea is to concentrate all the theoretical effort in the electronic structure. The physical justifications for such approach requires that the collision is done in gas phase as usual in atomic physics. With that requirement the projectile collides at most with one molecule in the target before being detected. Another condition is that the kinetic energy of the projectile is high enough so that the angle of deflection is negligible or at least can be obtained without solving step by step the kinematic state of the nuclei.

The opposite side of the spectrum is classical molecular dynamics that try to avoid the hard problem of solving the electronic structure at each time, and prefers to concentrate is efforts in the dynamics of the nuclei, assuming that the potentials produced by the electronic structure can be precomputed theoretically or tabulated experimentally.

In the middle between those extremes are the methods called ab-initio molecular dynamics. For those methods, the electronic structure is as important as the correct path followed by the nuclei and each aspect of the dynamics needs to be calculated taking in account the other element. The methods used in this work are based precisely in this assumption and the whole area will be briefly explored.

3.5.1 Classical Molecular Dynamics

There are two basic ingredients in classical molecular dynamics (CMD). The movement of atoms is determined by numerical integration of the Newton's equations of motion, and the potential generated by the electronic structure is precomputed in advance and used without any further first-principles calculation.

In CMD the complexity of the electronic structure is removed replacing the potential coming from the electronic structure by *effective potentials* or *force fields*. Those effective potentials try to capture the electronic, ionic and electron-ion interactions. Usually fixed, the potentials are function of the interatomic distances at least.

The derivation of the equations for CMD starts from the time-dependent Schrödinger equation

$$i\frac{\partial}{\partial t}\Phi(\mathbf{r},\mathbf{R};t) = \hat{\mathrm{H}}\Phi(\mathbf{r},\mathbf{R};t), \tag{3.41}$$

where the vector $\mathbf{r}$ is the set of electronic coordinates, $\mathbf{R}$ are the nuclear coordinates and the Hamiltonian can be described by

$$\hat{\mathrm{H}} = -\sum_i \frac{1}{2M_i}\nabla_i^2 + \hat{\mathrm{H}}_e(\mathbf{r},\mathbf{R}) \tag{3.42}$$

The classical molecular dynamics equations can be formally derivated as presented in [Marx and Hutter, 2000] that follows the route of Tully presented in some books [Berne *et al.*, 1998; Thompson, 1998]. The starting point is to assuming the complete separability of electronic and nuclear coordinates

$$\Phi(\mathbf{r},\mathbf{R};t) \approx \Psi(\mathbf{r};t)\chi(\mathbf{R};t)\exp\left[i\int_{t_0}^{t} dt'\tilde{E}_r(t')\right] \tag{3.43}$$

Introducing this separation into the Schrödinger equation and elaborating the Schrödinger equation associated to the nuclear coordinates, we can arrive to the Newtonian equations of motion for the nuclear positions

$$\begin{aligned} M_i\ddot{\mathbf{R}}_i(t) &= -\nabla_i \int \mathrm{d}\mathbf{r}\Psi^*\hat{\mathrm{H}}_e\Psi & (3.44)\\ &= -\nabla_i V_e^E(\mathbf{R}(t)) & (3.45)\end{aligned}$$

and the electronic Schrödinger equation for the electrons will be

$$\begin{aligned} i\frac{\partial\Psi}{\partial t} &= -\sum_i \frac{1}{2}\nabla_i^2\Psi + V_{n-e}(\mathbf{r},\mathbf{R}(t))\Psi(\mathbf{r},\mathbf{R};t)\\ &= \hat{\mathrm{H}}_e(\mathbf{r},\mathbf{R}(t))\Psi(\mathbf{r},\mathbf{R};t) & (3.46)\end{aligned}$$

The main message is that the nuclei move according to classical mechanics in an effective potential V_e^E that is created by averaging the electronic Hamiltonian $\hat{\mathrm{H}}_e$ over the electronic states. As the electronic structure is not computed during the simulation our present level of technology allows to compute millions of particles with large integration time. It is worth to mention than in CMD the quality of the simulations is very dependent of the choice of potentials.

Consider for example the most prototypical potential, the Lennard-Jones (LJ) [Jones, 1924]. The potential is defined as

$$\begin{aligned} V_{LJ} &= 4\varepsilon\left[\left(\frac{\sigma}{r}\right)^{12} - \left(\frac{\sigma}{r}\right)^{6}\right] & (3.47)\\ &= \varepsilon\left[\left(\frac{r_m}{r}\right)^{12} - 2\left(\frac{r_m}{r}\right)^{6}\right] & (3.48)\end{aligned}$$

where the parameters ε and σ are adjusted with experimental data or ab-initio calculations.

This potential is very simple, contains only two parameters and is a pair potential, ie, the interactions are established between two atoms. Those advantages are also its limitations. With only two parameters ε and σ, LJ potentials can be tuned for two physical quantities, for example bond length and energy of dissociation. Other physical properties can not be included and will typically

fail. LJ is a pair potential, so it is insensitive to the number of bonds that a particular atom creates or the coordination number in a crystal. For that reason LJ in crystals will try to maximize the coordination, producing hexagonal close-packed structures. Those potentials are also weak in representing the correct angles and dihedrals. In general, they are considered as appropriate for modeling noble gases at reasonable low temperatures. The interaction in such systems is dominated by van der Waals forces.

The main limitation of CMD in relation to the objective of this work is the complete lack of electronic structure dynamics. Charge transfer processes cannot be described at that level of theory.

3.5.2 Born-Oppenheimer Molecular Dynamics

An alternative to CMD consist in solving the electronic structure problem "on the fly" assuming static positions for the nuclei each time that the electronic structure is computed.

The physical justification for that comes from the mass disparity between nuclei and electrons. Consider the ratio between the mass of a proton and the mass of an electrons $m_p/m_e \approx 1836$. Adding to that the fact that the number of neutrons increase with the number of protons the disparity between the masses of nuclei and electrons becomes more and more evident.

This led Born and Oppenheimer [Born and Oppenheimer, 1927] to think that in order to alleviate the complexity of the Schrödinger equation the dynamics of nuclei and electrons could be decoupled. It means that the full many-body wavefunction for a set of electrons and nuclei could be separated as

$$\Phi_{\mathrm{BO}}(\mathbf{r}, \mathbf{R}; t) = \tilde{\Phi}_{\mathbf{R}}(\mathbf{r})\chi(\mathbf{R}; t). \tag{3.49}$$

Assuming a single state for the nuclear wavefunction. Notice that the Born-Oppenheimer eq. 3.49 separation differs from the CMD ansatz Eq. 3.43. The electronic wavefunction is static in BO but formally present in Eq. 3.43 but disappears in the mean field calculation.

The idea is that the coordinates of the nuclei $\mathbf{R_j}(j = 1 \cdots M)$ and the coordinates of the electrons $\mathbf{r_i}(i = 1 \cdots N)$ have very different nature and the electronic wavefunction $\Phi_{\{\mathbf{R_j}\}}(\mathbf{r_i})$ could simply depend parametrically of the nuclear coordinates.

This disentanglement of the wavefunction makes possible also the separation of the Hamiltonian into a Hamiltonian of the dynamics of electrons and nuclei separated plus a term of interaction between the nuclear and electronic parts. The Hamiltonian in those terms could be written in five terms

$$\hat{\mathrm{H}} = \hat{\mathrm{T}}_e + \hat{\mathrm{T}}_n + \hat{\mathrm{V}}_{e-e} + \hat{\mathrm{V}}_{n-e} + \hat{\mathrm{V}}_{n-n} \tag{3.50}$$

The subscript n means that the term is referring tho the nuclear part and the subscript e refers to the electronic part. The operator $\hat{\mathrm{T}}$ describes the kinetic energy and the $\hat{\mathrm{V}}$ is the potential energy. For a system of N electrons and M nucleus those five terms can be written as

$$\hat{\mathrm{T}}_e = -\sum_{i=1}^{N} \frac{1}{2} \nabla^2_{\mathbf{r}_i} \tag{3.51}$$

$$\hat{\mathrm{T}}_n = -\sum_{i=1}^{M} \frac{1}{2m_i} \nabla^2_{\mathbf{R}_i} \tag{3.52}$$

$$\hat{\mathrm{V}}_{e-e} = \frac{1}{2} \sum_{i=1}^{N} \sum_{j=1}^{N} (|\mathbf{r}_i - \mathbf{r}_j|)^{-1} \tag{3.53}$$

$$\hat{\mathrm{V}}_{n-n} = \frac{1}{2} \sum_{i=1}^{M} \sum_{j=1}^{M} Z_i Z_j (|\mathbf{R}_i - \mathbf{R}_j|)^{-1} \tag{3.54}$$

$$\hat{\mathrm{V}}_{n-e} = -\sum_{i=1}^{N} \sum_{j=1}^{M} Z_j (|\mathbf{r}_i - \mathbf{R}_j|)^{-1} \tag{3.55}$$

where m_i is the mass of the ith nuclei in the system. Z_i is the atomic number of the ith nuclei. The factor $\frac{1}{2}$ in $\hat{\mathrm{V}}_{e-e}$ (or $\hat{\mathrm{V}}_{n-n}$) comes from the double summation of the potential between the i and j electrons (or nuclei). The positive sign in $\hat{\mathrm{V}}_{e-e}$ and $\hat{\mathrm{V}}_{n-n}$ comes from the fact that the forces that they produce are repulsive.

The next important step is the consideration that the movement of nuclei is in general slow compared with the rapid movement of electrons. We can consider that electrons evolve in a potential generated by nuclei. It does not mean that the nuclei cannot move. It means that the dynamics of nuclei is of a different nature compared with the dynamics of electrons, that could eventually be treated classically. This procedure promotes Eq. 3.52 and Eq. 3.54 from the quantum domain to the classical domain and we end with a electronic Hamiltonian expressed as

$$\hat{\mathrm{H}}_{e\{\mathbf{R}\}} = \hat{\mathrm{T}}_e + \hat{\mathrm{V}}_{e-e} + \hat{\mathrm{V}}_{n-e} \tag{3.56}$$

With this the nuclear positions becomes parameters of the Schrödinger equation that now reads as

$$\hat{\mathrm{H}}^e_{\{\mathbf{R}\}} \Psi^e_{\{\mathbf{R}\}}(\mathbf{r}_i) = E^e_{\{\mathbf{R}\}} \Psi^e_{\{\mathbf{R}\}}(\mathbf{r}_i), \tag{3.57}$$

where $E^e_{\{\mathbf{R}\}}$ is the electronic energy of the system and $\{\mathbf{R}\}$ represent the parametric dependency on the M nuclear positions.

The complete expression can be reintroduced replacing the electronic terms of the Hamiltonian by the electronic eigenvalues. The complete Schrödinger equation including the nuclei can be written

$$\left(\hat{\mathrm{T}}_n + E_{e\{\mathbf{R}\}}\right) \Psi_i(\mathbf{R}) = E_{BO\{\mathbf{R}\}} \Psi_i(\mathbf{R}). \tag{3.58}$$

This decoupling of nuclear and electronic dynamics greatly simplifies the treatment of a set of many-body interacting particles, nuclei and electrons. However the solution of Eq. 3.57 is still a challenging problem. The big barrier

is created by the electron-electron interaction $\hat{\mathrm{V}}_{e-e}$ that correlates the dynamics of electrons. In the first section of this chapter, several approaches were considered to solve the electronic structure of a set of interacting electrons. Those approaches could be used to provide the electronic dynamics necessary by BO.

3.5.3 Ehrenfest Molecular Dynamics

In Ehrenfest molecular dynamics (EMD) the classical limit for nuclei is preserved as in Eq. 3.45 but the Schrödinger equation for the electronic part is preserved as Eq. 3.46 and not approximated as in CMD [Marx and Hutter, 2009].

Coupling the classical movement of nuclei with a quantum mechanical movement of electrons implies to solve the set of equations

$$M_i\ddot{\mathbf{R}}_i(t) = -\nabla_i \int \mathrm{d}\mathbf{r}\Psi^*\hat{\mathrm{H}}_e\Psi \tag{3.59}$$

$$i\frac{\partial\Psi}{\partial t} = \hat{\mathrm{H}}_e(\mathbf{r},\mathbf{R}(t))\Psi(\mathbf{r},\mathbf{R};t) \tag{3.60}$$

The traditional dimensionality explosion with nuclear dimensions for the computation of potential energy surfaces disappears when the time-dependent Schrödinger equation is solved "on-the-fly".

The nuclear forces are computed using the Hellmann-Feynman theorem in order to compute

$$\mathbf{F}_i = -\nabla_i \left\langle \Psi \middle| \hat{\mathrm{H}}_e \middle| \Psi \right\rangle . \tag{3.61}$$

By expanding the electronic wavefunction in terms of basis $\{\Psi_k\}$

$$\Psi(\mathbf{r},\mathbf{R};t) = \sum_{k=0}^{\infty} c_k(t)\Psi_k(\mathbf{r},\mathbf{R}) \tag{3.62}$$

where the coefficients $c_k(t)$ are constrained by the relation

$$\sum_k |c_k(t)|^2 = 1 \tag{3.63}$$

Using this expansion the equation Eq. 3.60 can be recast in terms of the coefficients c_k

$$M_i\ddot{\mathbf{R}}_i(t) = -\sum_k |c_k(t)|^2\nabla_i E_k - \sum_{k,l} c_k^* c_l (E_k - E_l)\mathbf{d}_i^{kl} \tag{3.64}$$

$$i\dot{c}_k(t) = c_k(t)E_k - i\sum_{i,l} c_l(t)\dot{\mathbf{R}}_i\mathbf{d}_i^{kl} \tag{3.65}$$

where the terms $\mathbf{d}_i^{kl}$ are given by

$$\mathbf{d}_i^{kl}(\mathbf{R}_i(t)) = \int d\mathbf{r}\Psi_k^*\nabla_i\Psi_l \tag{3.66}$$

With those c coefficients changing, the Ehrenfest dynamics allows for non-adiabatic transitions between different electronic states still preserving the classical nuclear motion for the nucleus.

This is the most natural method to produce molecular dynamics in explicit time-dependent methods such as Time-dependent Hartree-Fock (TDHF) or Time-Dependent density functional theory (TDDFT).

An illustrative example is the case with only one electronic state, in this case the Ehrenfest dynamics reduces to solve

$$M_i \ddot{\mathbf{R}}_i(t) = -\nabla_i \left\langle \Psi_0 \middle| \hat{\mathrm{H}}_e \middle| \Psi_0 \right\rangle \tag{3.67}$$

$$i\frac{\partial \Psi_0}{\partial t} = \hat{\mathrm{H}}_e \Psi_0 \tag{3.68}$$

where the electronic Hamiltonian $\hat{\mathrm{H}}_e$ is time-dependent via the nuclear movement.

Ehrenfest molecular dynamics is the method of choice in this work, and there are several number of reasons for that. Other methods like CMD and BO can not account for charge transfer processes, first because the electronic dynamics is completely missing (CMD) or computed for static atomic positions (BO). The limitation as usual is the number of degrees of freedom in the system. For TDDFT, Ehrenfest dynamics represents the natural alternative and it is the method of choice for collision problems with large systems.

Recently, for large-scale problems an efficient algorithm has been developed that automatically enforced orthogonalization of the Kohn-Sham orbitals, a typical limitation in other AIMD. [Andrade *et al.*, 2008; Andrade *et al.*, 2009]

3.5.4 Car-Parrinello Molecular Dynamics

Car-Parrinello is somehow a departure from the other methods like CMD, BO or EMD. Those methods can be formally presented stating from a certain factorization of the full Schrödinger equation as in Eq. 3.43 (CMD), Eq. 3.49 (BO) or Eq. 3.60 (EMD) and simplified with a series of physical arguments.

Car-Parinello Molecular Dynamics (CPMD) [Car and Parrinello, 1985] combines the good properties of EMD and BO using a radical new approach. In Ehrenfest the big limitation is the time scale that is dominated by the electrons, on the contrary in BO such limitation does not occur as the electronic structure is computed on frozen nuclear positions. That implies that the full electronic structure calculation must be done at each time step, something that is not required in Ehrenfest. Car-Parrinello molecular dynamics takes advantage of the smooth time-evolution of the electrons preserving the flow of the nuclear positions.

Instead of having a mixed quantum/classical system as in BO or EMD, CPMD recasts the problem in a purely classical envelope by proposing a classical Lagrangian for the set of nuclei and the classic-like electrons

$$\mathcal{L}_{\mathrm{CP}} = \underbrace{\sum_I \frac{1}{2} M_I \dot{\mathbf{R}}_I^2 + \sum_j \frac{1}{2} \left\langle \dot{\psi}_j \middle| \psi_j \right\rangle}_{\text{kinetic energy}} - \underbrace{\left\langle \Psi_0 \middle| \hat{\mathrm{H}}_e \middle| \Psi_0 \right\rangle}_{\text{potential energy}} + \underbrace{constraints}_{\text{for orthogonality}} \tag{3.69}$$

Imposing as usual the minimal action principle for the action of this Lagrangian

$$\delta S = \delta \int_{t_0}^{t_1} \mathcal{L} dt = 0 \tag{3.70}$$

we arrive to the Euler-Lagrange equations of motion

$$\frac{\mathrm{d}}{\mathrm{d}t} \frac{\partial \mathcal{L}}{\partial \dot{\mathbf{R}}_i} = \frac{\partial \mathcal{L}}{\partial \mathbf{R}_i} \tag{3.71}$$

$$\frac{\mathrm{d}}{\mathrm{d}t} \frac{\partial \mathcal{L}}{\partial \dot{\psi}_j} = \frac{\partial \mathcal{L}}{\partial \psi_j} \tag{3.72}$$

Applying the expression for $\mathcal{L}$ on these equations we obtain the Car-Parrinello set of equations of motion.

$$\begin{aligned} M_i \ddot{\mathbf{R}}_i(t) &= -\frac{\partial}{\partial \mathbf{R}_i} \left\langle \Psi_0 \middle| \hat{\mathrm{H}}_e \middle| \Psi_0 \right\rangle + \frac{\partial}{\partial \mathbf{R}_i} \{constraints\} \\ \mu_j \ddot{\psi}_j^*(t) &= -\frac{\partial}{\partial \psi_j} \left\langle \Psi_0 \middle| \hat{\mathrm{H}}_e \middle| \Psi_0 \right\rangle + \frac{\partial}{\partial \psi_j^*} \{constraints\} \end{aligned}$$

where μ_j is some sort of fake mass for the orbital ψ_j

The Car-Parrinello approach was groundbreaking since its publication. The method however has some limitations, the most important being the lack of a real electron dynamics. Also it is limited to account for strong electronic correlations in systems. Despite the fact that the CPMD method has improved in the last 25 years, the necessity to orthogonalize the electronic orbitals is a limit to the applicability for large systems.

3.6 Potential energy surfaces and surface hopping

Within the Born-Oppenheimer approximation the idea of potential energy surfaces (PES) is frequently mentioned. Using the nuclear positions as variables, the total energy forms a hypersurface. In the simple case of two atoms, the potential energy is a curve that resemble the traditional effective potentials used in classical molecular dynamics. In principle to model a reaction a potential energy surface must be created taking in account all the possible positions of reactant and product molecules, and the number of variables makes this task in practice unfeasible.

In practice, the energy surface is interpolated using a certain number of representative orientations, and the potential energy surface or projections of it are interpolated numerically.

Several points of a PES are particularly important. The global minimum correspond to the structure of the molecule in its ground state. The reaction path is the set of points that goes from the initial to the final configuration. Local minima are indications of reactive intermediates and saddle points are transition states.

For the description of processes beyond the Born-Oppenheimer approximation, we can mention two alternatives [Drukker, 1999]. One was Ehrenfest dynamics already described in the previous section. Using the idea of PES we have the surface-hopping method [Tully, 1990].

In the surface hopping method, the system jumps between different states. As the different states are in different levels of energy, the total energy is preserved by adjusting the velocity of the particles accordingly. During the path in the PES, a small gap between two states generally result in high transition probabilities and most of the hops occur in the vicinity of surface crossings.

3.7 Time-Dependent Density Functional Theory

Time-dependent density functional theory (TDDFT) [Gross and Burke, 2006] is an alternative to solve the time-dependent Schrödinger equation for a set of interacting electrons and is the method of choice for this work. The basics of the theory will be developed here.

TDDFT can be seen as an extension of the ground state density functional theory (GSDFT). However, the fundamental theorems [Runge and Gross, 1984] are demonstrated in a quite different way even if the results appear analogous to those of GSDFT. The fundamental theorem of TDDFT, called the Runge-Gross theorem, is the analogous of the Hohemberg-Kohn (HK) theorem that was shown for GSDFT.

Consider a wavefunction $\Psi(t)$, it represents the state of a system of N particles. The time evolution of such system is given by the solution of the Schrödinger equation :

$$\hat{\mathrm{H}}(t)\Psi(t) = i\frac{\partial\Psi(t)}{\partial t} \tag{3.73}$$

This is a first-order differential equation whose solution at time t requires the knowledge of an initial condition: the wavefunction $\Psi(0)$. The operator $\hat{\mathrm{H}}(t)$ is the Hamiltonian, this operator is usually separated in three terms:

$$\hat{\mathrm{H}}(t) = \hat{\mathrm{T}}(\mathbf{r}) + \hat{\mathrm{V}}_{ext}(\mathbf{r}t) + \hat{\mathrm{W}}(\mathbf{r}) \tag{3.74}$$

The kinetic energy operator $\hat{\mathrm{T}}(\mathbf{r})$ is expressed for a set of N particles as:

$$\hat{\mathrm{T}}(\mathbf{r}) = -\frac{1}{2}\sum_{i=1}^{N}\nabla_i^2 \tag{3.75}$$

The second term in the Hamiltonian is the external potential, that could explicitly depend on time and is separable in N terms, one for each particle in the system:

$$\hat{\mathrm{V}}_{ext}(t) = \sum_{i=1}^{N} v_{ext}(\mathbf{r}_i t) \tag{3.76}$$

The third term in the Hamiltonian $\hat{\mathrm{W}}(\mathbf{r})$ is in general the Coulomb term, this term is not explicitly dependent on time, is symmetric under the interchange of any two particles, and does not depend of a specific origin of coordinates:

$$\hat{\mathrm{W}}(\mathbf{r}) = \frac{1}{2} \sum_{i \neq j}^{N} \frac{1}{|\mathbf{r}_i - \mathbf{r}_j|} \tag{3.77}$$

As in GSDFT the focus is shifted from the wavefunction to the electronic density, a time-dependent scalar field in the domain of $\mathbb{R}$:

$$n(\mathbf{r}, t) = \langle \Psi(t) | \, \hat{\mathrm{n}}(\mathbf{r}) \, | \Psi(t) \rangle \tag{3.78}$$

Differently from the Hohenberg-Kohn theorem, the Runge-Gross theorem establishes the conditions under two densities $n(\mathbf{r}, t)$ and $n'(\mathbf{r}, t)$ evolves starting from the same initial state $\Psi(t = 0)$. The theorem uses extensively the current density given by

$$\mathbf{j}(\mathbf{r}, t) = N \int d^3 r_2 \cdots \int d^3 r_N \Im(\Psi \nabla \Psi^*), \tag{3.79}$$

where $\Psi = \Psi(\mathbf{r}, \mathbf{r}_2, \cdots, \mathbf{r}_N, t)$ and the integrand is the imaginary part of $\Psi \nabla \Psi^*$.

The link between the density and the paramagnetic current density is given by the continuity equation

$$\frac{\partial n(\mathbf{r}, t)}{\partial t} = -\nabla \cdot \mathbf{j}(\mathbf{r}, t). \tag{3.80}$$

For technical reasons revealed during the demonstration of the theorem, the external potential needs to be Taylor expandable

$$v_{ext}(\mathbf{r}, t) = \sum_{k=0}^{\infty} \frac{1}{k!} \partial_t^k v_{ext}(\mathbf{r}, t)|_{t=t_0} (t - t_0)^k, \tag{3.81}$$

this requirement is physically easy to satisfy as the fields change continuously. However, the theorem excludes the academically important case of potentials that are switched on instantaneously or changes in a step-like way.

Another important ingredient in the RG theorem is the condition under which two potentials are physically different, it means, the conditions under which the solution of the Schrödinger equation $\Psi(t)$ changes for more than a global phase. Without demonstration here if two potentials v_{ext} and v'_{ext} differ by more than a time dependent function

$$v'_{ext}(\mathbf{r},t) \neq v_{ext}(\mathbf{r},t) + \dot{\alpha}(t) \text{ for } t_0 \leq t \leq t_1, \tag{3.82}$$

the solutions $|\Psi(t)\rangle$ and $|\Psi'(t)\rangle$ will differ by more than a time dependent global phase,

$$|\Psi'(t)\rangle \neq e^{-iN\alpha(t)/\hbar}\,|\Psi(t)\rangle \text{ for } t_0 \leq t \leq t_1, \tag{3.83}$$

no matter if $|\Psi'(0)\rangle = |\Psi(0)\rangle$.

Now, we have all the ingredients to enunciate the Runge-Gross theorem. From a given initial state $|\Psi(t_0)\rangle$ there is an injective function (one to one) between the set of all potentials that satisfy Eq. 3.81 and Eq. 3.82,

$$\mathcal{V} = \{v_{ext}(\mathbf{r},t) \quad | \quad v_{ext}(\mathbf{r},t) = \sum_{k=0}^{\infty} \frac{1}{k!}\partial_t^k v_{ext}(\mathbf{r},t)|_{t=t_0}(t-t_0)^k; \\ v'_{ext}(\mathbf{r},t) \neq v_{ext}(\mathbf{r},t) + \dot{\alpha}(t)\} \tag{3.84}$$

and the set of associated time-dependent densities defined as Eq. 3.78, solution of Eq. 3.73 with $\hat{\mathrm{H}}$ defined as Eq. 3.74

$$\mathcal{N} = \{n(\mathbf{r},t) \quad | \quad n(\mathbf{r},t) = \langle\Psi(t)|\,\hat{n}(\mathbf{r})|\Psi(t)\rangle\,; \tag{3.85}$$

$$i\hbar\partial_t\,|\Psi(t)\rangle = \hat{\mathrm{H}}(t)\,|\Psi(t)\rangle \tag{3.86}$$

$$\hat{\mathrm{H}} = \hat{\mathrm{T}} + \int d^3r v_{ext}(\mathbf{r},t)\hat{n}(\mathbf{r}) + \hat{\mathrm{W}}; \tag{3.87}$$

$$v_{ext}(\mathbf{r},t) \in \mathcal{V}\} \tag{3.88}$$

the injective function being valid for all the values of t in the open (t_0,t_1).

Some remarks are relevant. First, notice that the RG theorem talks about an injective function, not a bijection, it means that the existence of a potential for any given density is not guarantee. Second, notice that the RG theorem is not pure density functional as the initial state $|\Psi(t_0)\rangle$ is required. the only exception is when the system starts from the ground state; in such case the HK theorem applies to the initial density and the RG theorem becomes a pure density-functional method. This is indeed how TDDFT is used in most cases.

The demonstration is splitted in two parts mediated by the intervention of the current density. In a first step the injective function is proved for the current and in a second step the injection is extended to the density.

Once the Runge-Gross theorem is demonstrated, a similar Kohn-Sham scheme can be proposed in a very similar way as is done in GS-DFT. Each one of those Kohn-Sham orbitals obey a time-dependent Schrödinger equation

$$i\frac{\partial\varphi_i(\mathbf{r},t)}{\partial t} = \hat{\mathrm{H}}_{\mathrm{KS}}(\mathbf{r},t)\varphi_i(\mathbf{r},t) \tag{3.89}$$

where $\hat{\mathrm{H}}_{\mathrm{KS}}(\mathbf{r},t)$ is the Kohn-Sham Hamiltonian defined by

$$\hat{\mathrm{H}}_{\mathrm{KS}}(\mathbf{r},t) = -\frac{\nabla^2}{2} + v_{\mathrm{KS}}[n](\mathbf{r},t). \tag{3.90}$$

The potential $v_{\mathrm{KS}}[n](\mathbf{r},t)$ is usually expressed in as the sum three terms: the external potential $v_{\mathrm{ext}}[n](\mathbf{r},t)$, the Coulomb interaction $v_{\mathrm{J}}[n](\mathbf{r},t)$ and finally the exchange-correlation potential $v_{\mathrm{xc}}[n](\mathbf{r},t)$.

3.7.1 Exchange-Correlation Potentials in TDDFT

TDDFT inherits also from GS-DFT that the fundamental approximation comes from the exchange-correlation potential v_{xc}. v_{xc} collects all the terms due to interaction between electrons beyond the Hartree term.

The exchange-correlation potential v_{xc} is a functional of the density, present or past, but also could be dependent on the Kohn-Sham wavefunctions and in principle from the many-body wavefunction. It is possible to produce v_{xc} with increasing complexity, starting from a pure density dependency to an v_{xc} depending in addition orbital dependency through the Kohn-Sham determinant.

The simplest v_{xc} starts assuming a instantaneous dependency on the density [Kohn and Sham, 1965]. That potential is called local density approximation (LDA) or in the case of systems with odd number of electrons local spin density approximation (LSDA) In LDA one considers a system whose spin densities are $n_\sigma(\mathbf{r})$ and computes the energy of exchange and correlation as

$$E_{xc}^{\mathrm{LDA}}[n_\downarrow, n_\uparrow] = \int d^3r\, n(\mathbf{r})\, e_{xc}^{\mathrm{HEG}}(n_\downarrow, n_\uparrow) \tag{3.91}$$

The potential v_{xc} is formally defined as the variational derivative with the density

$$v_{xc}(\mathbf{r},t) = \frac{\delta E_{xc}^{LDA}}{\delta n(\mathbf{r},t)} \tag{3.92}$$

Kohn and Sham realize the basic limitation of a local density approximation.

"Of course, the simple methods which are here proposed in general involve errors. These are of two general origins: a too rapid variation of density and for finite systems, boundary effects." [Kohn and Sham, 1965]

In spite of the warning, LDA has been remarkably successful and is the method of choice when its limitations are not proved for a particular kind of problems. This approximation has passed the test of time and it is still used nowadays. One step forward in complexity but not necessarily in accuracy are the semi-local functionals, in particular the generalized gradient approximation. In GGA, in addition to a dependency on the density, there is also a dependency on its gradient ∇n_σ,

$$E_{xc}^{\mathrm{GGA}}[n_\downarrow, n_\uparrow] = \int d^3r\, n(\mathbf{r})\, e_{xc}^{\mathrm{GGA}}(n_\downarrow, n_\uparrow, \nabla n_\downarrow, \nabla n_\uparrow) \tag{3.93}$$

The accuracy of semi-local functionals could be advanced with the inclusion of higher order derivatives of the density. Alternative we can make the functional to depend on the orbital kinetic energy density. As an example, recently a general class of functionals was proposed; the so-called meta-GGAs [Perdew *et al.*, 1999],

$$E_{xc}^{\mathrm{mGGA}}[n_\downarrow, n_\uparrow] = \int d^3r\, n(\mathbf{r})\, e_{xc}^{\mathrm{mGGA}}(n_\downarrow, n_\uparrow, \nabla n_\downarrow, \nabla n_\uparrow, \tau_\downarrow, \tau_\uparrow) \tag{3.94}$$

where $\tau_\sigma(\mathbf{r}) = \sum_i |\nabla \phi_{i\sigma}|^2$ denotes the orbital kinetic energy density.

All those functionals were designed for GS-DFT. They can be used also for TDDFT, in that case, the temporal dependency is neglected. The physical justification for that is that for slow varying systems, in the adiabatic approximation the exchange-correlation potential is instantaneous. For each functional designed for GS-DFT there is an adiabatic version for TDDFT.

$$v_{xc}^{\mathrm{adiabatic}}[n_\downarrow, n_\uparrow](\mathbf{r}, t) = v_{xc}^{\mathrm{LDA,GGA,mGGA,\cdots}}[n_\downarrow, n_\uparrow](\mathbf{r})|_{n_\sigma = n_\sigma(\mathbf{r},t)} \tag{3.95}$$

Several remarks can be done in respect to the use of adiabatic local or semilocal functionals in the context of atomic collisions. First, during a collision, the density changes radically not only in time, but also in space. The theoretical justification for LDA is a small variation of density and the adiabatic approximation is justified only if densities do not change much in time. Both conditions are heavily broken during collisions, in particular for the range of kinetic energies explored in this work.

During atomic collisions, one possible outcome could be the ejection of electrons from the system. This condition is also problematic in TDDFT with almost all the local and semilocal xc potentials. The problem is due to the incorrect asymptotic behavior of the tail of the potential. For finite systems, the exact xc potential decays as $-1/r$; but most of the functionals developed for GS-DFT show an exponential decay asymptotically. There are two ways of correcting for such deficiency, the use of a functional with the right behavior such as the van Leeuwen & Baerends functional [van Leeuwen and Baerends, 1994], or going into more elaborated functionals such as exact exchange and derive v_{xc} by a procedure called optimized effective potential (OEP) or optimized potential method (OPM)

3.7.2 Propagation of KS-states

Once in possession of a Kohn-Sham scheme as an auxiliary system, the next important step is the numerical integration of the set of Schrödinger equations.

Taking the time-dependent Schrödinger equation Eq. 3.73 and assuming a time-independent Hamiltonian, the quantum wavefunction at time t can be found from the wavefunction at time 0 as:

$$\Psi(\mathbf{r}, t) = G(t, 0)\Psi(\mathbf{r}, 0) \tag{3.96}$$

For a time-independent Hamiltonian, the propagator is simply

$$G(t, 0) = e^{-i\hat{\mathrm{H}}t} \tag{3.97}$$

The propagator for a time-dependent Hamiltonian is more elaborated

$$\Psi(\mathbf{r},t) = \hat{\mathrm{G}}(t,0)\Psi(\mathbf{r},0) \tag{3.98}$$

$$= \mathcal{T}\exp\left[-i\int_0^t d\tau\hat{\mathrm{H}}(\tau)\right]\Psi(\mathbf{r},0), \tag{3.99}$$

where $\mathcal{T}$ express the time ordering of the exponential, ie

$$\hat{\mathrm{G}}(t,0) = \sum_{n=0}^{\infty}\frac{(-i)^n}{n!}\int_0^t d\tau_1\int_0^t d\tau_2\cdots\int_0^t d\tau_n$$

$$= \times\mathcal{T}\left[\hat{\mathrm{H}}(\tau_1)\hat{\mathrm{H}}(\tau_2)\cdots\hat{\mathrm{H}}(\tau_3)\right] \tag{3.100}$$

Only in the case of a Hamiltonian that commutes with itself in the interval, the time-ordering operation becomes trivial. The propagator $\hat{\mathrm{G}}$ can be factored by intermediate propagations in the full interval

$$\hat{\mathrm{G}}(t) = \prod_{i=0}^{N-1} G(t_i+\Delta t_i, t_i) \tag{3.101}$$

This splitting of the propagator is motivated by two reasons. Assuming that the time dependency is continuous in time and its derivative is also continuous. During a very short time scale the Hamiltonian can be assumed constant. The second reason is for a small Δt the argument in the exponential decreases. So, the norm of the argument is also small.

Now, we can consider some of the symmetries present in the propagator $\hat{\mathrm{G}}$. If the Hamiltonian is Hermitian, the propagator is unitary

$$\hat{\mathrm{G}}^{\dagger}(t+\Delta t,t) = \hat{\mathrm{G}}^{-1}(t+\Delta t,t) \tag{3.102}$$

The second symmetry is connected with the non existence of time arrow in quantum mechanics. The time reversal symmetry.

$$\hat{\mathrm{G}}^{\dagger}(t,t+\Delta t) = \hat{\mathrm{G}}^{-1}(t+\Delta t,t) \tag{3.103}$$

This condition is valid for all cases present in this thesis, where no magnetic field are applied.

For the rest of the section, the discussion follows the lines of Castro et al. [Castro *et al.*, 2004], dividing the problem in two. First, the computational alternatives to approximate numerically the exponential of a time-independent operator. Second, the problem is concentrated in solutions for the quantum propagator of a time-dependent Hamiltonian. The propagators for the time-dependent Hamiltonian usually rely on the application of $\exp\hat{\mathrm{A}}(t)$ for several values of t.

For the numerical exponential of an operator $\hat{\mathrm{A}}$ the first approach could be the direct use of a Taylor expansion

$$e^{\hat{\mathrm{A}}} = \sum_{n=0}^{\infty}\frac{1}{n!}\hat{\mathrm{A}}^n. \tag{3.104}$$

The Taylor approach for evaluating the exponential for a given $\hat{\mathrm{A}}$ and a vector v consist in truncating Eq. 3.104 to a certain order k

$$e^{\hat{\mathrm{A}}}\mathbf{v} \approx \sum_{n=0}^{k} \frac{1}{n!}\hat{\mathrm{A}}^n\mathbf{v}. \tag{3.105}$$

The method requires k matrix-vector multiplications and $k-2$ matrix-matrix multiplications to compute the iteratively a series of matrices of the form $\{1, \hat{\mathrm{A}}, \hat{\mathrm{A}}^2, \cdots \hat{\mathrm{A}}^k\}$.

An alternative is Chebychev polynomials instead of using the standard base $\{1, \hat{\mathrm{A}}, \hat{\mathrm{A}}^2, \cdots \hat{\mathrm{A}}^k\}$. The Chebychev polynomials of first kind are defined by the recurrence relation

$$T_0(x) = 1 \tag{3.106}$$
$$T_1(x) = x \tag{3.107}$$
$$T_{n+1}(x) = 2xT_n(x) - T_{n-1}(x). \tag{3.108}$$

For $\hat{\mathrm{A}} = -i\hat{\mathrm{H}}\Delta t$ and a vector $\mathbf{v}$

$$e^{\hat{\mathrm{A}}}\mathbf{v} \approx \sum_{n=0}^{k}(2-\Delta_{n0})(-1)^n J_n(\Delta t)T_n(\hat{\mathrm{H}})\mathbf{v}, \tag{3.109}$$

where J_n are the Bessel functions. This method requires also k matrix-vector multiplications.

The next alternative consist in the use of a Krylov subspace expansion. The order-r Krylov subspace generated by $\hat{\mathrm{A}}$ and $\mathbf{v}$ is the linear subspace spanned by the images of $\mathbf{v}$ under the first r powers of $\hat{\mathrm{A}}$ (starting from $\hat{\mathrm{A}}^0 = I$), that is,

$$\mathcal{K}_r(\hat{\mathrm{A}}, \mathbf{v}) = \mathrm{span}\,\{\mathbf{v}, \hat{\mathrm{A}}\mathbf{v}, \hat{\mathrm{A}}^2\mathbf{v}, \ldots, \hat{\mathrm{A}}^{r-1}\mathbf{v}\} \tag{3.110}$$

Using a Lanczos method an orthonormal base can be constructed $\{v_i\}_{i=1}^r$. The basis is such that

$$\hat{\mathrm{A}}\hat{\mathrm{V}}_r = \hat{\mathrm{V}}_r\hat{\mathrm{H}}_r + h_{r+1,r}v_r e_r^T \tag{3.111}$$

where $\hat{\mathrm{V}}_r$ and $\hat{\mathrm{H}}_r$ are $r \times r$ matrices. e_r is the rth unit vector for $\mathbb{C}^r$

The exponential is approximated using the $\hat{\mathrm{H}}_r$

$$e^{\hat{\mathrm{A}}}\mathbf{v} \approx \hat{\mathrm{V}}_r \exp(\hat{\mathrm{H}}_r)e_1 \tag{3.112}$$

All the three methods presented, are accurate enough for a sufficiently small time-step. Castro and coworkers [Castro *et al.*, 2004], test those method for the propagation of s, p and d orbitals in equal number of atoms. Their results are not conclusive on which method performs better. For the purpose of this thesis, the Lanczos approach was used extensively.

Now, let us consider the problem of approximate the evolution operator $\hat{\mathrm{U}}(t+\Delta t, t)$. The biggest challenge is that most of the methods of approximation

require the knowledge of the wavefunction and the Hamiltonian in some points in the interval $(t, t + \Delta t)$. Several alternatives are considered: extrapolation, self-consistency. As will be presented in a next chapter, the self-consistency must be deactivated when velocity phase factors are applied.

For the propagators, Castro and coworkers present a series of methods: Implicit midpoint rule (Crank-Nicholson), explicit midpoint rule, propagators that enforce, exactly or approximately the time-reversal symmetry, methods based on the splitting of the Hamiltonian and the so-called Magnus expansions.

For the purpose of this thesis, the method used ubiquitously was a time-reversal symmetry based operator. This method is based on the observation that quantum mechanics has no time arrow (except when magnetism is included). So, propagating forward from t to $t + \Delta t$ should be the same as propagating backward from $t + \Delta t$ to t should produce the same result. This statement for a movement of $\Delta t/2$ produces the condition

$$\exp\left(i\frac{\Delta t}{2}\hat{\mathrm{H}}(t+\Delta t)\right)\psi(t+\Delta t) = \exp\left(-i\frac{\Delta t}{2}\hat{\mathrm{H}}(t)\right)\psi(t) \tag{3.113}$$

The expression for the propagator becomes

$$\hat{\mathrm{U}}(t+\Delta t, t) = \exp\left(-i\frac{\Delta t}{2}\hat{\mathrm{H}}(t+\Delta t)\right)\exp\left(-i\frac{\Delta t}{2}\hat{\mathrm{H}}(t)\right) \tag{3.114}$$

3.8 Conclusions

In this chapter, a wide number of methods, theories and techniques were presented, each of them trying to grasp a different level of the complexity involved in the solution of a quantum system of several interacting particles.

For the electronic structure, the method of choice was time-dependent density funtional theory. The reason for that choice comes from the need of an efficient theory capable to scale to a large number of electrons and still be able to describe reasonably well the electronic structure of the system. A method like Hartree-Fock lacks completely the correlation, and Post-HF methods, such as CI, becomes prohibitive when the number of electrons and atoms increase.

For the movement of nuclei, the kind of collisions that we are interested to model are such that the velocity of the nuclei is comparable to or higher than the average velocity of the valence electrons. Adiabatic approximations, such as Born-Oppenheimer are not able to describe the transition of charge from one atom to another during a collision. The method of choice in this level was Ehrenfest molecular dynamics, with the added advantage that the orthogonalization of the wavefunctions can be automatically included in the algorithm, one of the bottlenecks of the other methods.

As in collisions we require explicit evolution of the time-dependent Schrödinger equation, TDDFT was the method of choice, using adiabatic LDA as the exchange-correlation potential to start exploring the possibilities of the method in high energy collisions.

4 Atomic Charges and Charge-Exchange Ionization

4.1 Introduction

Compared to classical molecular dynamics, the use of TDDFT to explore dynamical processes such as collisions, offers the possibility to describe the evolution of the charge in the system. As a result of a collision, electrons can be transferred from one atom to another or being ejected out of the system. Atoms change their charge states and their interaction with other atoms also changes. This kind of behaviour is not well modelled at all in classical molecular dynamics because the potentials used for each atom usually remains unchanged during propagation.

In the specific case of TDDFT, a theory based on the electronic density, the density and the KS wavefunctions need to be represented in space. Three alternatives are commonly used to represent those entities: localized basis functions, spatial grids and in the particular case of periodic systems, plane waves. Each of these alternatives has its strengths and weaknesses, but the use of spatial grids is privileged to represent phenomena were electrons could eventually escape in open systems. That is done at the cost of using large grids that extend far beyond the location of the atoms in order to avoid reflections with the boundaries of the box; otherwise, absorbing boundary conditions could be also used to avoid the reflections. For absorbing boundaries, there are traditionally two approaches: To use negative imaginary potentials [Neuhasuer and Baer, 1989; Nakatsukasa and Yabana, 2001] or using a perfectly matched layer [Zheng, 2007]. The former was used with $\sin^2$ imaginary potential as the absorbing boundary always was needed.

An important element is to decide how to analyse the repartition of charge and how to associate a certain amount of charge to a particular atom. In order to quantify the charge transfer between atoms, it is necessary to have a way to count the amount of charge associated to each atom for a given distribution of charge. The main problem in such an association is that atomic charges are not observables from the point of view of quantum mechanics. They cannot be measured and theoretically they are deduced from physical observables using

a more or less arbitrary method. The method pretends to capture the idea of *ionicity* for a set of molecules or surfaces. During the last decades, several methods have appeared to model theoretically or experimentally the charge associated to atoms. Wiberg and Rablen [Wiberg and Rablen, 1993] computed the charge on atoms using seven different methods for a set of organic molecules. One year after, Meister and Schwarz [Meister and Schwarz, 1994] collected statistical data about 25 different methods to account for charges in atoms, both theoretical and experimental. The authors concluded that even if those models diverge in their values for different cases, they point to the same physical concept from a statistical point of view. A single principal component is responsible for most of the physics behind the different charge analysis.

In this chapter we will explore some of them, those that will be extensively used in the next chapters. Ideally the method to account for charges should have these properties:

(a) Should be simple and scale linearly with the number of atoms

(b) If the method relies on the wavefunctions, it should be independent of a basis, otherwise we should convert the real space mesh into a basis representation in order to get the associated charge. These kind of conversions are in general non trivial.

(c) Should not have arbitrary parameters

(d) It should be able to represent charges that are not attached to a particular atom during the evolution.

Let us consider several methods found in the literature and discuss them in light of the conditions mentioned above.

The problem of separating molecules in atoms is particularly important in chemistry where such knowledge allows to quantify, for example, the strength of a bond or how easy it is to remove charge from one particular atom in a molecule. We can separate the different methods in several categories: wavefunction-based, density-based and spatial-based methods. The oldest method to account for charges is probably the Mulliken population analysis [Mulliken, 1955c,d,a,b], based on wavefunctions. In the density-based methods we can distinguish the Bader analysis [Bader, 1990] and Hirshfeld analysis [Hirshfeld, 1977]. Those method rely strongly on the electronic density to split the charges between the different atoms. For one example of purely geometric methods, we can mention the Voronoi charge analysis [Guerra *et al.*, 2004].

In scattering processes, we can use the fact that projectile and target start and end separated in space. This fact induces us to consider also schemes that rely preferentially on some sort of easy spatial separation and account for the charges using that. For example we can split the space in fixed spheres around each atom and integrate the charge inside. We can also split the charge using slices perpendicular to the direction of propagation and use them also to account for the charge.

The main advantage of those methods is that they allow to represent charges that are not attached to a particular atom during the evolution. The spatial

separation is probably the simplest way to quantify dynamically the amount of charge of a distribution of atoms, but there is great arbitrariness on the shape of the containers: slices, boxes, spheres and their sizes. Another issue is when the atoms get closer to each other: those boxes will overlap and the total charge is not longer the sum of the different boxes plus its complement. That is not particularly important in scattering processes because what is measured usually is the asymptotic state of the system.

On the other side of the spectrum, methods such as Bader analysis or Hirshfeld analysis offers a far more elaborate way to account for the charge associated to an atom. However, those methods were designed for static charge configurations and are not able to represent charges being ejected out of the system.

4.2 Atomic Charges

4.2.1 Mulliken

The Mulliken charge analysis [Mulliken, 1955c,d,a,b] is probably the oldest of all methods to separate the charge in atoms. The method is based on wavefunctions and in particular expanded in atom centered basis functions of the atoms constituting the system. For this reason, it is not very well suitable for densities expressed in a mesh. We describe it here to have a full description of methods developed in the last century but this method will not be used for this thesis.

Consider a molecule whose many-body molecular wavefunction could be separated in molecular orbitals $\psi_i(\vec{r})$. Those molecular orbitals can be expanded in a basis of wavefunctions centered on the atoms of the molecule

$$\psi_i(\vec{r}) = \sum_{\tau}^{M} \sum_{\nu \in \tau} c_\nu \phi_\nu(\vec{r}), \tag{4.1}$$

where the sum over τ runs over the M atoms of the molecule, and the parameter ν runs over the dimension of the basis where ψ_i is expanded and the orbitals are centered on atom τ.

The total number of electrons could be expressed as:

$$\begin{aligned} N &= \sum_{i}^{\text{occ}} n_i \int d\mathbf{r} |\psi_i(\mathbf{r})|^2 && (4.2)\\ &= \sum_{\tau,\varsigma} \sum_{\nu \in \tau, \mu \in \varsigma} \sum_{i}^{\text{occ}} n_i c_{\nu i} c_{\mu i} \int d\mathbf{r} \phi_\mu(\mathbf{r}) \phi_\nu(\mathbf{r}) && (4.3)\\ &= \sum_{\tau,\varsigma} \sum_{\nu \in \tau, \mu \in \varsigma} \mathbf{D}_{\mu,\nu} S_{\mu,\nu} && (4.4) \end{aligned}$$

where D is the density matrix $\mathbf{D}_{\mu,\nu} = \sum_i^{\text{occ}} n_i \, c_{\nu i} \, c_{\mu i}$ and S is the overlap $S_{\mu,\nu} = \langle \phi_\mu | \, \phi_\nu \rangle$

The diagonal elements $D_{\mu,\mu}S_{\mu,\mu}$ are the fractions of the charge that belongs purely to one of the atom centered basis functions, and correspondingly the charge belongs to the atom μ. The non diagonal elements are symmetrically split between the atoms ν and μ. The Mulliken charge associated to the atom τ in the orbital ν:

$$Q_\nu = D_{\nu,\nu}S_{\nu,\nu} + \frac{1}{2}\sum_{\mu\neq\nu}(D_{\nu,\mu}S_{\nu,\mu} + D_{\mu,\nu}S_{\mu,\nu}) \tag{4.5}$$

The total Mulliken charge for one particular atom results of the addition of all the contributions from the orbitals centered on the atom.

As was mentioned before, this scheme is not well adapted for densities and wavefunctions expressed in spatial grids, because it implies to project the grid in atom-centered basis with computational overhead. The use of Mulliken charges has been questioned because the values not always converge with the size of the atom-centered basis. Even more, Mulliken charges for static electronic structures produce values of charge that are not correlated with the degree of ionicity of specific atoms in molecules and the utility in periodic systems is also limited.

4.2.2 Bader Analysis

Richard Bader [Bader, 1990] created a natural way to separate a molecule in regions using its electronic density. Consider for example a bi-atomic molecule; normally, in some place between the two atoms the density will reach a minimum and that is the natural place to split the charge in the system. Even more, there is an entire plane, such that for points out of that plane, if the gradient is followed, the path will end on one of the two atoms and no path will cross the plane. That is called a "zero-flux" surface. For more complex molecules or crystals the same idea is followed: discover the surface were the density is a minimum perpendicular to the surface. Those surfaces split the entire space in volumes and the charges can be computed using those volumes.

For an electronic density $\rho(\mathbf{r})$, a zero-flux surface can be expressed as the set of points in $\mathbb{R}^3$ such as:

$$\nabla\rho(\mathbf{r_s}) \cdot \hat{n}(\mathbf{r_s}) = 0 \tag{4.6}$$

where $\hat{n}(\mathbf{r})$ is an unitary vector perpendicular to the surface $S(\mathbf{r})$ such that $r_s \in S(\mathbf{r})$.

The procedure to construct the "zero-flux" surfaces starts by identifying the critical points in the mesh. Critical points $\mathbf{r}_c$ are characterized by the zero value of the gradient in those points:

$$\nabla\rho(\mathbf{r}_c) = \frac{\partial\rho(\mathbf{r}_c)}{\partial x}\hat{u}_x + \frac{\partial\rho(\mathbf{r}_c)}{\partial y}\hat{u}_y + \frac{\partial\rho(\mathbf{r}_c)}{\partial z}\hat{u}_z = 0. \tag{4.7}$$

Those critical points could be maxima, minima, or saddle node points. Typically, the position of nuclei would be at a maximum, but also critical points could be in places where no nuclei is present, in the center of a bond

for example. To further characterize those critical points an extra derivative is necessary, the Hessian matrix

$$A(\mathbf{r}_c) = \left(\begin{array}{ccc} \frac{\partial^2\rho(\mathbf{r})}{\partial x^2} & \frac{\partial^2\rho(\mathbf{r})}{\partial x\partial y} & \frac{\partial^2\rho(\mathbf{r})}{\partial x\partial z} \\ \frac{\partial^2\rho(\mathbf{r})}{\partial y\partial x} & \frac{\partial^2\rho(\mathbf{r})}{\partial y^2} & \frac{\partial^2\rho(\mathbf{r})}{\partial y\partial z} \\ \frac{\partial^2\rho(\mathbf{r})}{\partial z\partial x} & \frac{\partial^2\rho(\mathbf{r})}{\partial z\partial y} & \frac{\partial^2\rho(\mathbf{r})}{\partial z^2} \end{array} \right)_{r=r_c} . \tag{4.8}$$

This matrix, being real and symmetric, can be diagonalized

$$\Lambda(\mathbf{r}_c) = \left(\begin{array}{ccc} \frac{\partial^2\rho(\mathbf{r})}{\partial x'^2} & 0 & 0 \\ 0 & \frac{\partial^2\rho(\mathbf{r})}{\partial y'^2} & 0 \\ 0 & 0 & \frac{\partial^2\rho(\mathbf{r})}{\partial z'^2} \end{array} \right)_{r=r_c} , \tag{4.9}$$

with its values characterizing the curvature of ρ in the critical point $\mathbf{r}_c$.

The critical points that are maxima can be reached by following the gradient of the density. The basin of each nuclei, ie. the set of points that goes to that nuclei following the gradient, constitutes the Bader volume. The boundary of those Bader volumes is the Bader surface, and has the property that no path of gradient crosses the surface. That is the reason why they are called "zero-flux" surfaces. Those surfaces naturally limit the volumes of each atom.

Typical implementations will search for critical points. They will interpolate the mesh and look for the Bader surface accurately. When the surfaces are determined, numerical volume integration is performed to get the Bader charges. That algorithm is particularly expensive, mainly because it involves many interpolations in the grid and solving non-linear equations.

More recently, Henkelman and co-workers [Henkelman *et al.*, 2006; Sanville *et al.*, 2007; Tang *et al.*, 2009] developed an algorithm that implements Bader's idea for the electronic density in a grid. The algorithm avoids to determine explicitly the Bader surfaces, instead of that, it searches for the basin of each atom following a steepest ascent path. It follows the gradient of the density jumping from a grid point to another grid point until it reaches the maximum. Commonly the maximum will be the closest grid point to the position of one nuclei. Identifying the grid point that goes to each nucleus, the grid points could be grouped in sets of basin grid points. The Bader charges are found by adding the density contributions of each grid point and interpolating in the boundaries of the different basins

4.2.3 Hirshfeld Analysis

Another way to account for charges is the Hirshfeld charge analysis [Hirshfeld, 1977]. The Hirshfeld analysis uses previously computed radial density distributions. That information is used to split the charge in a given point of space using weights, determined from the sum of the overlapping (original) atomic densities for all the atoms in the system. The figure 4.1 shows the values of charge for the lightest elements in the periodic table. These all-electron density data have been generated using the FHI98PP code [Fuchs and Scheffler, 1999],

in the LDA (PW92 XC functional). The data could be found in the website of the ABINIT software package (http://www.abinit.org).

Consider a differential volume dv located in the position of space $\mathbf{r}$. The radial density of an atom $h_i(r)$ is a function of the radius and the atomic species i. The density $n_\tau(\mathbf{r})$ that belongs to the atom τ in the position $\mathbf{r}$ with a local density of $n(\mathbf{r})$ is:

$$n_\tau(\mathbf{r}) = n(\mathbf{r}) \frac{h_\tau(|\mathbf{r} - \mathbf{r}_\tau|)}{\sum_\mu h_\mu(|\mathbf{r} - \mathbf{r}_\mu|)}. \tag{4.10}$$

The total charge associated to the atom τ results in the integration of $n_\tau(\mathbf{r})$ in all the space,

$$Q_\tau = \int n_\tau(\mathbf{r}) d^3\mathbf{r}. \tag{4.11}$$

The Hirshfeld charges offers an intuitive way to account for charges yielding meaningful charges when comparing the degree of ionicity of bonds. Hirshfeld charge analysis was created to account for static charges. In process such as collisions, electrons could be ejected out of the molecule. Those charges will always been associated to the atoms in the system. The use of Hirshfeld charge analysis should be, for the purpose of this thesis, complemented with other schemes to be able to identify the amount of ejected charges.

4.2.4 Voronoi Charge Analysis

The Voronoi charge analysis (VCA) [Guerra *et al.*, 2004] method offers a simple geometric partition of charges based on a natural partition of space. The origin of the Voronoi method comes from the so-called Voronoi tessellation. The position of the nuclei plays the role that in mathematics are the seeds for the Voronoi diagram. The volume R_τ that belongs to an atom τ is the set of points in space that are closer to the atom τ than any other atom $\varsigma \neq \tau$.

$$R_\tau = \{\mathbf{r} \in \mathbb{R}^3 \mid |\mathbf{r} - \mathbf{r}_\tau| \leq |\mathbf{r} - \mathbf{r}_\varsigma| \text{ for all } \varsigma \neq \tau\}. \tag{4.12}$$

As an example the figure 4.2.4 shows a slice of the Voronoi tesselation for a molecule of Anthracene.

The charge that belongs to the atom τ is naturally the density integrated in the volume R_τ. This method, as well as the Hirshfeld will always integrate to the total charge in the system.

4.2.5 Spatial Charge Analysis

The traditional methods used to account for charges in general are unable to describe charges that escape from the system. In scattering processes, the analysis is focused in the asymptotic states of the system. In those cases, it is natural to encapsulate the projectile and target in volumes. However, the shape and size of those volumes remains arbitrary and could only be justified by comparison with the other methods.

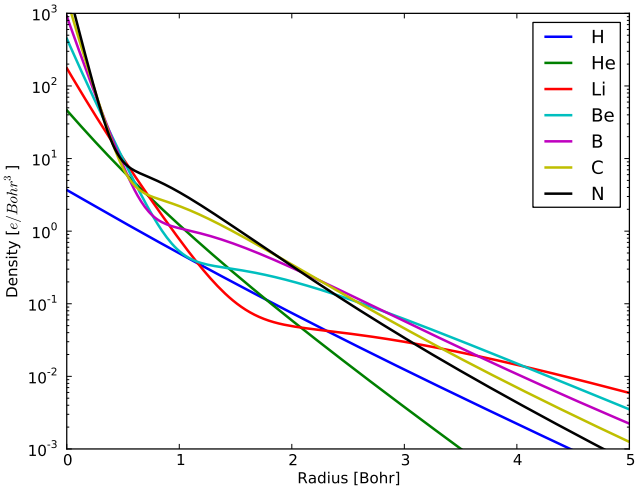

Figure 4.1: Radial averaged distribution of charge for the lightest elements in the periodic table.

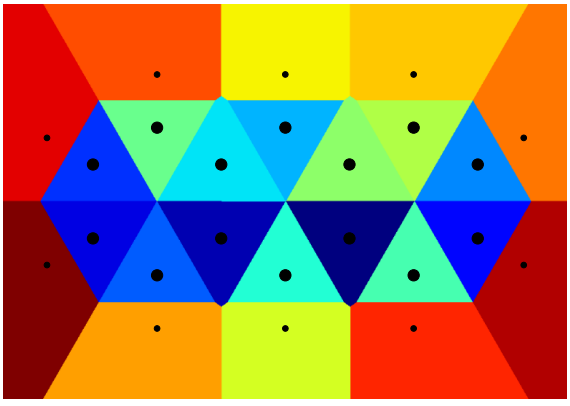

Figure 4.2: Voronoi tesselation for a molecule of anthracene ($C_{10}H_{14}$). Slice in the plane of the molecule. Medium black dots represent the location of carbon nuclei and small black dots are the positions of Hydrogen nuclei. As the molecule is flat, the Voronoi volumes are found by simply projecting the Voronoi tessellations perpendicular to the plane of the molecule.

Storing the density for a full time-dependent trajectory, requires an important amount of disk space. Instead of storing the entire density, integrated quantities consume less space, are easier to write in disk and allow us to analyze the charges using spatial separation analysis. Two integrated quantities were implemented: integrating in planes perpendicular to the direction of propagation, and radial integration on spheres centered on each of the nuclei in the system.

Both schemes are useful to encapsulate charges close to the atoms. This scheme will be used in the next chapter for a proton - He collision.

4.3 Conclusions

In this chapter, we have presented several methods to analyze charge repartition on a finite system. Hirshfeld, Bader and Voronoi are traditional methods used in the literature for splitting the charge in atoms. However, those methods integrate the charges in the whole space and they are unable to describe electrons escaping from their original host atoms. Also the necessity of a simplified scheme is imposed for the cases of many-electron systems. The solution was to account for charges using geometrical volumes like slabs and spheres. Those schemes will be extensively used all along the next chapters.

5 First Applications

Quando você quer alguma coisa, todo o Universo conspira para que você realize seu desejo

O Alquimista
Paulo Coelho

5.1 Introduction

In this chapter are present the first applications of fast atomic collisions using time-dependent density functional theory (TDDFT). For the first case, one H^+ atom impacts a neutral helium atom. The system is simple enough and an experimental results from several sources are available. For the second case, a more challenging problem was addressed, the collision of an atom of gold with a molecule of Butane. Those two problems show the possibilities for computing charge transfer processes with reasonable accuracy. They also raise some of the challenges that induce the creation of new tools. Those tools, in particular, the velocity phase factor are not used here and will be the purpose of the next chapter. This first applications of TDDFT in fast collisions were published [Avendaño-Franco *et al.*, 2012].

5.2 Proton Impacting Helium

Our first case corresponds to the simulation of a collision between a proton and a Helium atom. This is a well-studied problem in atomic physics [Keim *et al.*, 2005; Rudd *et al.*, 1985; Belkić, 1978; Belkić *et al.*, 1979; Mergel *et al.*, 1997; Hasan *et al.*, 2006], for which a wealth of experimental data as well as results from higher levels of theory are available.

For the simulation, a rectangular parallelepiped of 16.94 Å along the direction of impact, and 10.58 Å in the transversal directions is used. The simulation

box is defined by its extremes:
$(-8.47, -5.29, -5.29)$ and $(8.47, 5.29, 5.29)$. Proton kinetic energies were explored between 16 keV and 1.2 MeV. The spacing between points in the mesh is 0.1 Bohr (that is, 0.0529 Å). The total number of points in the mesh is $321 \times 201 \times 201 = 12,968,721$ grid-points plus some extra points outside of the boundary to properly compute spatial derivatives.

The Helium atom originally located along the major central axis of the parallelepiped is impacted by a proton that starts in one of the faces of the box with a certain kinetic energy and impact parameter. The starting coordinates for the He target is $(-4.2, 0, 0)$, and for the proton projectile is $(-8.47, b, 0)$, where b is the impact parameter (the perpendicular distance between the path of a projectile and the center of the target).

In scattering processes usually only the final product of the collision is considered. First principles methods also allow to understand the dynamics during the collision. With the aim to gain understanding of computational as well as physical aspects, we monitor the dynamics of the electronic structure during the entire evolution. However, the amount of data accumulated per time step is quite large, and thus must be handled with care. To fix the idea, the storage of electronic density for 12968721 grid points will require a binary file of about 96 MB. Supposing a total of 25000 time steps, storing the data each hundred steps will require 24 GB. Instead of storing such amount of data for post-processing purposes only, we decided to introduce small modifications to the Octopus source code to extract the relevant data in a less detailed way during the execution, focusing on selected integrated quantities, described later. Those modifications are only affecting the output of the density : the physics and algorithms implemented in Octopus were not changed.

As the kinetic energy of the proton spans several orders of magnitude, the time step needs to be properly adjusted for each value of kinetic energy. However, for low kinetic energies, the time step is fixed by electrons. The optimal value was computed for the most energetic proton in such a way that the total energy of the system be constant under a tolerance of 0.03 eV. The larger deviations for the total energy occurs when the proton reaches the closest distance with the He nucleus. After the time step was scaled proportionally for the different energies in such a way that the same number of time steps are needed to move the proton the entire length of the simulation box. The number of time steps required to move the proton from one side of the box to the opposite one is around 30000. The simulation is stopped at 25000 time steps when the proton is sufficiently far from the He nucleus and around 3 Å far from the end of the simulation box. At this point the electronic capture is complete.

As the proton follows its path, coming close to the Helium atom, the electronic structure of the latter is perturbed. Depending on the initial kinetic energy of the projectile and its impact parameter, some charge is ejected out of the Helium atom region, and either becomes attached to the proton projectile, or is ejected in all directions of space, including backwards the direction of impact.

In the TDDFT formalism for a two-electron spin-saturated system such as the Helium atom, only one Kohn-Sham orbital is explicitly treated. Contrary

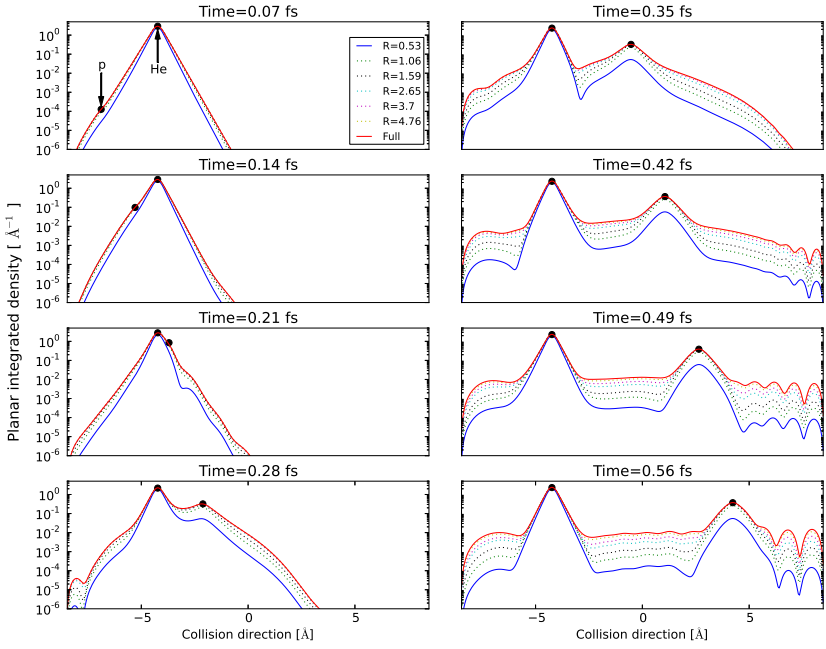

Figure 5.1: Snapshots of the integrated planar charge density during a typical proton - Helium collision. The impact parameter is 0.74 Å, the initial kinetic energy of the proton is 26.8 keV. The direction of propagation is x. The different lines show the density integrated inside a disc of radius R (in Å) in the $y-z$ plane (or inside the full box) centered on a line that passes through the Helium atom at rest. Small black dots are used to show the locations of the nuclei in the direction x (see text).

to wavefunction-based methods, the knowledge of the final state of the system does not allow a unambiguous interpretation of the final result in term of probabilities of one- and two- electron transfer. However, the one-electron transfer probability is much larger than the two-electron transfer probability, and in the present context, we will assume that the charge density outside the Helium region, is a direct image of the one-electron transfer process. This is consistent with the results obtained in Refs. [Wang *et al.*, 2011, 2012]

Fig. 5.1 presents several snapshots of the time evolution of the electronic density inside the simulation box, for a typical collision. For the purpose of visualisation, the electronic density is integrated in planes perpendicular to the direction of propagation, inside discs of different radii in the $y - z$ plane. One notices that before the collision, the lines for radii larger or equal to $R = 1.59$ Å are undistinguishable from the line obtained in the whole plane, while the spread between different radii increases steadily after the collision, meaning that the electronic charge that is localized within 1.59 Å before the collision, is scattered and occupies the whole simulation box after the collision, as expected.

To measure the amount of charge being transferred to the proton, we integrate the charge around the two nuclei after the scattering and when they are sufficiently separated to measure a stable number of electrons to each of them. In this simulation, the proton carries at the end about 0.4 electrons in a sphere of 1 Å of radius.

In order to examine the stability of the quantitative estimation of the charge transfer, Fig. 5.2 presents the evolution of the integrated charge in slices of 2 Å, centered on each atom. For completeness, we also present in this graph, the integral of the charge density in the region of space with x lower than -1 (called "Back-scattering slice"), and with x larger than +1 (called "Forward-scattering slice").

At the beginning of the simulation, using a slice of 2 Å for the Helium atom, a charge 1.967 electrons is inside the "Helium slice", the charge that spills out of the slice represent the tail of the charge density, split in 0.018 electrons for the "Back-scattering slice" and 0.015 electrons for the "Forward-scattering slice". It means that more than 98% of the charge is initially contained inside the "Helium slice". As the proton gets closer to the Helium, part of the charge associated to the He is also associated to the proton, as the two slices overlap. Finally, when the proton leaves the region of interaction, some charge follows the proton, reducing the charge associated the Helium atom.

The charges associated to proton and He stabilizes around a well-defined value. While the back-scattered charge is quite small, the difference between forward-scattered charge and the charge centered on the proton, after the collision, is non negligible, and calls for further analysis, especially with respect to its angular dependence. Such analysis could be possible, for example by calculating the photoelectron spectrum [Pohl *et al.*, 2000; De Giovannini *et al.*, 2012]. Artefacts due to the reflecting nature of the simulation box must also be analysed. At the end of the time simulation corresponding to Fig. 5.2, the charge present in the "Back-scattering slice" is 0.023, the charge present in the "Helium slice" is 1.504, the charge present in the "Forward-scattering slice" is 0.473, while the charge present in the "Proton slice" is 0.367.

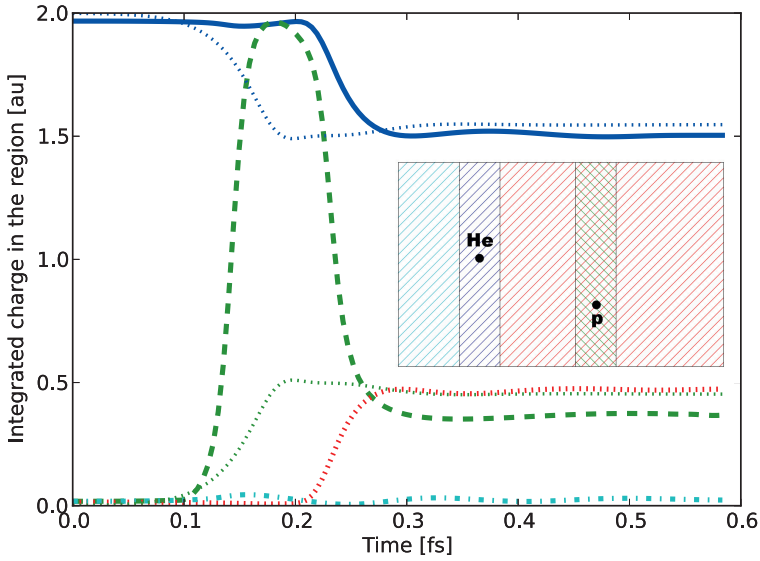

Figure 5.2: Amount of charge present in different regions of space during the proton-He collision. Both atoms are allow to move and the simulation is done in a reference where the He atom is initially at rest. The initial kinetic energy and impact parameter are the same than the ones used in Fig. 5.1. Full line (blue) : integrated charge in a slice with x between -5.2 and -3.2, that is, between -1 and $+1$ Å with respect to the Helium atom, defining the "Helium slice". Dotted line (red) : integrated charge with x higher than -3.2, that is, in the "Forward-scattering slice". Dash-dotted line (light blue) : integrated charge with x lower than -3.2, that is, in the "Back-scattering slice". Dashed line (green) : integrated charge in a moving slice, with the difference in x with respect to the proton being between -1 and $+1$, that is, in the "Proton slice". Note that this slice overlaps first with the "Back-scattering slice", then with the "Helium slice", then with the "Forward-scattering slice". Small dotted line (blue), upper : Hirshfeld charge for the Helium nucleus. Small dotted line (green), lower : Hirshfeld charge for the proton.

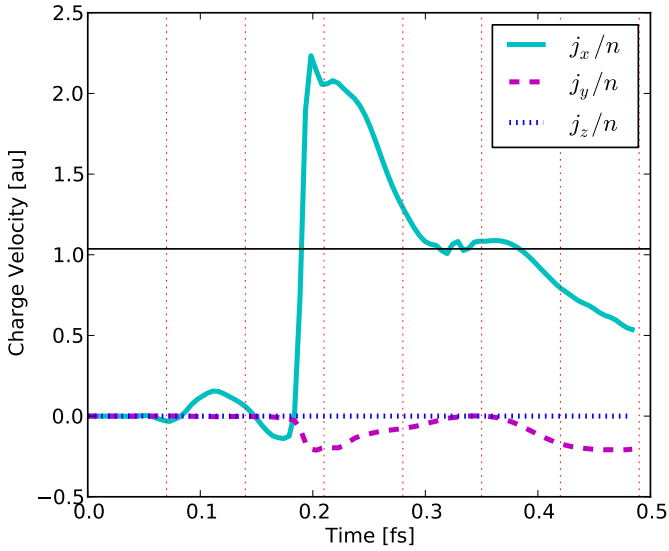

Figure 5.3: Components of the planar average charge velocity (j/n) as a function of time, for the plane $x = -0.5$ Å. The physical conditions shown here are the same as Fig. 5.2; the vertical dashed red lines indicate the times of the snapshots of Fig. 5.1. The velocity of the proton is also shown with a horizontal line.

Fig. 5.2 also presented the Hirshfeld partitioning [Hirshfeld, 1977] of the total charge, as a function of time. The Hirshfeld partitioning attributes the charge at each point in space either to the Helium or to the proton, according to a weight that is proportional to the radial densities of the neutral (ground-state) Helium or Hydrogen atoms. The implementation of this partitioning is rather easy. Although it completely neglects the possibility that a fraction of electronic charge density might not be attributed to one of both atoms, it constitutes a useful characterisation tool, that can be transposed easily to more complex situations, as described in the next section [Meister and Schwarz, 1994]. For the present proton-Helium case, after the collision, the Hydrogen Hirshfeld charge is 0.453, and the Helium Hirshfeld charge is 1.547. The Helium Hirshfeld charge is slightly higher than the charge in the "Helium slice". It seems to gather most of the charge excluded from the "Back-scattering slice". Analogously, the proton Hirshfeld charge is larger than the "proton slice charge", and smaller than the charge in the "Forward-scattering slice". In both cases, they stabilize after the collision, and can be used to perform an analysis of the transfer of charge.

As seen on Fig. 5.2, the amount of charge being transferred becomes stable for a given value of initial kinetic energy and impact parameter. The understanding of the long-term evolution of the charge clearly identified to be in the

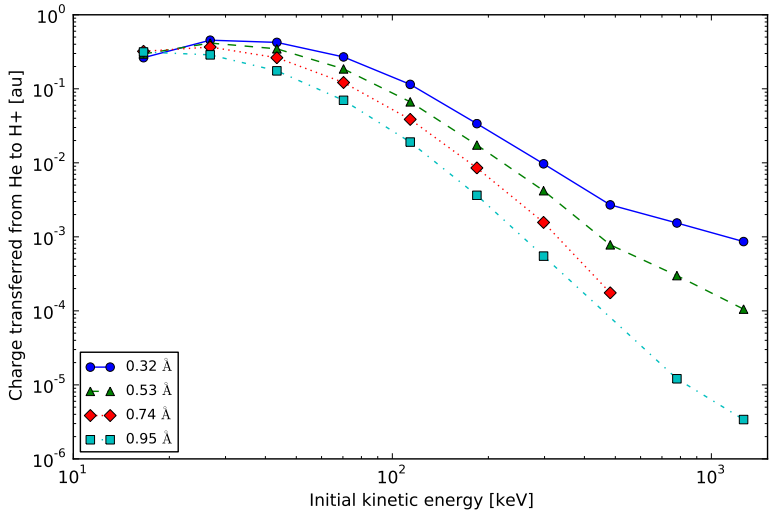

Figure 5.4: Electronic charge capture for the proton-Helium collision, as function of the initial kinetic energies for several different impact parameters. The charge depicted is the charge from the proton slice when the transfer is completed.

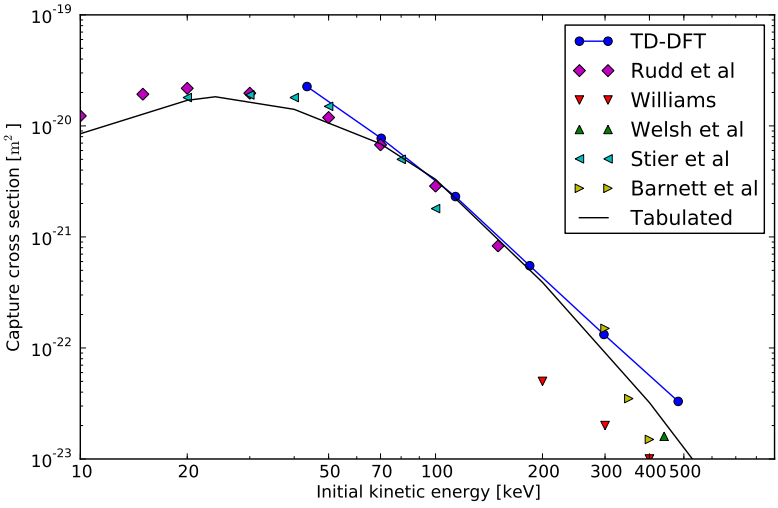

Figure 5.5: Electronic capture cross section by proton in Helium. Experimental results [Rudd *et al.*, 1983] [Stier and Barnett, 1956] [Barnett and Reynolds, 1958] [Williams, 1967] [Welsh *et al.*, 1967] are shown for comparison.

He and H regions seems rather obvious, unlike the charge in other regions.

In Fig. 5.3, we examine one aspect of the behavior of the charge that remains between the two nuclei. In this respect, we define the planar average velocity as the integral of the local current divided by the local density in the plane perpendicular to the x direction. This figure shows the planar average velocity during the proton-He collision for a reference plane in the scattering region at $x = -0.5$ Å. As the proton approaches the He atom ($t < 0.20$ fs), the charge oscillates at the reference plane, inducing oscillations in the charge velocity. Immediately after the proton-He atom collision ($x = -4.2$ Å, $t = 0.21$ fs) some charge crosses the reference plane, causing a sudden jump in the charge velocity shown in Fig. 5.3. When the proton crosses the reference plane, (t=0.35 fs) the charge crosses the plane with the same velocity as the proton, as is evident in the plateau found around 0.35 fs. After the crossing of the proton the velocity of the charge in the plane decreases exponentially. Also some charge goes back to the Helium atom, visible as a negative value in the current along y. The quantification of the amount of charge going in the different channels (including e.g. electron scattering) has not been attempted.

Fig. 5.4 gathers the electronic charge transfer values, after collision, as a function of the initial kinetic energy of the projectile, for several values of the impact parameter. Assuming an exponential behaviour of the electronic capture as a function of the impact parameter the capture cross section based on the proton slice integrated charge density, can be computed as a function of the initial kinetic energy of the projectile. The corresponding data are presented in Fig. 5.5 There is a good agreement with the experimental data [Rudd *et al.*, 1983; Stier and Barnett, 1956; Barnett and Reynolds, 1958; Williams, 1967; Welsh *et al.*, 1967] in the energy range below 150 keV.

One can wonder why the agreement is quite good, although it is well-known that TDDFT usually overestimates charge transfer. [Jamorski *et al.*, 2002; Dreuw and Head-Gordon, 2004] However, during collisions, the electronic transfer occurs close to the nuclei, where the electronic density is high. The contribution to the capture cross section is dominated by collisions with small impact parameter. The known problem, actually related to the presence of region of spaces weakly populated (exponential decay of the wavefunction) seems not to be encountered here. Even the lack of a non-local exchange [Dreuw *et al.*, 2003] does not affect the capture cross section. We performed some additional calculations, with the self-interaction correction present in Octopus. We observed that differences in the final outcome of the simulation are negligible.

5.3 Gold-Butane Collision

The collision of an atom of gold and a molecule of butane includes some extra challenges compared with the previous case. Instead of 2 electrons, now we have a total of 113 electrons. By using pseudopotentials, the number of electrons treated explicitly can be reduced to 37. The gold atom being spin-polarized, we have to treat independently each spin channel. The total number of Kohn-Sham spin-orbitals to be handled is thus 37.

As the butane molecule and the gold atom are bigger than the entities of

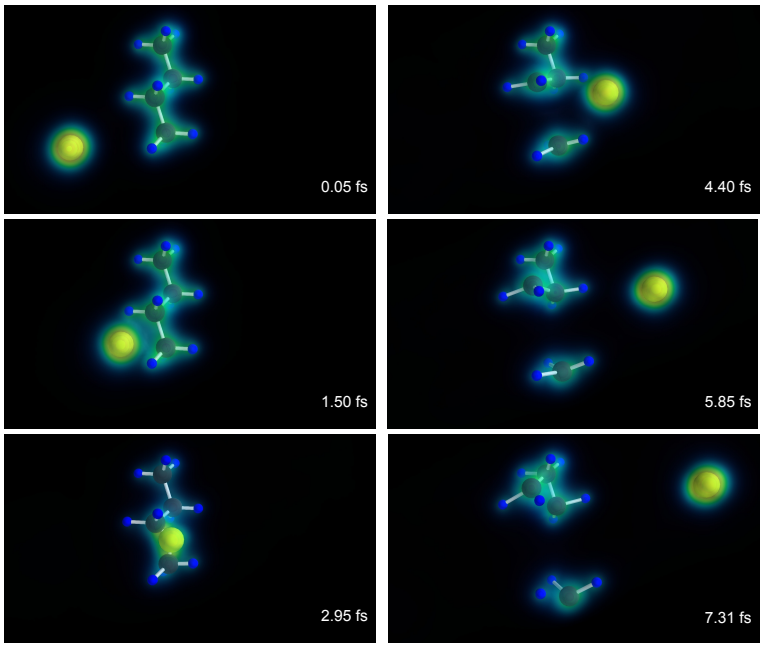

Figure 5.6: Snapshots of the collision of a gold atom with a butane molecule. The initial kinetic energy of the projectile is 23.9 keV.

the previous case, the simulation box needs also to be bigger: the box is 22 Å along the direction of collision and 10.5 Å in the transversal directions. As the projectile (Au) now contains electrons, its initial position must be inside of the box.

In the proton-Helium case the mass ratio between projectile and target was 1:4. With Au as projectile, the proportion is inverted to about 3:1. The simulation presented in Fig. 5.6 shows an atom of gold, with initial kinetic energy of 23.9 keV, impacting the bond region between two carbon atoms of the butane molecule. We observe that the gold atom breaks the molecule precisely on that bond, and continues its path without major deflection. Two fragments are formed from the former butane : one CH_3 ion (lower part of each sub-figure) and one C_3H_7 ion (upper part of each sub-figure). However, the latter can be seen to decompose in a CH_2 entity (moving upwards), and a C_2H_5 entity (nearly static).

This work is intended to simulate the kind of processes occurring in secondary ion mass spectrometry (SIMS). From a SIMS perspective, the fragmentations present in our simulations should be similar to those occurring in organic polymers due to secondary collision of the atoms from a gold deposit surface as is the case in Metal-assisted SIMS (MetA-SIMS). They should have an important role in the ionization of those organic fragments, allowing them to be identified when sputtered.

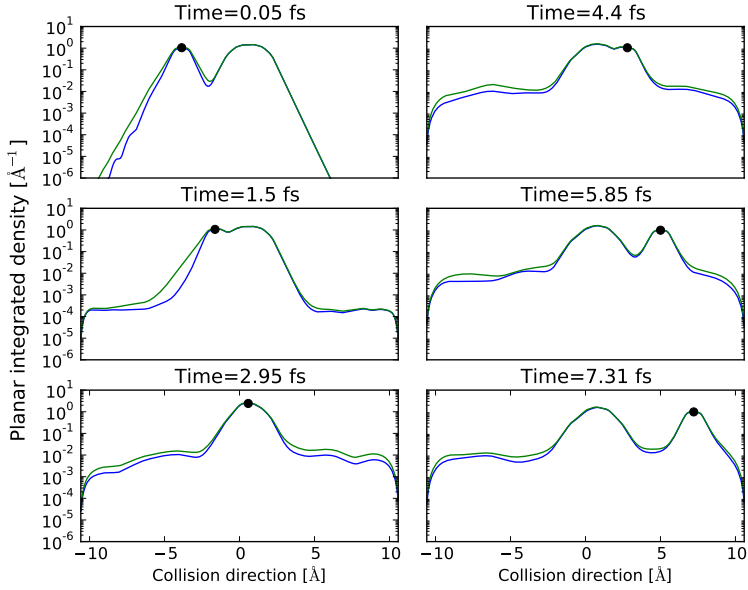

Figure 5.7: Planar integrated charge density, during the simulation of an atom of gold in collision with a butane molecule, corresponding to the six snapshots of Fig. 5.6. Each spin channel (up and down) is plotted with different colors (blue and green).

Following the same methodology than the one used to understand the case of proton and He collision, the planar integrated density was computed along the direction of impact. It is represented in Fig. 5.7. As for the proton-Helium collision, such charge density representation allows to visualize the dynamic evolution of the electronic clouds. The two clouds, initially well separated, merge, and then separate, while a small component is present outside of the two major regions.

For kinetic energies as high as in the case presented, and with similarly large impact parameter, the fragments of the butane molecule acquire a relatively small velocity, making easier to partition the charge. We also tested lower kinetic energy cases. However, for some of these, the fragments have a velocity close the one of the projectile. Measures of charge based on a one-dimensional integrated partition of the space are not as effective. The partition of space must be three-dimensional (as was done with cylinder for the proton-Helium collision) to provide usable results.

In Fig. 5.8, the Hirshfeld analysis is carried out for each spin component. It shows a well-defined realocation of the spins charges for the gold atom. As the total amount of charge for each component remains constant, it means that the spin rearrangement is done at the expense of the spin components of the carbon and hydrogen atom. While the charge and spin on the gold atom quickly stabilizes after the collision, on each fragment, the time-dependent Hirshfeld

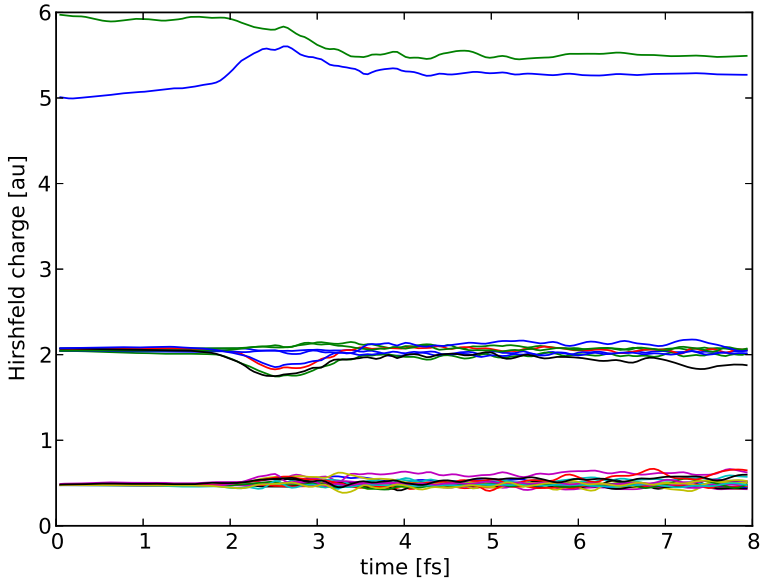

Figure 5.8: Evolution of the Hirshfeld charges, during the simulation of the collision between an atom of gold and a butane molecule, with the same parameters as in Fig. 5.6. Each spin contribution is displayed independently for each atom. The upper curves are for the spin up and spin down Hirshfeld charges on the gold atom. The Carbon Hirshfeld charges start at a value of about two (for both spin up and spin down, making four valence electrons for each carbon atom as expected), and the Hydrogen Hirshfeld charges start at a value of about one half (for both spin up and spin down, making one valence electrons for each hydrogen atom as expected)

analysis shows some fluctuation between atoms, which is expected (even if confined in a fragment, the electrons continue to oscillate, due to the Ehrenfest dynamics). For a well-separated fragment, like the CH_3 going downwards on Fig. 5.6, the stabilization is expected to be faster than for each atom separately.

The Hirshfeld analysis shows that the gold atom loses a charge of 0.477 electrons in the spin up channel, and gains a charge of 0.280 electrons in the spin down channel, with a global loss of 0.197 electrons. The CH_3 fragment charge change (U,D) is $(+0.297, -0.135)$, for a global gain of 0.162 electrons, the CH_2 fragment charge change (U,D) is $(+0.134, -0.039)$, for a global gain of 0.095 electrons, the C_2H_5 fragment charge change (U,D) is $(+0.047, -0.106)$, for a global loss of 0.059 electrons.

5.4 Conclusions

Those two examples shows the feasibility of computing charge transfer processes in atomic and molecular collisions. They also raise some of the limitations. In the case of the collision of proton with Helium, it was assumed that most of the contribution for charge transfer comes from single electron processes. This could be reasonably justified in this case, but the justification will be weaker in the case of more highly ionized projectiles or target. In those cases, several charge states are possible in the final state and a simple measure based on the density will be not enough. It is important to clarify that the fractional charges in the final configuration must be interpreted in a probabilistic sense. In a experimental measure, a define charge state will be obtained.

Also for this case, the use of a proton as projectile avoids the use of a velocity phase factor. For projectiles with electronic states described explicitly, the use of a velocity phase is mandatory for the range of kinetic energies presented. That will be the topic of the next chapter.

For the collision of gold with butane, the use of a phase becomes more relevant. In this case, a small dipole moment in the direction of propagation appears. The balance here is established between the high kinetic energy of 23 keV and the also heavy mass of the projectile, Au. As a result, an effective velocity of $0.07au$ is low enough to avoid charge loss when the velocity phase is missing. This problem also shows how for molecules the configuration space increases significantly , even if the target is rather symmetric. Those elements were instrumental in the selection of the problem for a next chapter, where a collision of $Li^+$with a C_{60} molecule is considered.

6

Initial Conditions and the Velocity Phase Factor

A TI, donaire alado, forma en vuelo,
Raudo volumen que la luz reanima
y en el movible espacio determina
la paralela sombra de su anhelo.

A ti, persecución, múltiplo en celo,
círculo en fuga, aljaba y jabalina;
rebelión de lo extático y divina
dinámica arcangélica del cielo.

A ti, soplo contrario a lo imposible,
perpetua agilidad, tallo flexible,
sangre en tensión, feliz musculatura.

La vida de la vida es promoverte.
Tu victoria, la muerte de la muerte.
A ti, libertador de la Pintura.

Al movimiento
Rafael Alberti

6.1 Introduction

As was shown in chapter 3, TDDFT is a pure density functional method only if the system starts from the ground state. Otherwise, the Hamiltonian is also a functional of the initial full many-body wavefunction and the initial Kohn-Sham states. In practical cases, TDDFT operates as a pure density functional theory. The ground state is computed as the initial state of the system. The evolution is applied on the Kohn-Sham set of orbitals starting from that initial condition. In the case of dynamical processes such as collisions, it is also natural to assume that the particles that will interact start from their ground state. The target, usually at rest, is assumed to be in the ground state and the projectile comes from far away and impacts the target.

In practice, the two entities, target and projectile, start as far as the method of choice allows. In this initial step, two issues appear that could induce im-

portant effects in the outcome of a simulation. First, once the electronic wavefunction is computed for its ground state the proper kinetic energy should be added to the electrons that belong to the moving particles. Second, in the case of ion projectiles, if the ground state is computed for the ensemble of projectile and target, the ground state could eventually result into a redistribution of the charges, ie, neutralizing the projectile and ionizing the target. In such a case, the ground state must be computed independently for target and projectile, and reintegrated to start the propagation.

This chapter will focus on the first issue, the correct introduction of the electronic kinetic energy for the electrons associated to moving particles. The content of this chapter is part of a paper to be submitted soon.

6.2 Velocity Phase Factor

As was said, TDDFT starts from the GS because in such case the HK-theorem guarantees that the potential is a pure density functional. The usual procedure to evolve the Kohn-Sham scheme under TDDFT starts by computing the ground state of the system and later evolving the set of Kohn-Sham states. It is important at this point to realize that computing the ground state of a moving particle is not equivalent to compute the ground state of same particle at rest. Consider the state $\Psi_{\mathbf{v}}(\mathbf{r},t)$ of a particle moving with velocity $\mathbf{v}$, the particle is under the influence of a potential $\hat{\mathrm{V}}(\mathbf{r}-\mathbf{v}t)$. The time-dependent Schrödinger equation can be written as

$$\left[-\frac{1}{2}\nabla^2+\hat{\mathrm{V}}(\mathbf{r}-\mathbf{v}t)\right]\Psi_{\mathbf{v}}(\mathbf{r},t)=i\frac{\partial}{\partial t}\Psi_{\mathbf{v}}(\mathbf{r},t). \tag{6.1}$$

At $t=0$, the solution $\Psi_{\mathbf{v}}(\mathbf{r},t=0)$ is not equal to the solution of the static problem

$$\left[-\frac{1}{2}\nabla^2+\hat{\mathrm{V}}(\mathbf{r})\right]\Psi_{\mathbf{0}}(\mathbf{r},t)=i\frac{\partial}{\partial t}\Psi_{\mathbf{0}}(\mathbf{r},t), \tag{6.2}$$

however, as we plan to show, the solution to the dynamical problem can be expressed from the solution of the static problem.

Consider the ground state of the static problem, factorized in space and time

$$\Psi_{\mathbf{0}}(\mathbf{r},t)=\Phi_{\mathbf{0}}(\mathbf{r})\cdot e^{-iE_{\mathbf{0}}t}, \tag{6.3}$$

equation 6.3 solves the time-dependent Schrödinger equation

$$\left[-\frac{1}{2}\nabla^2+\hat{\mathrm{V}}(\mathbf{r})\right]\Phi_{\mathbf{0}}(\mathbf{r})\cdot e^{-iE_{\mathbf{0}}t}=i\frac{\partial}{\partial t}\Phi_{\mathbf{0}}(\mathbf{r})\cdot e^{-iE_{\mathbf{0}}t}. \tag{6.4}$$

Applying the derivative in the right hand side and canceling the exponential in both sides we arrive to the usual result that the spatial component $\Phi_{\mathbf{0}}(\mathbf{r})$ is solution of the time-independent Schrödinger equation

$$\left[-\frac{1}{2}\nabla^2 + \hat{\mathrm{V}}(\mathbf{r})\right]\Phi_{\mathbf{0}}(\mathbf{r}) = E_{\mathbf{0}}\Phi_{\mathbf{0}}(\mathbf{r}). \tag{6.5}$$

Now we show that the wavefunction

$$\Psi_{\mathbf{v}}(\mathbf{r},t) = \Phi_{\mathbf{0}}(\mathbf{r})\cdot e^{-iE_{\mathbf{v}}t}\cdot e^{i\mathbf{v}\cdot\mathbf{r}}, \tag{6.6}$$

is solution of the dynamical Schrödinger equation. This is a well know result for non-relativistic particles [Lévy-Leblond, 1967]

$$\left[-\frac{1}{2}\nabla^2 + \hat{\mathrm{V}}(\mathbf{r}-\mathbf{v}t)\right]\Psi_{\mathbf{v}}(\mathbf{r},t) = i\frac{\partial}{\partial t}\Psi_{\mathbf{v}}(\mathbf{r},t). \tag{6.7}$$

Developing the time derivative in the right hand side of 6.7:

$$\begin{aligned}
i\frac{\partial}{\partial t}\Psi_{\mathbf{v}}(\mathbf{r},t) &= i\frac{\partial}{\partial t}\Phi_{\mathbf{0}}(\mathbf{r}-\mathbf{v}t)\cdot e^{-iE_{\mathbf{v}}t}\cdot e^{i\mathbf{v}\cdot\mathbf{r}} \\
&= i\left[\sum_\alpha \frac{\partial r_\alpha}{\partial t}\frac{\partial}{\partial r_\alpha}\Phi_{\mathbf{0}}(\mathbf{r}-\mathbf{v}t)\right]\cdot e^{-iE_{\mathbf{v}}t}\cdot e^{i\mathbf{v}\cdot\mathbf{r}} \\
&\quad +i\Phi_{\mathbf{0}}(\mathbf{r}-\mathbf{v}t)\cdot[-iE_{\mathbf{v}}]\, e^{-iE_{\mathbf{v}}t}\cdot e^{i\mathbf{v}\cdot\mathbf{r}} \\
&= \left[i\sum_\alpha \frac{\partial r_\alpha}{\partial t}\frac{\partial}{\partial r_\alpha} + E_{\mathbf{v}}\right]\Phi_{\mathbf{0}}(\mathbf{r}-\mathbf{v}t)\cdot e^{i\mathbf{v}\cdot\mathbf{r}}\cdot e^{-iE_{\mathbf{v}}t} \\
&= \left[i\sum_\alpha v_\alpha\frac{\partial}{\partial r_\alpha} + E_{\mathbf{v}}\right]\Phi_{\mathbf{0}}(\mathbf{r}-\mathbf{v}t)\cdot e^{i\mathbf{v}\cdot\mathbf{r}}\cdot e^{-iE_{\mathbf{v}}t}.
\end{aligned} \tag{6.8}$$

The left hand side of 6.7:

$$\begin{aligned}
\left[-\frac{1}{2}\nabla^2 + \hat{\mathrm{V}}(\mathbf{r}-\mathbf{v}t)\right]\Psi_{\mathbf{v}}(\mathbf{r},t) &= \Big[-\frac{1}{2}\nabla^2\Phi_{\mathbf{0}}(\mathbf{r}-\mathbf{v}t)\cdot e^{i\mathbf{v}\cdot\mathbf{r}} \\
&\quad +\hat{\mathrm{V}}(\mathbf{r}-\mathbf{v}t)\Phi_{\mathbf{0}}(\mathbf{r}-\mathbf{v}t)\cdot e^{i\mathbf{v}\cdot\mathbf{r}}\Big]\, e^{-iE_{\mathbf{v}}t}.
\end{aligned} \tag{6.9}$$

Cancelling $e^{-iE_{\mathbf{v}}t}$ from 6.8 and 6.9, substracting both terms and going into the limit $t = 0$

$$
\begin{aligned}
0 &= -\frac{1}{2}\nabla^2\Phi_{\mathbf{0}}(\mathbf{r})\cdot e^{i\mathbf{v}\cdot\mathbf{r}} + \hat{\mathrm{V}}(\mathbf{r})\Phi_{\mathbf{0}}(\mathbf{r})\cdot e^{i\mathbf{v}\cdot\mathbf{r}} \\
&\quad - \left[i\sum_{\alpha} v_\alpha \frac{\partial}{\partial r_\alpha} + E_{\mathbf{v}} \right] \Phi_{\mathbf{0}}(\mathbf{r})\cdot e^{i\mathbf{v}\cdot\mathbf{r}} \\
&= -\frac{1}{2}\left[\nabla^2\Phi_{\mathbf{0}}(\mathbf{r}) - 2i\sum_{\alpha} v_\alpha \frac{\partial}{\partial r_\alpha}\Phi_{\mathbf{0}}(\mathbf{r}) - v^2\Phi_{\mathbf{0}}(\mathbf{r})\cdot \right] e^{i\mathbf{v}\cdot\mathbf{r}} \\
&\quad + \hat{\mathrm{V}}(\mathbf{r})\Phi_{\mathbf{0}}(\mathbf{r})\cdot e^{i\mathbf{v}\cdot\mathbf{r}} - \left[i\sum_{\alpha} v_\alpha \frac{\partial}{\partial r_\alpha} + E_{\mathbf{v}} \right] \Phi_{\mathbf{0}}(\mathbf{r})\cdot e^{i\mathbf{v}\cdot\mathbf{r}} \\
&= -\frac{\nabla^2}{2}\Phi_{\mathbf{0}}(\mathbf{r})\cdot e^{i\mathbf{v}\cdot\mathbf{r}} + \frac{v^2}{2}\Phi_{\mathbf{0}}(\mathbf{r})\cdot e^{i\mathbf{v}\cdot\mathbf{r}} + V(\mathbf{r})\Phi_{\mathbf{0}}(\mathbf{r})\cdot e^{i\mathbf{v}\cdot\mathbf{r}} \\
&\quad - E_{\mathbf{v}}\Phi_{\mathbf{0}}(\mathbf{r})\cdot e^{i\mathbf{v}\cdot\mathbf{r}} \\
&= \left[-\frac{\nabla^2}{2} + \frac{v^2}{2} + \hat{\mathrm{V}}(\mathbf{r}) \right] \Phi_{\mathbf{0}}(\mathbf{r}) - E_{\mathbf{v}}\Phi_{\mathbf{0}}(\mathbf{r}).
\end{aligned}
$$

The last relation is satisfied if $E_{\mathbf{v}} = E_0 + v^2/2$. As conclusion, the ground state of a free moving particle is derivable from the ground state of the same particle at rest introducing the phase $e^{i\mathbf{v}\cdot\mathbf{r}}$.

In the context of wavefunction based methods a similar issue appears. The orbitals are expanded in a basis set centered on each of the nuclei. The so called *electron translation factors* resemble the velocity phase factor, but they are used all along the propagation instead of at the beginning as it is the case here. The electron translation factors are relevant even in near-adiabatic collisions and has been studied for several decades. Thorson and Delos [Thorson and Delos, 1978] develop a method to treat the electron translation factors applicable to near-adiabatic collisions using switching functions and a geometric approach to associate an electron to its closest nuclei. More recently Illescas and Riera [Illescas and Riera, 1998] develop a method applicable in close coupled expansions for the treatment of atomic collisions. Their method uses classical trajectory MonteCarlo (CTMC) to predict the appropriate electronic translation factors at intermediate distances.

In the context of this work, the velocity phase factor is only introduced before the propagation takes place. Once the KS is propagated in time, the TD Schrödinger equation is expected to follow naturally the orbitals with the proper velocity phase. Now, we concentrate the attention in detail about the application of the VPF for a single particle. After that we can consider the case of more moving atoms, in particular, atomic collisions.

6.3 One Moving Particle

The velocity phase $e^{i\mathbf{v}\cdot\mathbf{r}}$ for a single particle system is straightforward to apply, in particular for wavefunctions described on real space grids. Physically, the correct Galilean transformation is applied to a wavefunction from a static

framework into a moving one. When is the use of a velocity phase relevant? It is obvious that for sufficiently low velocities this correction is also small, not only because the phase is small but also because that is exactly the limit of the Born-Oppenheimer approximation where ab-initio MD based on ground-state DFT is theoretically justified.

The logical step now is to present arguments to define the meaning of the expression "sufficiently low velocities". The velocity phase factor will be now studied for a particularly simple system to get some intuition about the limit where such correction becomes relevant in problems involving collisions. We concentrate our attention in two physical quantities that are easy to compute and reveal the domain where the lack of a VPF shows its limitations. Consider a single atom moving freely in space. If the initial state is indeed an eigenstate of equation 6.7, the density should move unperturbed with the movement of the nuclei. This means

$$n(\mathbf{r}, t) = n(\mathbf{r} + \mathbf{v}(t' - t), t') \qquad \forall \quad (\mathbf{r}, t, t'). \tag{6.10}$$

An approximate way to verify this condition is to measure the amount of charge enclosed inside a sphere around the nuclei, the value must remain constant. A second way is to verify that no dipole moment appears in any direction. When the nuclei is propagated from a GS that is not the GS of the dynamic Schrödinger equation, ie, without the proper VPF, two phenomena can be expected; a partial loss of charge left behind when the nuclei propagates forward or the creation of an oscillating dipole when the charge is not spherically symmetric due also to the propagation of the nuclei.

Consider the simplest case, an atom of Hydrogen moving freely. The atom of Hydrogen is simulated in a big box of 24 Bohr along the direction of propagation and 16 Bohr in the perpendicular directions. The ground state is computed as usual and the particle is let to propagate a distance of 8 Bohr inside the box. The hydrogen atom was propagated in a range of values of kinetic energy from 10 to 10^5 eV. Once the particle has advanced by 8 Bohr, the amount of charge enclosed in a sphere of radius 4 Bohr is measured. The figure 6.1 shows the charge loss in the sphere compared with the initial value. Physically no charge should be lost in the process of propagation if the electronic wavefunction is correctly started from the ground state in the framework where it is moving. However, if the GS is computed in a different framework, the electrons have not the right direction and speed and some charge will be left behind as a result. That is exactly what is observed on figure 6.1: for kinetic energies larger than 1 keV an increasing amount of charge is left behind. When the VPF $e^{i\mathbf{v}\cdot\mathbf{r}}$ is introduced, the charge inside the sphere surrounding the moving proton is preserved.

Propagating the nuclei without adding the phase generates an effect of kicking the electronic structure. This effect is used for example in a different context to compute the polarizability from real-time propagations. In that case, instead of moving the nuclei, the wavefunction is kicked and propagated with the nuclei at rest. Consider a system perturbed with a sudden short-time electric pulse

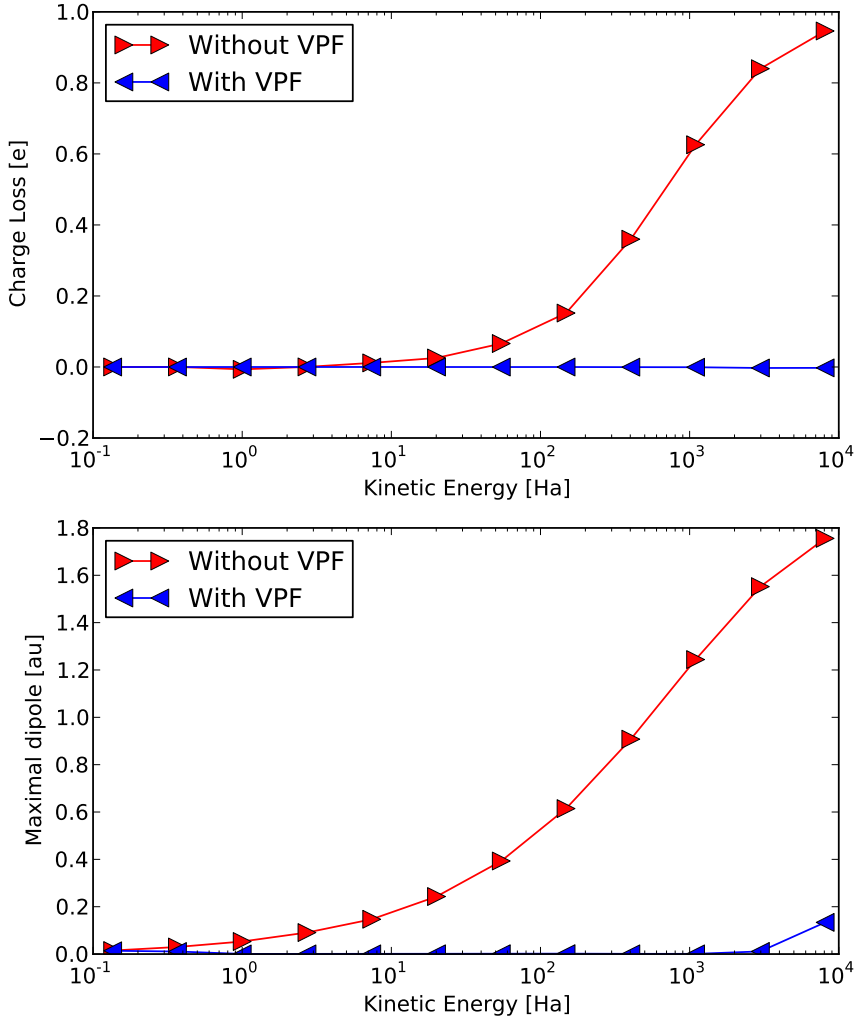

Figure 6.1: Hydrogen atom moving freely 8 Bohr in a large box. Up: Charge loss after propagation. Down: Maximal value of the dipole in the x direction for the entire propagation. The red line with right-oriented triangles shows the results when the propagation is applied to the ground state of the atom at rest. The blue line with left-oriented triangles shows a propagation for the same distance but introducing the velocity phase factor to the initial wavefunction.

$$E(t) = E_0 \delta(t) \hat{\mathbf{z}}, \tag{6.11}$$

in frequency space that is equivalent to perturb all the frequencies homogeneously.

$$E(\omega) = E_0 \hat{\mathbf{z}} \tag{6.12}$$

The dynamical polarizability can be obtained as the variation of the dipole moment with respect to the intensity of the kick

$$\alpha_z z(\omega) = \frac{\delta Z(\omega)}{E_0} \tag{6.13}$$

The variation in the dipole moment is obtained from the time-dependent density

$$\delta Z(\omega) = \int dt\, e^{i\omega t} \delta Z(t) \tag{6.14}$$

where $\delta Z(t)$

$$\delta Z(t) = \int d^3\, r\, n(\mathbf{r}, t) z - Z_0 \tag{6.15}$$

Notice that the wavefunction kick has two effects according to the intensity E_0. It produces in general an oscillating dipole moment but if the intensity is high enough the system will also ionize in a similar way as the charge is lost when the nuclei is propagated without the velocity phase factor.

Figure 6.1 shows the effect of the use of the VPF to preserve the correct propagation of the KS orbitals. In the figure, the dipole moment in the direction of propagation is measured inside a sphere of radius 4 Bohr. One collects the magnitude of the dipole at each time-step, the maximal dipole is taken and plotted as a function of the initial kinetic energy. The effect is visible for kinetic energies starting from around 10 eV

Notice how those two artifacts emerge at different values of kinetic energy. On figure 6.1 the loss of charge starts being evident for kinetic energies on the order of keV; for the dipole, the effect is non-negligible even for kinetic energies of a few eV. As a conclusion, the lack of this correction will cause the presence of an artificial dipole oscillation starting from a few Ha to the kHa, while for higher energies, the dominant effect is a loss of charge. It is expected that the effect is driven by the actual velocity of the particle, so for heavy elements the effect should be shifted in the range of energy.

6.4 Velocity Phase for non-Local Potentials

We can now consider the effect of the VPF for atoms with increasing number of electrons. Notice that the application of the VPF is strictly correct if the potential $V(\mathbf{r})$ is local. That is in general not the case for most of the norm-conserving pseudopotentials currently used. Take for example, the Kleinman

and Bylander scheme [Kleinman and Bylander, 1982]. The potential for the ion is written as:

$$V_{ion} = V_{loc} + \sum_{l\,m} \frac{|\psi_{lm}\delta V_l\rangle \langle \delta V_l \psi_{lm}|}{\langle \psi_{lm}| \delta V_l |\psi_{lm}\rangle}, \tag{6.16}$$

where V_{loc} is an arbitrary local potential, ψ_{lm} are the pseudo-atom wavefunctions, and δV_l is defined through

$$\delta V_l = V_{l,\mathrm{NL}} - V_{\mathrm{LOC}}, \tag{6.17}$$

where $V_{l,\mathrm{NL}}$ is the l angular momentum component of a non-local pseudopotential. Writing the pseudopotential in this form allows the calculation to be faster than the direct computation of

$$V_{ion} = \sum_{l\,m} |Y_{l\,m}\rangle\, V_l\, \langle Y_{l\,m}|\,. \tag{6.18}$$

The attention will be now concentrated on the effect of the application of VPF when the potential is not completely local. Consider for example the figure 6.2, the twelve lightest atoms in the periodic table were propagated a distance of 10 Bohr inside a box of $30 \times 20 \times 20$ Bohr. The difference in charge inside a sphere of radius 4 Bohr is computed and plotted respect to the initial value. Pseudopotentials were created using FHI98PP [Fuchs and Scheffler, 1999] following the Troullier-Martins scheme [Troullier and Martins, 1991b].

Notice how in most of cases the non-linear part of the pseudopotentials causes charge loss during the propagation, with the notable exception of Li, that is gaining charge, ie, the charge is concentrating inside the sphere close to the nuclei. Also artifact dipoles are created during the propagation 6.3. In order to compare the effect of the non-locality of the pseudopotentials, consider the comparison with pseudopotentials from Hartwigsen, Goedecker and Hutter [Hartwigsen *et al.*, 1998] using semicore electrons when available. In that case the pseudopotentials for atoms until Be are local and can be compared with the previous FHI pseudopotentials.

When the pseudopotentials are purely local the artifact effect of the loss of charge and dipoles disappear. That is visible in figures 6.4 and 6.5 showing the maximal charge loss and maximal dipoles created by the propagation of each atom a distance of 10 Bohr. The pseudopotentials for Be and Li are local when all the electrons are included in the valence.

Notice that the non-locality of pseudopotentials, even using VPF, prevents the zeroing of dipoles during the propagation that could eventually have important physical effects in the case of collisions.

Lets consider now how the equations 6.8 and 6.9 are modified by the introduction of a non-local potential. The most general form for a potential $\hat{\mathrm{V}}$ that could include local and non-local contributions, can be written as an integral operation of the form

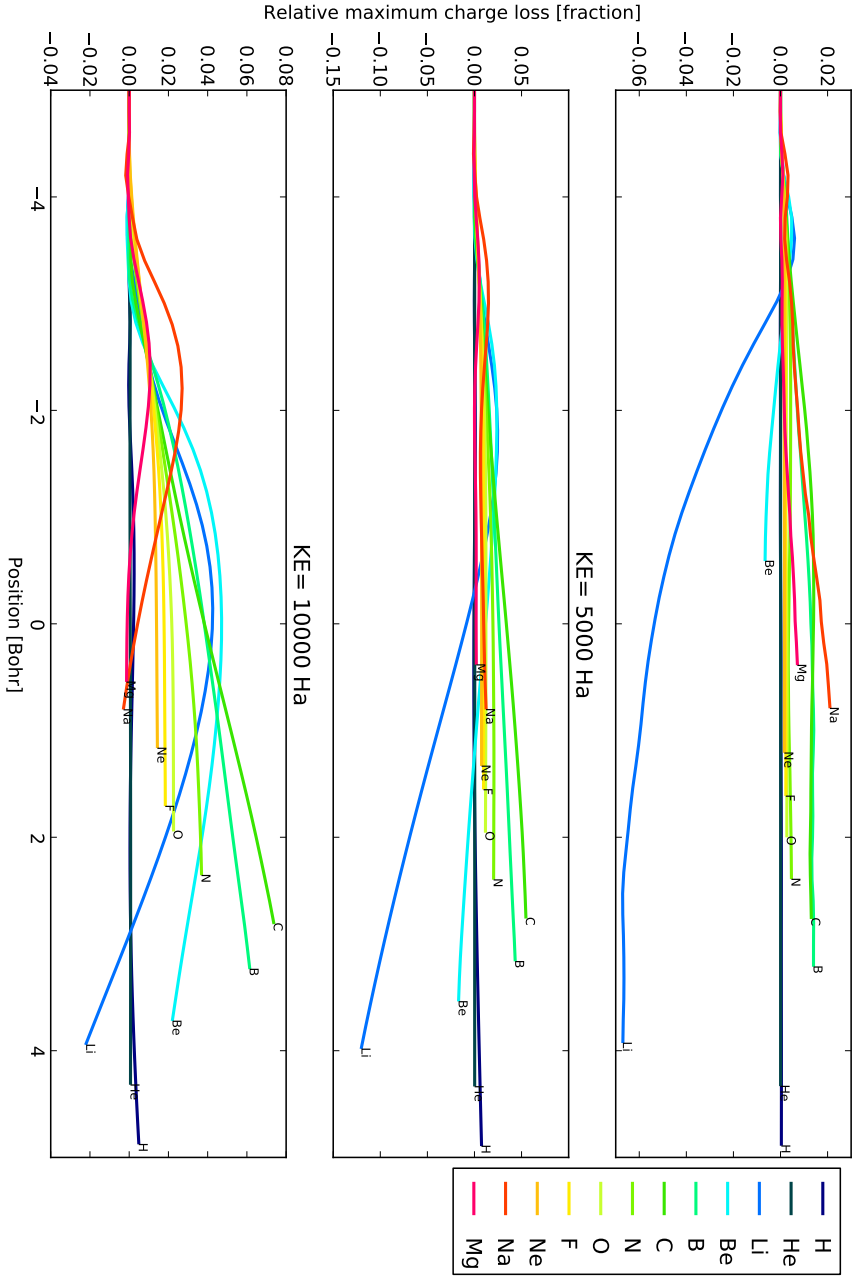

Figure 6.2: Charge loss when the velocity phase factor is applied for the 12 atoms in the periodic table. The propagation was computed for three values of kinetic energy: 1kHa, 5kHa and 10kHa. Only the pseudopotentials for H and He are local.

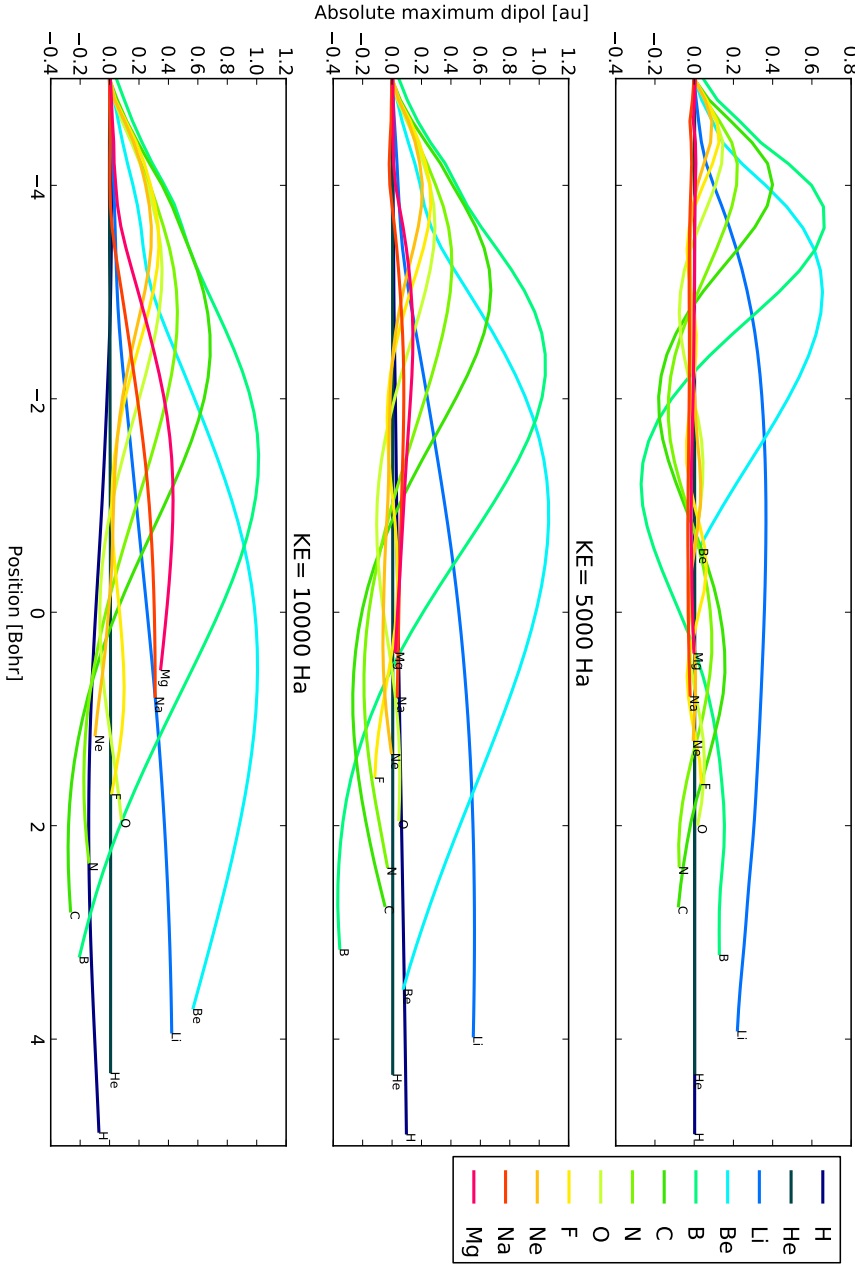

Figure 6.3: Dipole in the direction of propagation when the velocity phase factor is applied for the 12 atoms in the periodic table. The propagation was computed for three values of kinetic energy: 1kHa, 5kHa and 10kHa.Only the pseudopotentials for H and He are local.

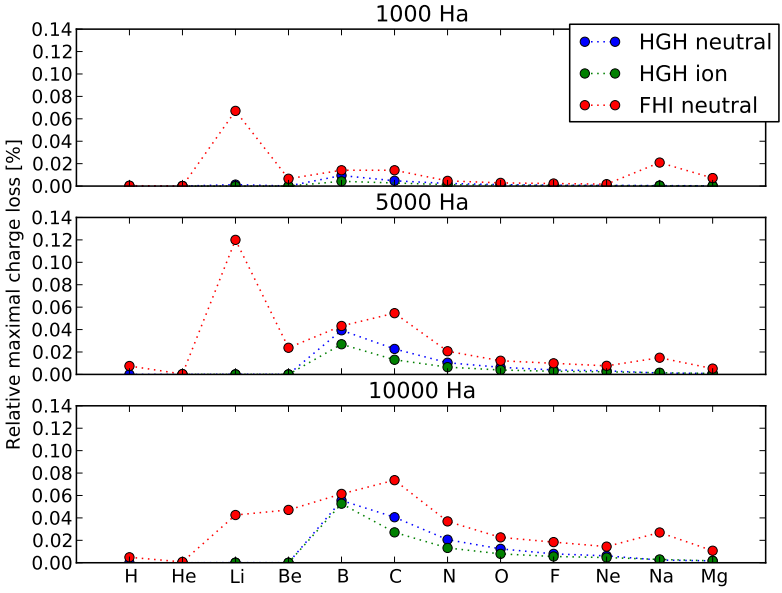

Figure 6.4: Relative Maximal charge loss for an atom propagated 10 Bohr inside a large box. The red dots correspond to pseudopotentials in the Troullier-Martins scheme by the FHI. Blue and green correspond to pseudopotentials in Hartwigsen-Goedecker-Hutter parametrization. for both neutral and single ionized atoms respectively. The propagation was computed for three values kinetic energy 1kHa, 5kHa and 10kHa.

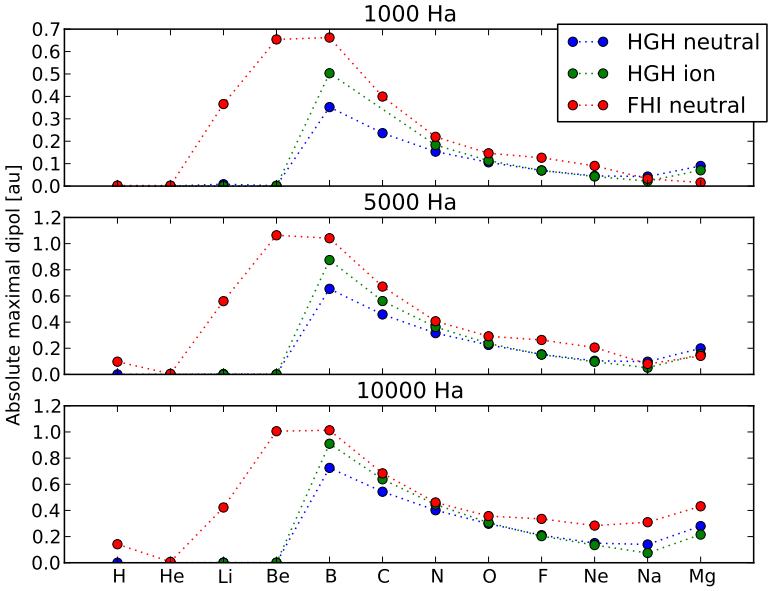

Figure 6.5: Absolute maximal dipole in the direction of propagation for an atom propagated 10 Bohr inside a large box. The red dots correspond to pseudopotentials in the Troullier-Martins scheme by the FHI. Blue and green correspond to pseudopotentials in Hartwigsen-Goedecker-Hutter parametrization. for both neutral and single ionized atoms respectively. The propagation was computed for three values of kinetic energy: 1kHa, 5kHa and 10kHa.

$$\begin{aligned}\left\langle \mathbf{r}\right|\hat{\mathrm{V}}\left|\psi\right\rangle &= \int d^3\,r'\left\langle \mathbf{r}\right|\hat{\mathrm{V}}\left|\mathbf{r}'\right\rangle\left\langle \mathbf{r}'\right|\left.\psi\right\rangle \\ &= \int d^3\,r' V(\mathbf{r},\mathbf{r}')\psi(\mathbf{r}') \end{aligned} \tag{6.19}$$

This potential $V(\mathbf{r},\mathbf{r}')$ is symmetric

$$V(\mathbf{r},\mathbf{r}') = V(\mathbf{r}',\mathbf{r}) \tag{6.20}$$

.

A local potential can be written removing all the non-diagonal elements as

$$V(\mathbf{r},\mathbf{r}')_{\mathrm{LOC}} = V(\mathbf{r})\delta(\mathbf{r}-\mathbf{r}') \tag{6.21}$$

We can say that a potential is local only if

$$\left\langle \mathbf{r}\right|\hat{\mathrm{V}}\left|\psi\right\rangle = V(\mathbf{r})\psi(\mathbf{r}) \tag{6.22}$$

Replacing 6.19 in the Schrödinger equation 6.7 we get the integro-differential Schrödinger equation

$$-\frac{1}{2}\nabla^2\Psi_{\mathbf{v}}(\mathbf{r},t) + \int d^3\,r' V(\mathbf{r},\mathbf{r}')\Psi_{\mathbf{v}}(\mathbf{r}',t) = i\frac{\partial}{\partial t}\Psi_{\mathbf{v}}(\mathbf{r},t). \tag{6.23}$$

The left hand side develops identical as 6.8 resulting in

$$i\frac{\partial}{\partial t}\Psi_{\mathbf{v}}(\mathbf{r},t) = \left[i\sum_\alpha v_\alpha\frac{\partial}{\partial r_\alpha} + E_{\mathbf{v}}\right]\Phi_{\mathbf{0}}(\mathbf{r}-\mathbf{v}t)\cdot e^{i\mathbf{v}\cdot\mathbf{r}}\cdot e^{-iE_{\mathbf{v}}t}$$

The right hand side is changed as:

$$\begin{aligned}-\frac{1}{2}\nabla^2\Psi_{\mathbf{v}}(\mathbf{r},t) + \int d^3\,r' V(\mathbf{r},\mathbf{r}')\Psi_{\mathbf{v}}(\mathbf{r}',t) = \\ \left[-\frac{1}{2}\nabla^2\Phi_{\mathbf{0}}(\mathbf{r}-\mathbf{v}t)\cdot e^{i\mathbf{v}\cdot\mathbf{r}}\right. \\ \left. + \int d^3\,r' V(\mathbf{r},\mathbf{r}')\Phi_{\mathbf{0}}(\mathbf{r}'-\mathbf{v}t)\cdot e^{i\mathbf{v}\cdot\mathbf{r}'}\right] e^{-iE_{\mathbf{v}}t}\end{aligned} \tag{6.24}$$

Cancelling $e^{-iE_{\mathbf{v}}t}$ from 6.24 and 6.25, substracting both terms and going into the limit $t=0$

$$
\begin{aligned}
0 &= -\frac{1}{2}\nabla^2\left(\Phi_{\mathbf{0}}(\mathbf{r})\cdot e^{i\mathbf{v}\cdot\mathbf{r}}\right) + \int d^3\,r' V(\mathbf{r},\mathbf{r}')\Phi_{\mathbf{0}}(\mathbf{r}')\cdot e^{i\mathbf{v}\cdot\mathbf{r}'} \\
&\quad - \left[i\sum_\alpha v_\alpha \frac{\partial}{\partial r_\alpha} + E_{\mathbf{v}}\right]\Phi_{\mathbf{0}}(\mathbf{r})\cdot e^{i\mathbf{v}\cdot\mathbf{r}} \\
&= -\frac{1}{2}\left[\nabla^2\Phi_{\mathbf{0}}(\mathbf{r}) - 2i\sum_\alpha v_\alpha \frac{\partial}{\partial r_\alpha}\Phi_{\mathbf{0}}(\mathbf{r}) - v^2\Phi_{\mathbf{0}}(\mathbf{r})\cdot\right] e^{i\mathbf{v}\cdot\mathbf{r}} \\
&\quad + \int d^3\,r' V(\mathbf{r},\mathbf{r}')\Phi_{\mathbf{0}}(\mathbf{r}')\cdot e^{i\mathbf{v}\cdot\mathbf{r}'} \\
&\quad - \left[i\sum_\alpha v_\alpha \frac{\partial}{\partial r_\alpha} + E_{\mathbf{v}}\right]\Phi_{\mathbf{0}}(\mathbf{r})\cdot e^{i\mathbf{v}\cdot\mathbf{r}} \\
&= -\frac{\nabla^2}{2}\Phi_{\mathbf{0}}(\mathbf{r})\cdot e^{i\mathbf{v}\cdot\mathbf{r}} + \frac{v^2}{2}\Phi_{\mathbf{0}}(\mathbf{r})\cdot e^{i\mathbf{v}\cdot\mathbf{r}} \\
&\quad + \int d^3\,r' V(\mathbf{r},\mathbf{r}')\Phi_{\mathbf{0}}(\mathbf{r}')\cdot e^{i\mathbf{v}\cdot\mathbf{r}'} \\
&\quad - E_{\mathbf{v}}\Phi_{\mathbf{0}}(\mathbf{r})\cdot e^{i\mathbf{v}\cdot\mathbf{r}}
\end{aligned}
$$

Canceling the common factor $e^{i\mathbf{v}\cdot\mathbf{r}}$:

$$
\begin{aligned}
E_{\mathbf{v}}\Phi_{\mathbf{0}}(\mathbf{r})\cdot e^{i\mathbf{v}\cdot\mathbf{r}} &= \left[-\frac{\nabla^2}{2} + \frac{v^2}{2}\right]\Phi_{\mathbf{0}}(\mathbf{r})\cdot e^{i\mathbf{v}\cdot\mathbf{r}} \\
&\quad + \int d^3\,r' V(\mathbf{r},\mathbf{r}')\Phi_{\mathbf{0}}(\mathbf{r}')\cdot e^{i\mathbf{v}\cdot(\mathbf{r}'-\mathbf{r})} \qquad (6.25)
\end{aligned}
$$

We observe that the non-local pseudopotential should be modified by a velocity phase $e^{i\mathbf{v}\cdot(\mathbf{r}'-\mathbf{r})}$. It is no longer possible to compute the dynamic ground state by the simple introduction of the VPF to the static ground state. In what follows, we will restrict ourselves to the local pseudopotential case.

6.5 Several Moving Particles

The application of the velocity phase $e^{i\mathbf{v}\cdot\mathbf{r}}$ is straightforward when there is only one nucleus, and its electronic cloud. Nevertheless, our interest is focused in processes where several particles interact. For example, two atoms in collision or an atom impacting a big molecule or surface. In those cases, we have several particles initially separated and with different states of movement.

To properly initialize a KS scheme in this case, the direct solution is to apply the correct phase to the wavefunctions attached to the nuclei that are moving. However, this solution requires the knowledge about which wavefunction is associated to which ion. Also, the application of different phases to the wavefunction in a given place will break the orthogonality of the wavefunctions.

Our approach is to develop a scheme that could be applied without specific knowledge of the wavefunctions. Also, we require that the orthogonality is preserved for the KS set and easily applicable to the case of atomic collisions beyond the Born-Oppenheimer limit. The basic idea is to localize the effect of the velocity phase according to the position of the moving atoms and limit somehow their range in space.

Two basic strategies were considered to localize the effect of the phase, a radial sigmoid around the atom or stabilize the value of the phase beyond a certain plane perpendicular to the direction of propagation. The first alternative can be expressed for a system of M atoms as

$$\Phi(\mathbf{r})_v = \Phi(\mathbf{r})_0 \prod_{\tau=1}^{M} e^{i\mathbf{v}_\tau \cdot (\mathbf{r}-\mathbf{r}_\tau)\, S(\mathbf{r}-\mathbf{r}_\tau)}, \tag{6.26}$$

where $S(\mathbf{r}-\mathbf{r}_\tau)$ is a sigmoid introduced to limit the range of application of the phase

$$S(\mathbf{r}-\mathbf{r}_\tau) = 1 - (1 + e^{-\alpha(|\mathbf{r}-\mathbf{r}_\tau|-r_{cut})})^{-1}. \tag{6.27}$$

The equation 6.26 is correct if the spheres created in the nuclei centers $\mathbf{r}_\tau$ with radius $\mathbf{r}_{cut}$ are sufficiently distant one of each other.

The parameter α controls how steep is the change of the phase for a radius of r_{cut}. Beyond this radius the phase decays to zero. The figure 6.6 shows how the sigmoid limits the range of application of the velocity phase factor around the position of the moving particle.

The application of this scheme effectively localizes the VPF around the nuclei. However, it also produces a slope in the phase with opposite sign with respect to the original phase. Physically it means that the electronic density in the frontier of a sphere of radius r_{cut} is moving backwards with respect to the direction inside the sphere. In this case, the solution is to make the radius large enough to ensure that the minimal amount of charge is located in the frontier to the sphere defined by r_{cut}.

The second alternative is to freeze the phase beyond a plane in the forward direction. The frozen phase approach could be written as:

$$\begin{aligned} \Phi(\mathbf{r})_v \quad = \quad & \Phi(\mathbf{r})_0 \prod_{\tau=1}^{M} \exp\left[i\mathbf{v}_\tau \cdot (\mathbf{r}-\mathbf{r}_\tau)\,(1 - H(\hat{v}\cdot(\mathbf{r}-\mathbf{r}_\tau) - r_{cut})\right) \\ & + i|\mathbf{v}_\tau| r_{cut}\, H(\hat{v}\cdot(\mathbf{r}-\mathbf{r}_\tau) - r_{cut})] \end{aligned} \tag{6.28}$$

where $H(\hat{v}\cdot(\mathbf{r}-\mathbf{r}_\tau) - r_{cut})$ uses the Heaviside step function formally defined as

$$H(x) = \int_{-\infty}^{x} \delta(s)\, \mathrm{d}s \tag{6.29}$$

Again, this scheme is also restricted for non-overlapping VPF. This could be important for example in poly-atomic projectiles, a case that we are not considering here.

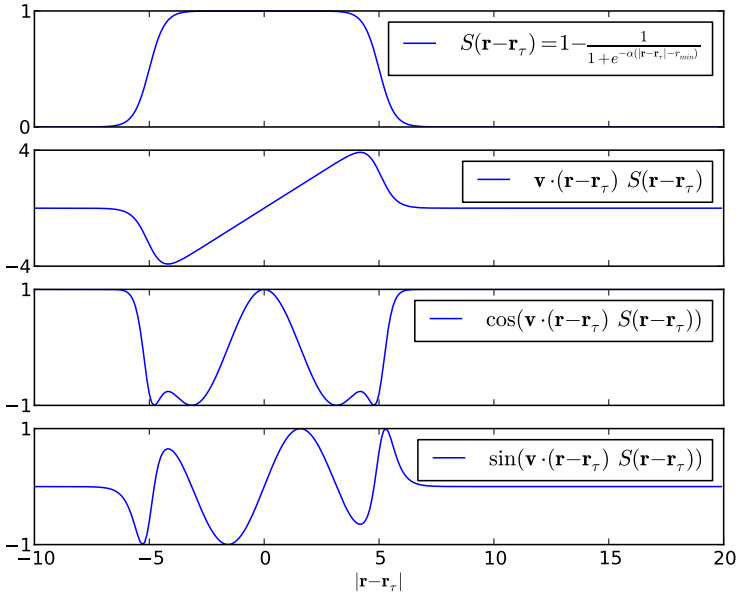

Figure 6.6: The different plots show the effect of a sigmoid to localize the velocity phase. The figure in the second row shows clearly the slopes in the opposite direction when this scheme is used.

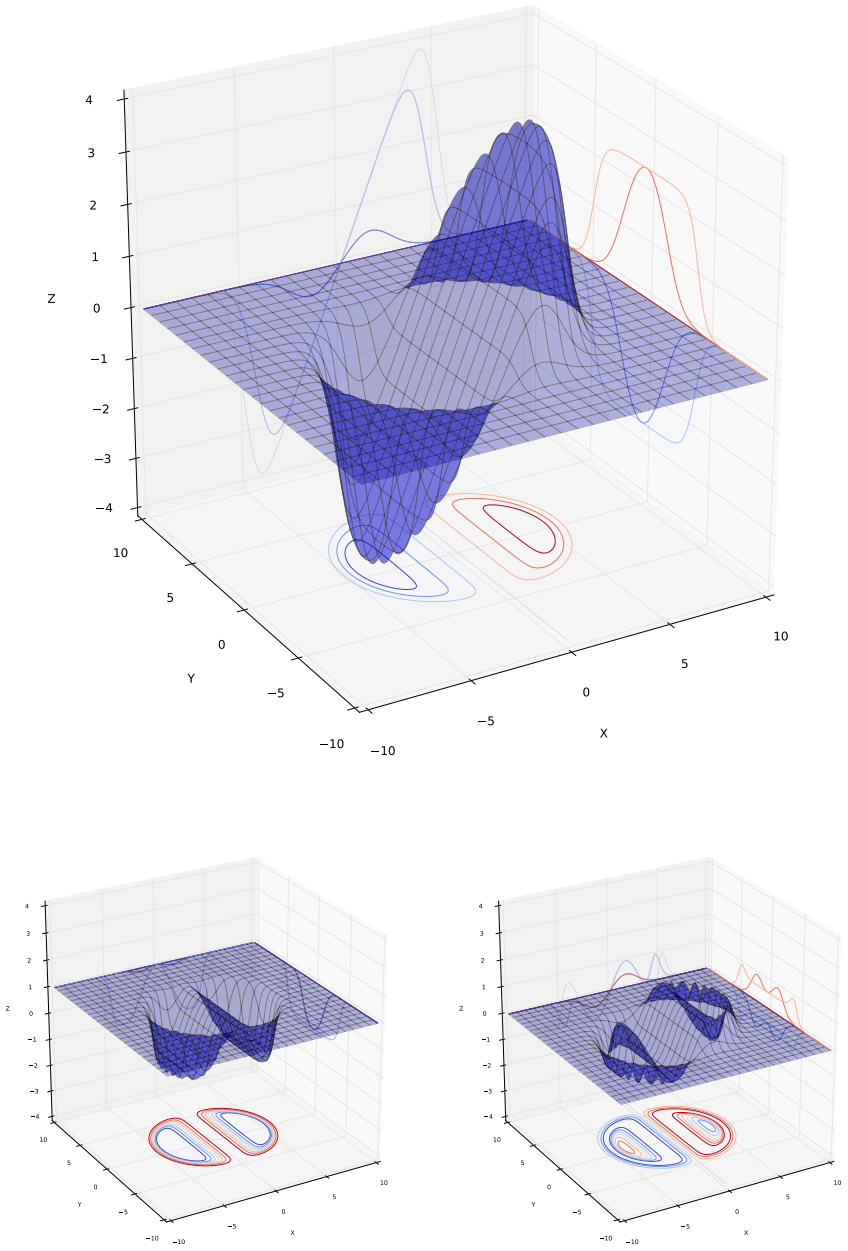

Figure 6.7: Up: Plot of the phase $\mathbf{v}_\tau \cdot (\mathbf{r} - \mathbf{r}_\tau)\, S(\mathbf{r} - \mathbf{r}_\tau)$ with the sigmoid introduced as a factor to limit the range of action of the phase around the location of each moving atom. Down: The components real (cos) and imaginary (sin) of the phase

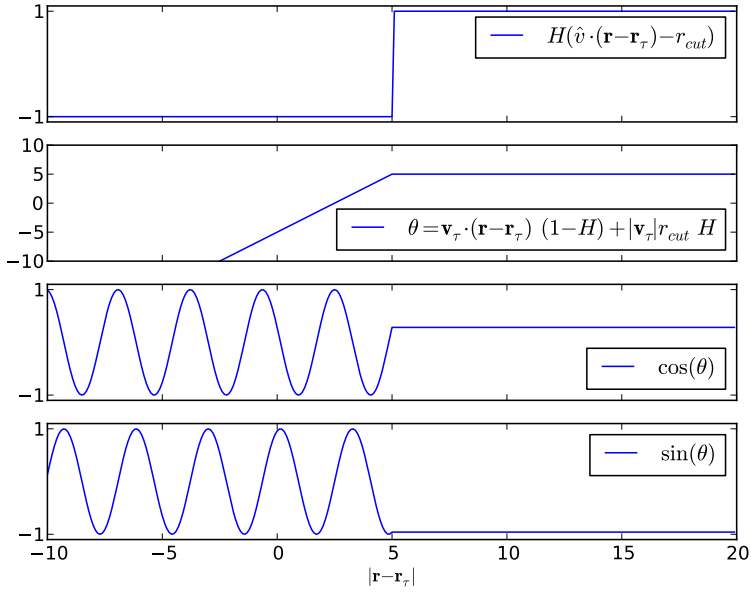

Figure 6.8: The different plots show the effect of the a Heaviside step function introduce as a factor in the velocity phase

The Heaviside approach is based on the fact that any observable in quantum mechanics is not sensible to a global phase in the wavefunction. It preserves the continuity of the phase in the whole domain, but not the continuity on the derivative. To solve the last issue, the Heaviside function could be also replaced with a sigmoid and we call it a planar sigmoid. This alternative was also implemented to compare with the sharp Heaviside version. The figure 6.8 shows how the phase is modified in the direction of propagation.

To see the reliability of each option, a test was done on a simple system, an atom of He in collision with an Be^+. In this case, both pseudopotentials are local, namely Hartwigsen, Goedecker and Hutter [Hartwigsen *et al.*, 1998] pseudopotentials with semicore electrons for Be.

Consider an atom of He impacting a singly ionized Be. We test the collision under two values of kinetic energy in the center of mass, 50 keV and 100 keV. The impact parameter in both cases was fixed to 1 Bohr. For each initial kinetic energy the same physical collision was computed under three different frameworks: in the center of mass of the system, and putting at rest each atom and moving the other. For each case we test the evolution with and without the velocity phase factor including each of the three options considered above. As the three frameworks represent the same physical collision they should produce identical results for the charge transfer after the collision. As an example the figure 6.10 shows the evolution of the planar integrated charges for a collision simulated in the center of mass framework.

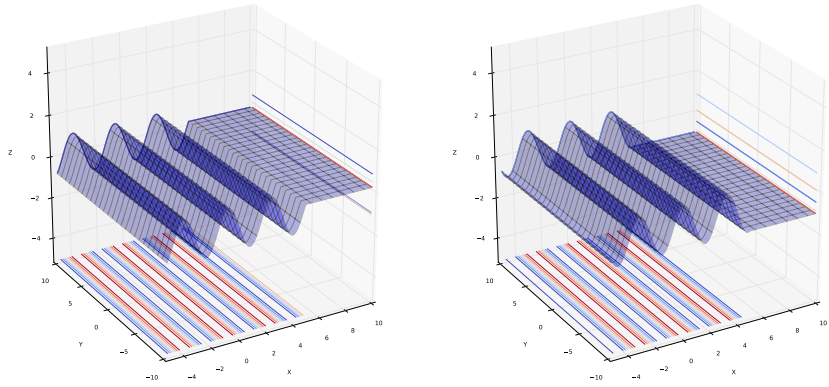

Figure 6.9: Plot of the phase $\mathbf{v}_\tau \cdot (\mathbf{r} - \mathbf{r}_\tau)\, S(\mathbf{r} - \mathbf{r}_\tau)$ with the Heaviside step function introduced as a factor to limit the range of action of the phase a certain distance beyond the location of each moving atom

Notice that the use of a VPF correctly reproduces the dynamics of the electrons in the three frameworks. Also, it is important to remark that the Hirshfeld analysis here is not able to account for the fact that both atoms are losing charge after the collision. The values of charge loss are in general overestimated when the velocity phase is missing. The large size of the simulation box and the particularly strong parameters used for this simulation enforces the good behavior of all versions. In fact, it does not matter which scheme is chosen to localize the phase, both of them agree in the amount of charge being loss after the collision.

Fig. 6.11 shows the amount of charge lost by each atom after the collision. In those cases, the charge is measured inside a sphere with radius of 4 Bohr. Similarly, fig. 6.12 shows the Hirshfeld analysis for the same situation.

Notice how the lack of VPF has an important effect in the charge transfer phenomena as well as in the Hirshfeld charge analysis. That difference is produced by the charge loss in the onset of the propagation.

6.6 Conclusions

In this chapter, it was shown how the ground state in the correct framework plays an important role when atoms are initially moving. It was also shown that the velocity phase factor is exact only for local potentials and it will fail in general for most of the norm-conserving pseudopotentials normally used. Two physical quantities, the charge and the dipole moment computed inside a sphere, were used to compare the correct preservation of the wavefunction during the time propagation. For the case of several moving particles, in the non-relativistic regime, two schemes were presented and shown that they correctly preserve the Galilean invariance during atomic collisions.

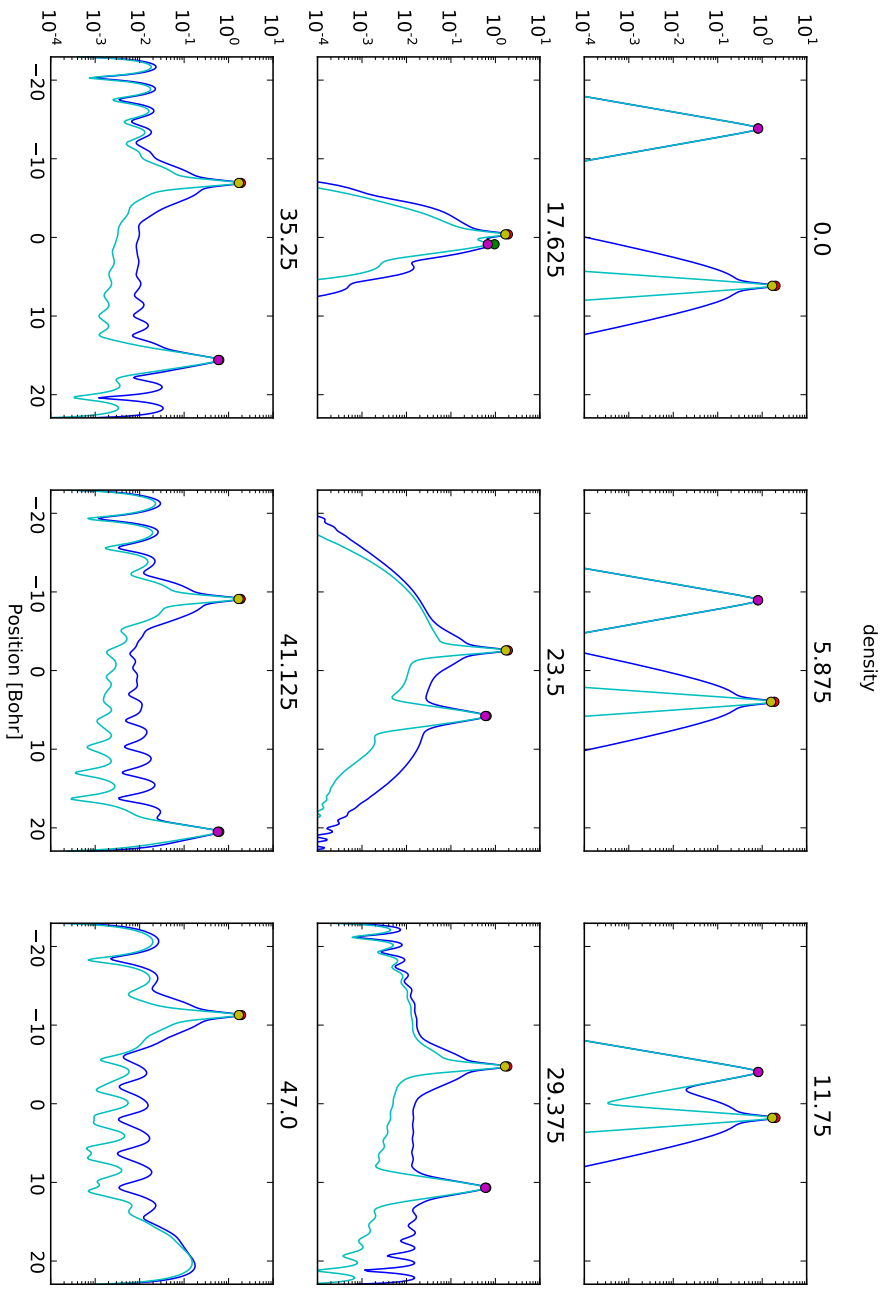

Figure 6.10: Evolution of the planar integrated charges for a simulation of an atom of He in collision with an atom of Be^{+}. The simulation is done in the center of mass of the system. The kinetic energy is 100 keV and integrated charges for each spin channel are depicted for each snapshot.

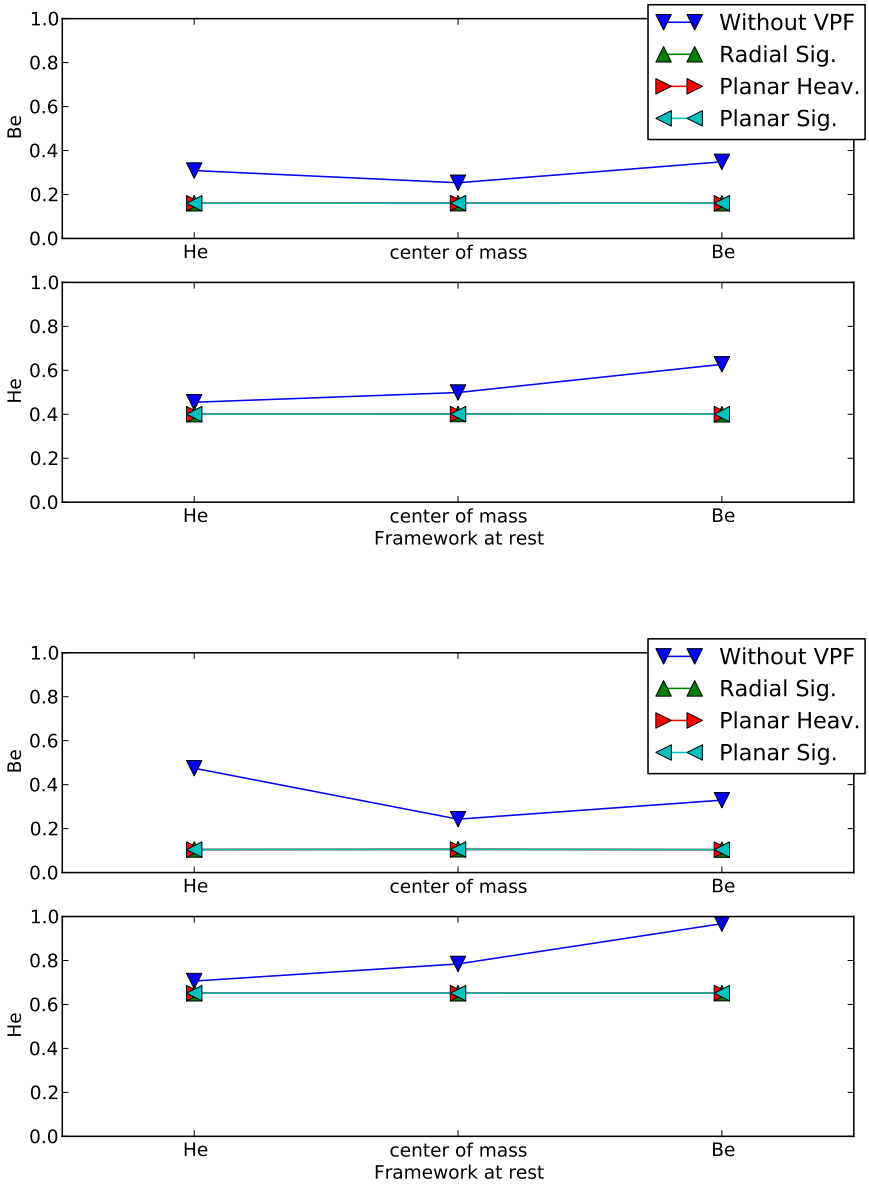

Figure 6.11: Charge loss after the collision of an atom of He and an ion of Be^{+}. The impact parameter is 1.0 Bohr. The simulation was computed for the same equivalent kinetic energy, but simulating in three different frameworks, with either the He atom or the Be atom at rest and a simulation with the center of mass at rest. The kinetic energy in the center of mass is 50 keV for the figure in top and 100 keV for the figure in the bottom

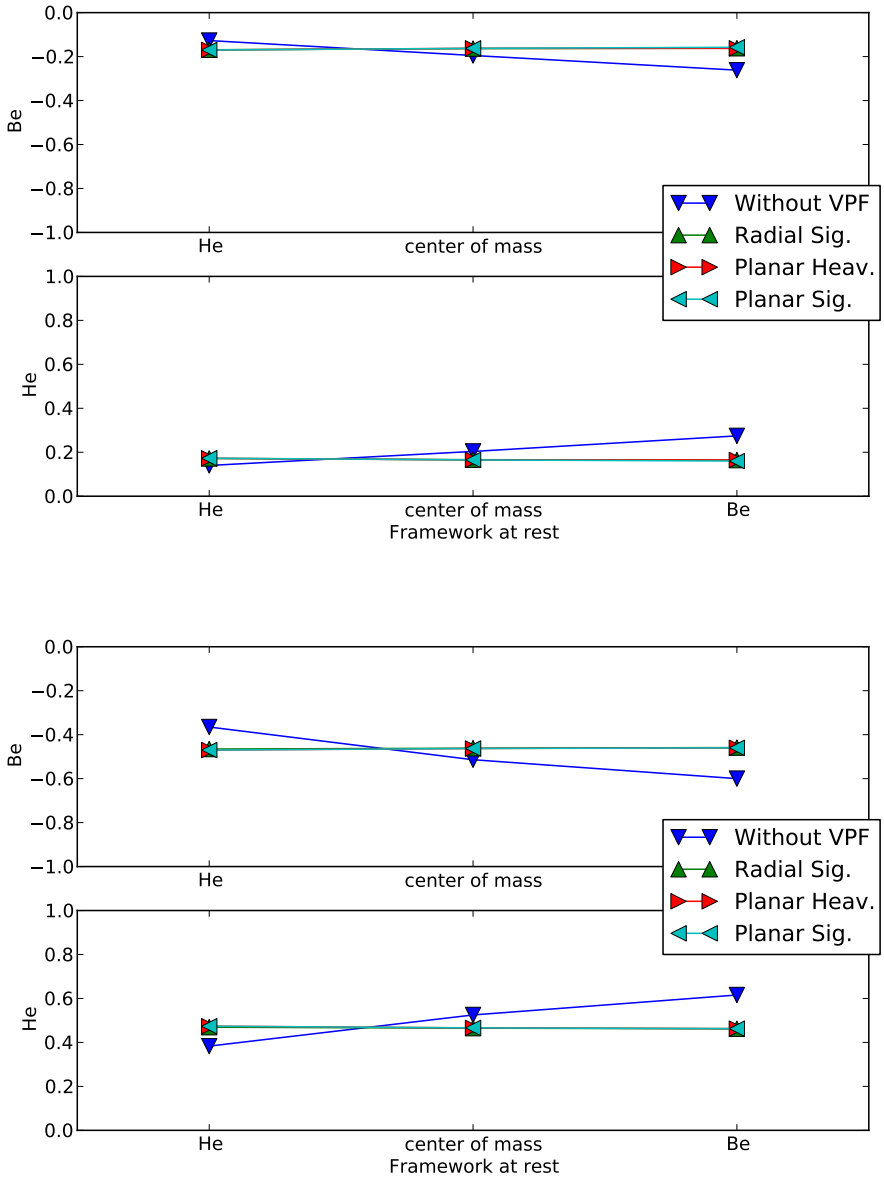

Figure 6.12: Hirshfeld analysis for the collision of an atom of He and an ion of Be^{+}. The impact parameter is 1.0 Bohr. The simulation was computed for the same equivalent kinetic energy, but simulating in three different frameworks, with either the He atom or the Be atom at rest and a simulation with the center of mass at rest. The kinetic energy in the center of mass is 50 keV for the figure in top and 100 keV for the figure in the bottom

7

Impact of Li^{+}2 MeV on C_{60}

Los idealistas arguyen que las salas hexagonales son una forma necesaria del espacio absoluto o, por lo menos, de nuestra intuición del espacio. Razonan que es inconcebible una sala triangular o pentagonal. (Los místicos pretenden que el éxtasis les revela una cámara circular con un gran libro circular de lomo continuo, que da toda la vuelta de las paredes; pero su testimonio es sospechoso; sus palabras, oscuras. Ese libro cíclico es Dios.) Básteme, por ahora, repetir el dictamen clásico: La Biblioteca es una esfera cuyo centro cabal es cualquier hexágono, cuya circunferencia es inaccesible.

The idealists argue that the hexagonal rooms are a necessary form of absolute space or, at least, of our intuition of space. They reason that a triangular or pentagonal room is inconceivable. (The mystics claim that their ecstasy reveals to them a circular chamber containing a great circular book, whose spine is continuous and which follows the complete circle of the walls; but their testimony is suspect; their words, obscure. This cyclical book is God.) Let it suffice now for me to repeat the classic dictum: The Library is a sphere whose exact center is any one of its hexagons and whose circumference is inaccessible.

Jorge Luis Borges
(La biblioteca de Babel)

7.1 Introduction

Fullerenes form a family of closed molecules composed entirely of carbon atoms. The smallest most stable fullerene is the C_{60} molecule known as Buckminsterfullerene in honor of the architect Richard Buckminster Fuller, who popularized such shapes for structural and architectonic purposes [Smalley *et al.*, 1985]. There are also fullerenes with larger and smaller number of carbons. However, these fullerenes are more unstable or produced with a lower probability, both, naturally or artificially. Small fullerenes are produced in laboratory [Milani, 1996] for the synthesis of carbon clathrates [San-Miguel and Toulemonde, 2005]. Bigger fullerenes, ranging from C_{70} to C_{90}, can be produced in several ways including C_{60} - C_{60} collisions [Rohmund *et al.*, 1996], laser irradiation [Hedén *et al.*, 2005] and atomic impact of highly ionized projectiles and high energies [Zettergren *et al.*, 2010].

C_{60} fullerenes are made of 12 pentagons and 20 hexagons. Each carbon atom is in the vertex of one pentagon and two hexagons. The C_{60} molecule has two bond lengths. On average, the bond length is 2.64 Bohr (1.4 Å).

As the C_{60} molecule is a truncated icosahedron, it is clear that they both have the same symmetry group S which is isomorphic to $A_5 \times S_2$. From S we can extract a subgroup of rotational symmetries R. The point group symbols for S and R are I_h and I. The 12 pentagons form 6 pairs of opposite faces. A rotation axis through the centres of two such faces is an axis of a 5-fold rotation. The 20 hexagons of the fullerene C_{60} form 10 pairs of opposite faces through the centres of which each have an axis of a 3-fold rotation. This 3-fold symmetry orientation will be used further on in this chapter.

Carbon fullerenes were first identified experimentally by Smalley and coworkers [Smalley *et al.*, 1985]. Their research aimed at reconstructing the conditions under which carbon molecules are formed in interstellar space and circumstellar shells. The characteristic signature of those molecules in interstellar medium (ISM) has been detected recently [Foing and Ehrenfreund, 1994; Cami *et al.*, 2010; Cami, 2012; Berne *et al.*, 2012; García-Hernández *et al.*, 2011].

Theoretical predictions for the existence of such molecules, go back to 1970 by Eiji Osawa (Japan)[Osawa *et al.*, 1993]. Also, independently, R. W. Henson (USA) and in 1973 Prof Bochvar (USSR) studied theoretically their chemical stability. All those works remained independent one of each other because they were published in Japan for the first one, never accepted for publication for the second and published in Russia only for the third.

Fullerenes are currently applied in cosmetics in anti-aging creams [Bakry *et al.*, 2007]. Since C_{60} molecules have a high electron affinity, they are used to absorb free radicals that are responsible for aging of the skin [Jensen *et al.*, 1996]. They are also candidates as mediators in photodynamic therapy [Mroz *et al.*, 2007]. The are commonly employed in organic photovoltaic (OPV) cells as electron-acceptor pairs [Fendrich *et al.*, 2006; Hong *et al.*, 2007; Huang *et al.*, 2009; Dutton *et al.*, 2010; Ren *et al.*, 2012]. The synthesis of diamonds from C_{60} has been experimentally demonstrated [Bocquillon *et al.*, 1993]. Amorphous diamond has been synthesize from C_{60} [Hirai *et al.*, 1994]. A fullerene

derivative, the [6,6]-phenyl-$C_6$1-butyric acid methyl ester (PCBM) is currently as a candidate for organic solar cells [Björström *et al.*, 2005]. Also they are of fundamental importance in fundamental research. In astrochemistry of interstellar medium, they are one of the exotic big carbon molecules formed in the particular conditions of space [Ehrenfreund and Foing, 1995; Leach, 1995; Sellgren, 2001; Cami, 2012; García-Hernández and Díaz-Luis, 2013].

Theoretically, the high level of symmetry (I_h), to be composed of a single species of atom and the availability of experimental results, has inspired a wealth of works, from structure to electronic properties, including the dynamical properties such as collisions in all sort of circumstances.

From the experimental point of view, fullerenes have been used as projectiles as well as the target. In the first case, C_{60} ions or neutrals are sent to collision against targets composed of various gases [Caldwell *et al.*, 1992]. A second approach, is the use of atomic ions impacting a gaseous environment of C_{60} [Majima *et al.*, 2002; Basir and Anderson, 1997; Rentenier, 2004]. Collisions of protons on C_{60} have been shown to induced single and double-electron capture [Martin, 2004]. Ions of C_{60}^{2+} fragment by emission of C_2 [Chen *et al.*, 2007; Martin *et al.*, 2008]. C_{60} - C_{60} collisions have been also experimentally explored [Shen *et al.*, 1995]. Fullerenes are often used in SIMS as projectiles [Weibel *et al.*, 2003; Klerk *et al.*, 2010; Smith *et al.*, 2011]

In all those cases, a rich set of phenomena can be present, such as: inelastic collisions, electron capture, fragmentation, collective ionization and even multifragmentation [Campbell, 2003]. All those effects are integrated experimentally, making its understanding a challenge. Also, it calls for a theoretical approach that could be able to discriminate the different effects under a very controlled environment.

In the case of ions as projectiles, two variants of projectiles are usually considered in the literature. First, slow but highly charged ions. Using them, it has been demonstrated that multiple-electron capture makes the C_{60} unstable and induces multi-fragmentation. The second variant is the use of single, double or triple ionized fast projectiles. This is the variant that will be explored in this chapter, using a single ionized lithium atom as projectile.

This study focuses on the interaction of a fast Li^+ impacting on a C_{60} molecule. For this, a bottom-up approach is proposed. First, we study the collision of an atom of lithium at 2 MeV with a single atom of carbon. The idea is to analyze for this two-nuclei system the probabilities of transfer of charge and kinetic energy. Second, the impact Li^+- C_{60} is studied. Both cases are studied in the framework of TDDFT and adiabatic LDA. Finally, the results obtained for C_{60} are correlated with those from the binary collision in order to extract a simplified model of the processes of charge transfer in the large system.

7.2 Li^+ at 2 MeV in Collision with a Single Carbon Atom

Before entering into the study of the collision with C_{60}, we start by considering the dynamics of the interaction between an atom of lithium at 2 MeV and a single carbon initially at rest. The purpose of this preliminary study is to obtain an initial idea about how such impact could effectively introduce a change in the state of charge for the carbon atom. In particular, we focus our attention on the possible transfer of kinetic energy and eventually also, changes in the charge state by charge transfer to the lithium or electron ejection from the carbon atom.

Atomic collisions in the MeV range, raise important questions that should be mentioned before any claim that could arise from our results.

At the most fundamental level, all moving charged particles produce magnetic fields. A more elaborate theory could include the Maxwell equations correctly coupled with a TDDFT KS scheme.

In general, we are not considering atomic impacts with exactly zero impact parameter or sufficiently small such that the interaction between nuclei goes beyond the Coulomb interaction. The justification is that in practice the probability of such events is negligible for molecules such as a C_{60} in gas phase, in the typical conditions of the experiments. DFT assumes in general that nuclei are point-like particles that interact only by a Coulomb potential.

The speed of light in atomic units is approximately 137; a lithium ion at 2 MeV has a velocity of approximately 3.43 au, which means that the velocity of the projectile is 2.5% of the speed of light. At such velocity, relativistic corrections could enter in consideration. However, the gain of mass is still marginal.

At the level of TDDFT, there are also theoretical considerations to expose. TDDFT works based on a Kohn-Sham set of orbitals that interacts with each other indirectly through an exchange-correlation functional. In our case, we use the so called adiabatic LDA (ALDA), that is the natural extension of LDA for time-dependent problems. The use of ALDA raises the traditional questions about the reliability of a local exchange and correlation. In the case of ALDA, the XC assumes that this functional operates only on the present values of density. Such assumptions should be questioned for rapidly changed densities during the small time compared with the electronic time scale on which that the ion crosses their target.

In the practical level, there are also some limitations. The TDDFT code used for this study makes use of norm-conserving pseudopotentials. Those pseudopotentials are used with two purposes, to reduce the number of electrons treated explicitly and to smooth the behavior of the potential close to the nuclei. Otherwise, treating all the electrons explicitly will increase the number of Kohn-Sham wavefunctions needed. The spacing of the mesh will need to be reduced to describe the potential and the nodes in the wavefunctions of the most internal states. All those elements increase significantly the effective memory requirements and the computational time needed for the simulation.

At 2 MeV, the energy of the collision is high enough to excite the lowest

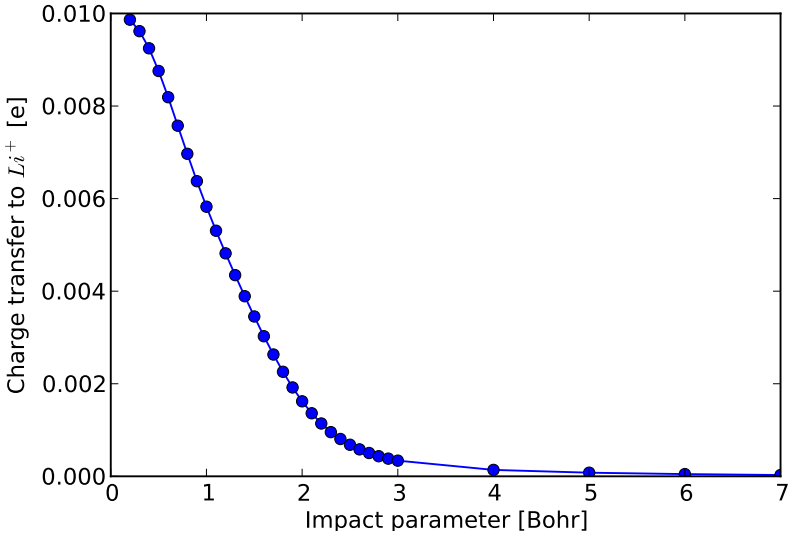

Figure 7.1: Charge transfer to the Li^+after the collision with a single carbon atom. The kinetic energy of the projectile is 2 MeV. The charge is measure by integrating the density on a sphere of 4.5 Bohr centered on the Li atom

levels of both target and projectile. The approach proposed is to freeze those low-level states and phenomena such as Auger electrons are missing in the present approach.

Also important, is the fact that those pseudopotentials smooth the potential close to the nuclei until a certain radius where it matches with the all-electron potential in the frontier of a sphere around each nuclei. The problem arises when the collision is such that the distance between ions is small enough that spheres of two atoms overlap. Also the finite size of the simulation box could be a source of error, that is the reason why large boxes are used in for this simulation. In this particular case absorbing boundaries were used using a $\sin^2$ imaginary potential to absorb the scattered electronic wavefunction. This procedure is not a perfect absorbing boundary, due to this, a large simulation box is still used.

For the simulation of a Li^+- C collision, the impact parameter was varied from 0.1 to 8 Bohr. The simulation box is a parallelepiped and its size was adjusted such that both, projectile and target are distant 10 Bohr from any border. The initial distance between the two atoms is 12 Bohr considering the planes perpendicular to the propagation direction that contain the two atoms.

Due to the high kinetic energy of the projectile, the amount of kinetic energy transferred to the carbon is lower than 1 meV. The projectile is deflected less than 10^{-3} rad for all the impact parameters. In the figure 7.1 the charge transfer is plotted as a function of the impact parameter. The maximal value of charge transfer to the carbon, saturates to 0.011 [e] in the limit of direct impact.

From the simulations with the binary collision, we can expect that a similar behavior is present in the collision with the entire C_{60} molecule. The projectile, for example, should be deflected a negligible amount when it crosses the molecule. After the impact, no significant movement of the target is expected. The fragmentation, in the context of our simulations is not due to a direct transfer of kinetic energy, but probably by instabilities when the C_{60} becomes ionized. However, the experimental results show that the fragmentation by ionization is relevant only starting from a double ionization. Lets now to consider the problem of the collision of $Li^+$with the entire molecule of fullerene.

7.3 Li^+at 2 MeV in Collision with C_{60}

The Li^+- C_{60} collision present some challenges compared with the binary collision. The system contain a total of 362 electrons. This value is reduced to 240 by using norm-conserving pseudopotentials for carbon and lithium. The system is treated without spin polarization. This also reduces the total number of Kohn-Sham states to 120. The Li projectile has no KS orbital associated to it.

The simulation box is a parallelepiped with 40 Bohr length along the direction of propagation and 36 Bohr on the directions perpendicular to the direction of propagation. The direction of propagation of the projectile is parallel to the x axis. The fullerene is positioned in such a way that the center of mass of the C_{60} molecule is located in $(6, 0, 0)$ Bohr. For the pseudopotential used (FHI), the Li projectile has no Kohn-Sham states associated to it, the x coordinate for the initial conditions of the projectile can be located in the boundary of the simulation box ($x = 20$ Bohr).

This geometrical configuration, ensures that the distance between the plane of the projectile and the center of mass of the C_{60} target is 14 Bohr. As the C_{60} molecule has a typical radius of 6.7 Bohr, the projectile will be at least 7.3 Bohr far from the closest carbon in the initial step.

The C_{60} fullerene is a very symmetric molecule. However, there are many possible orientations for the impact of one atom on the molecule. For the purpose of this work, we select two particular orientations, one completely random orientation and the other along one of the symmetry axis of the C_{60}. For the second orientation, two hexagons are parallel and perpendicular to the direction of propagation. This orientation is three-fold symmetric in the axis of propagation. For each orientation of C_{60} the ground state is computed by DFT until the relative difference in the density in successive cycles is less than 10^{-8}.

For the non-symmetric orientation (Up on fig. 7.2), 189 initial conditions were chosen. For the symmetric orientation (Down on fig. 7.2), 180 initial conditions are present.

For each orientation and each initial position of the projectile, the $Li^+$is propagated until it crosses completely the C_{60}. At the end of the simulation, the plane perpendicular to the direction of propagation is $x = -14$. The distance between this plane and the closest carbon atom is 13.3 Bohr. In all

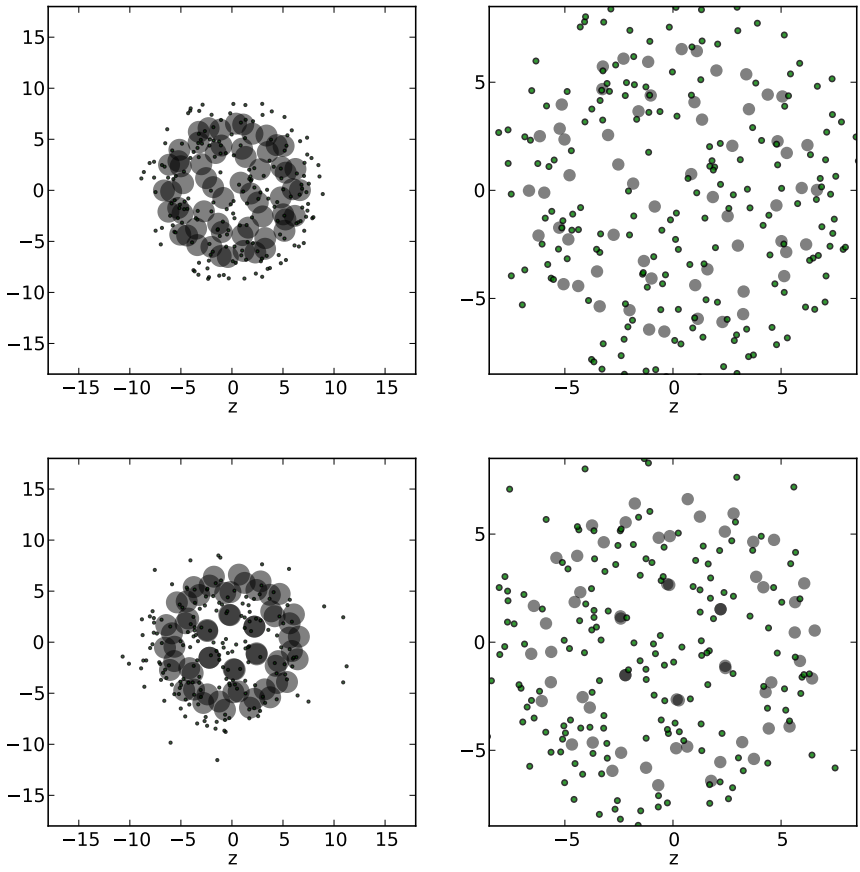

Figure 7.2: Initial conditions for the Li^+. The locations of the carbon atoms are projected in the background. The figure in the left side shows the system in the scale of the simulation box considered of 36 Bohr each side. The figure in the right side shows a closer view of the initial conditions. The gray circles indicate the projections of the carbon atoms in the yz plane. The small green dots are the randomly selected initial positions for the Li^+projectile. Up: Non-symmetric orientation. Down: Symmetric orientation

the cases considered, the charge-transfer value is stable when the projectile reaches the $x = -14$ plane.

The time step was fixed in 0.005 au and each initial condition was propagated for 2000 iterations. The total energy is relatively stable all along the simulation, with an average of 0.15 Ha of deviation from the initial total energy.

After each collision, the charge associated to the lithium was measured by integrating it inside a sphere of radius 4 Bohr.

7.4 Results and Discussion

As was expected from the analysis with $Li^+$and C, the deflection of the projectile is negligible: less than 1 mrad on average for all the initial conditions. It is fair to assume that the projection of the initial condition on the perpendicular plane is consistent with the actual trajectory of the projectile, not only out of the cage, but also when it enters inside the molecule. With this assumption, the charge transfer to the projectile can be mapped according with its initial position in the plane yz.

The figure 7.3 shows the values of charge transfer interpolated on the plane yz. For the interpolation, a 1000×1000 grid is produced in the range $(-11, 11)$ in the plane yz. The values in the mesh are interpolated using a Clough-Tocher piecewise cubic, continuously differentiable (C1), and approximately curvature-minimizing polynomial surface [Alfeld, 1984].

The charge transfer process is lower through the holes in the fullerene. It is significantly higher in the bonds and close to each carbon. The maximal charge transfer is 0.016 e. This value is close to the maximal charge transfer obtained in the single Li^+- C collision (0.011 e).

We can assume that the charge transfer is mostly due to one electron being transferred to the lithium. Using the interpolated values we can compute the capture cross section. For the non-symmetric case the value is $5.4 \times 10^{-17}\text{cm}^2$, while for the symmetric orientation is $5.2 \times 10^{-17}\text{cm}^2$. The values are smaller than the geometrical cross section of around $1.9 \times 10^{-16}\text{cm}^2$, indicating that most of the charge transfer is produced inside the cage as mentioned before. The values are considerably higher than the experimental results of $1.6 \times 10^{-18}\text{cm}^2$ for the one electron transfer. In this case, we encounter the known result that TDDFT usually overestimates charge transfer [Jamorski *et al.*, 2002; Dreuw and Head-Gordon, 2004]. Introducing self-interaction correction could help in this case. It also remains to be explored, if the lack of a dynamical description of the $1s$ orbital, for the Li atom, is also responsible for the overestimation. The $1s$ state for the lithium atom is frozen in the pseudopotential not allowing for processes where the projectile becomes even more ionized ($Li^+ \rightarrow Li^{2+}$) and ($Li^+ \rightarrow Li^{3+}$).

In the experiments, a lithium could cross the C_{60} without capture but ionizing the C_{60} molecule. This event has a significantly high cross section ($5 \times 10^{16}\text{cm}^2$).

Apart from global quantities such as the cross section, some information can be extracted from the individual impacts, and their dependency with the configuration space. The different impacts can be grouped according to the

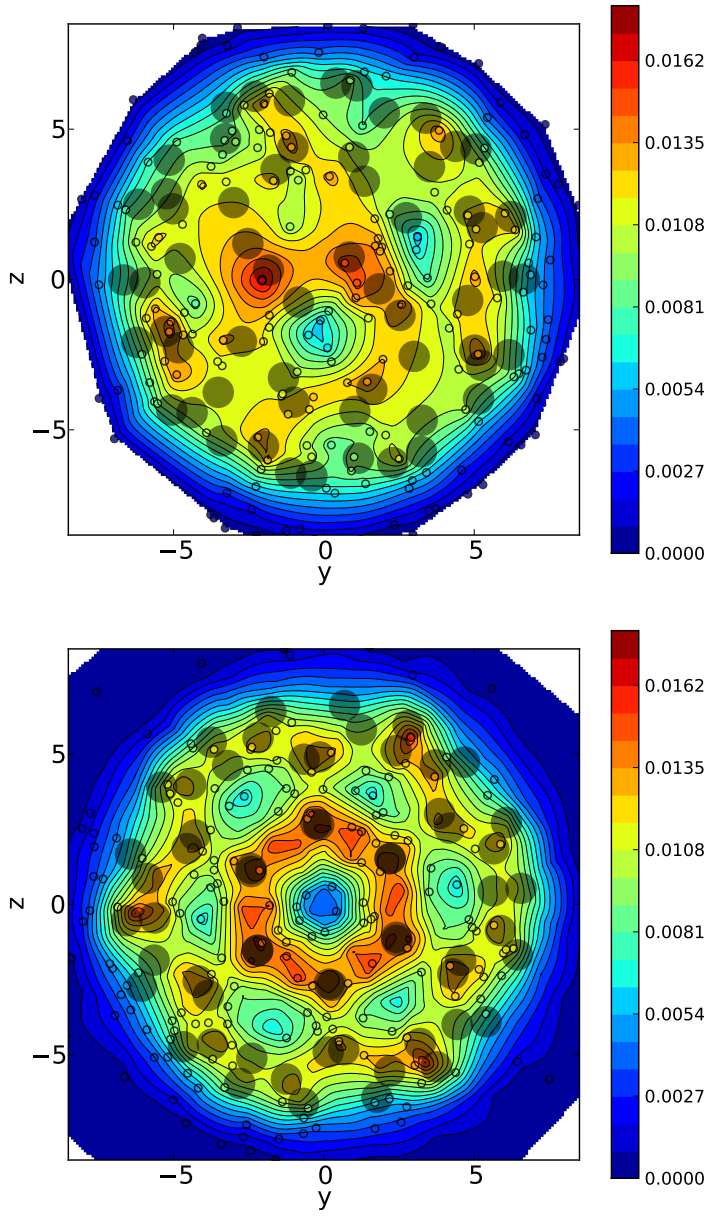

Figure 7.3: Symmetric orientation: Charge transfer interpolated from the random selected initial conditions for the Li^+projectile. A cubic interpolation was used (see text). The color indicates the amount of charge transfer for an projectile that is projected in that particular point in the yz plane. The values are in fractions of the one electron charge. Up: Non-symmetric orientation. Down: Symmetric orientation

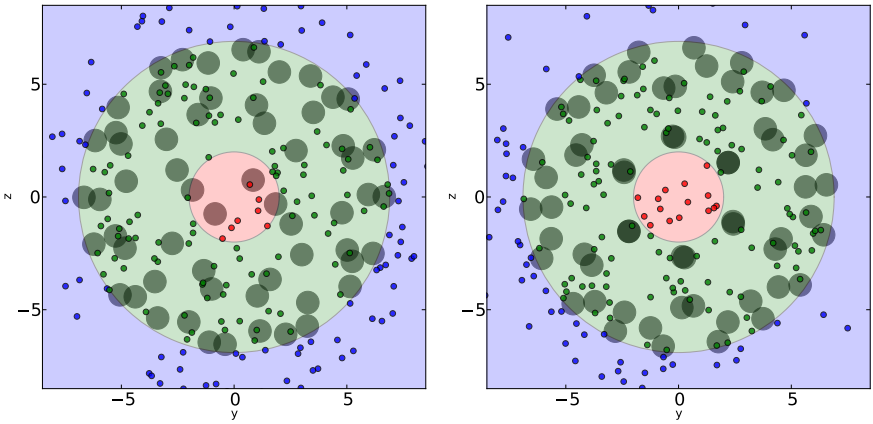

Figure 7.4: The different impacts grouped by the radius to the central axis of the C_{60}. The blue region are external collisions. The green collects most of the internal collisions, with the exception of the very central red region where there is a hole in the symmetrical orientation. The left side shows the non-symmetric orientation, the right side the symmetric one.

radius with the central axis of the C_{60}. In particular the collision that enter in the cage can be differentiated from those that crosses out the molecule. For both orientations the regions are shown in fig. 7.4

Using the colouring schema in 7.4 for the three regions, the charge transfer to the projectile can be plotted as a function of the minimal perpendicular distance from any carbon atom to the trajectory of the Li projectile. From figure 7.5 is clear that collisions that enter in the cage has an enhanced probability of capture charge compare with collisions that crosses outside of the cage even if the distance to the closest carbon is small. That effect is even more evident for the symmetric orientation where the impacts in the central hole capture much more charge that close non-penetrating collisions.

7.5 Independent Charge Transfer Model

It is possible to correlate the results obtained for the Li^+- C_{60} collision with the previous results for the Li^+- C collision. Consider two ansatz for the charge transfer process. It is clear from the figure 7.1 that most of the charge is transferred with the minimal impact parameter. It is logical to make a guess, that most of the contribution to the charge being transferred to the lithium atom comes from its encounter with the closest carbon atom during the collision. The charge really transferred to the lithium can be compared with the one atom contribution. The figures 7.6 shows those correlations for both the non-symmetric and symmetric orientations. Some interesting observations arise. As could be expected, assuming one atom contribution tends to systematically underestimate the charge transfer. However, for external collisions (blue dots)

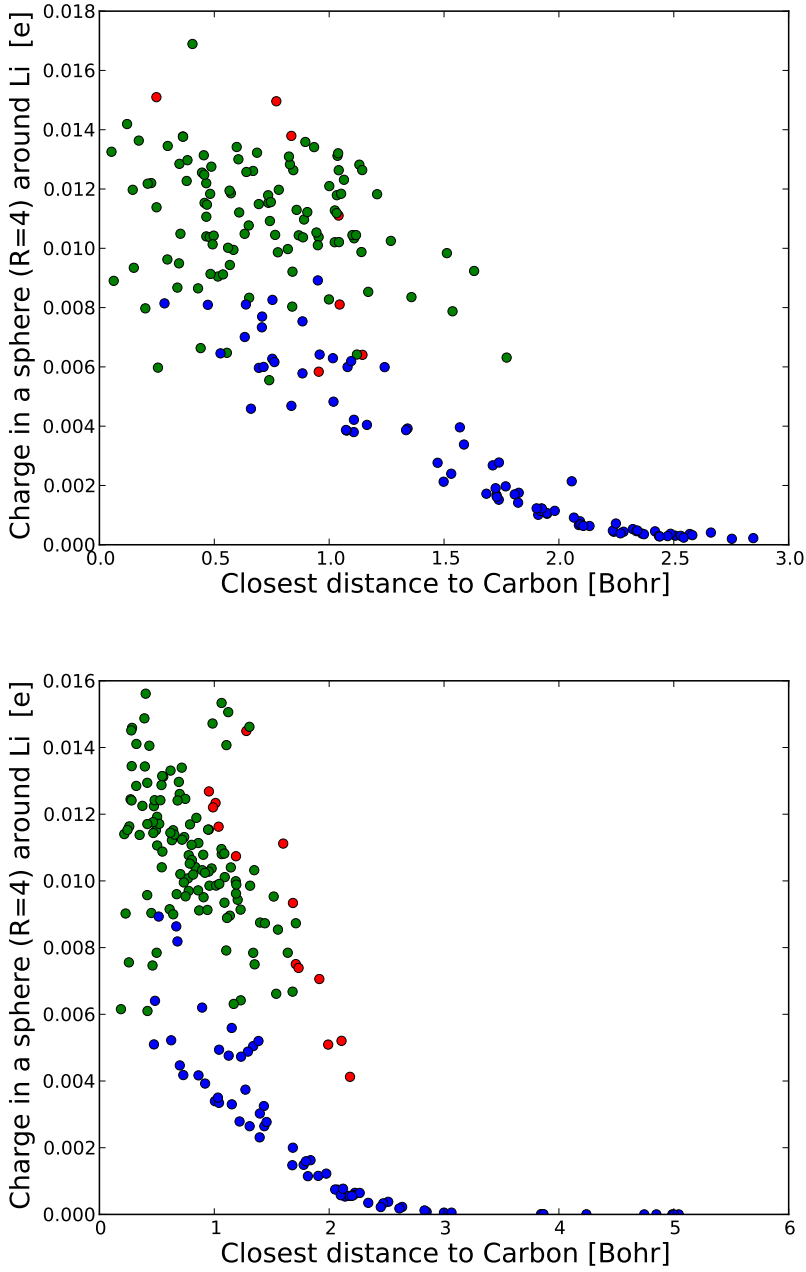

Figure 7.5: Charge transfer in the Li^+- C_{60} collision as a function of the minimal perpendicular distance from any carbon atom to the trajectory of the Li projectile. Up: Non-symmetric orientation. Down: Symmetric orientation.

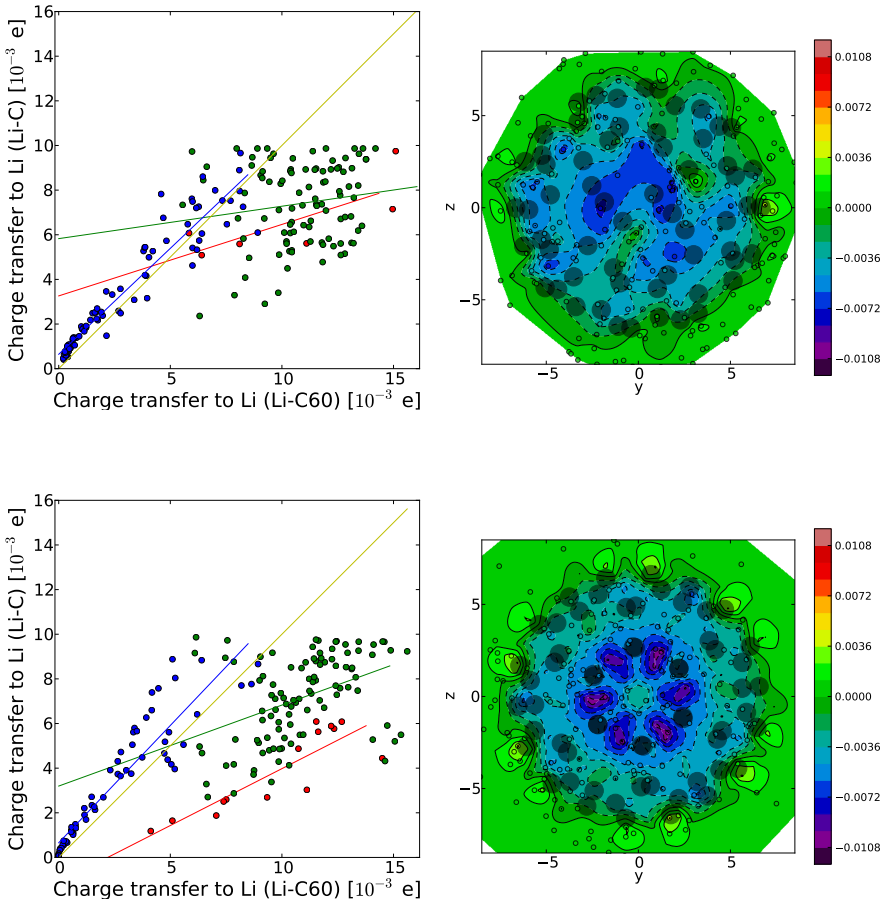

Figure 7.6: Correlation between the charge transfer in the Li^+- C_{60} and the charge transfer by the closest atom in the Li^+- C collision. Up: Non-symmetric orientation. Down: Symmetric orientation.

this ansatz is closer to the actual transfer.

The second possible ansatz is somehow the complementary to the first one: one assumes that the charge transfer is produced by individual contributions from all the carbon atoms to the lithium, using the perpendicular distance to the trajectory to account for the charge that is transferred. In this case, the charge transfer is systematically overestimated for the three regions, but with a remarkable alignment of most of the points. In particular, the external collisions and the internal ones are aligned. The exception is constituted by the central points in the symmetric orientation. Using the least square method for the external collisions, the slope can be determined. The value of the slope is 2.38 for the non-symmetric orientation and 2.54 for the symmetric one. The good correlation of the data allow to present a simplified model for the charge transfer in fullerene cages. The charge that is transferred can be computed

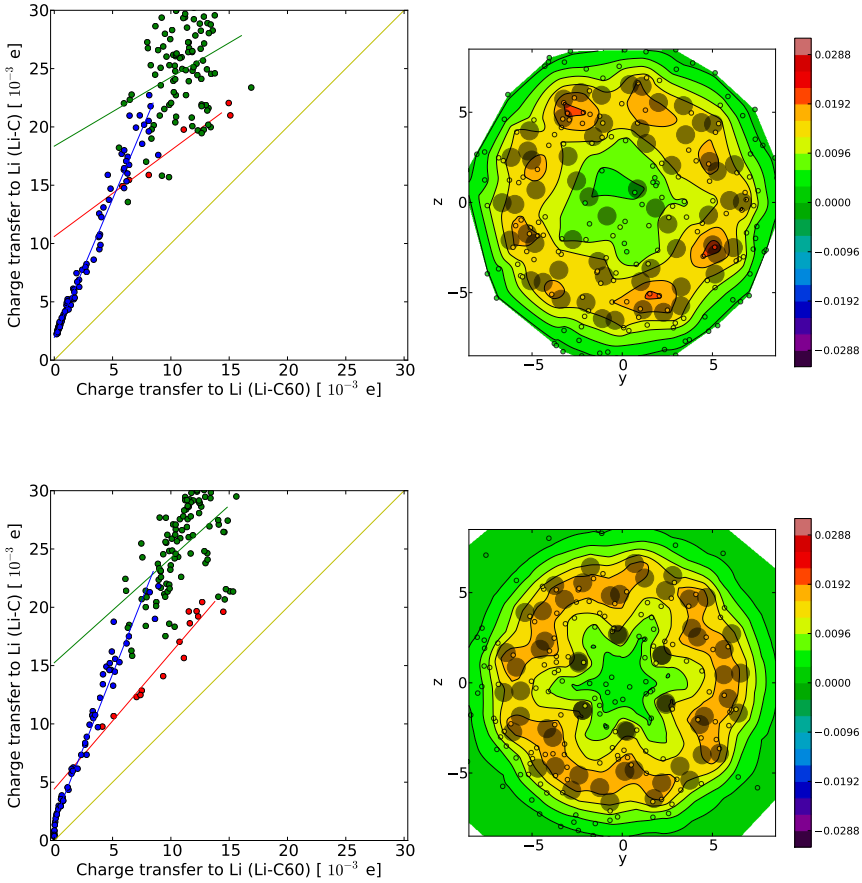

Figure 7.7: Correlation between the charge transfer in the Li^+- C_{60} and the sum of all the contributions to the charge transfer using the perpendicular distance to the trajectory to determine the value from 7.1. Up: Non-symmetric orientation. Down: Symmetric orientation.

using 7.1 weighted by a "screening factor", the inverse of the slope, that is dependent of the orientation of the molecule. The screening factor has its origin in the bonds created between the carbon atoms in the C_{60} molecule and reduces the capture compared with an isolated atom.

7.6 Conclusions

In this chapter, we have presented simulations of fast ions impacting molecules. The particular case treated, was a 2 MeV Li^+ion impacting on a C_{60} molecule. From all possible orientations for the C_{60} molecule two were chosen: a random, non-symmetrical and one molecule with two parallel hexagons perpendicular to the trajectory. The simulations show an overestimation of the charge transfer

compared with experimental results. Two simplified models were proposed to analyze the charge transfer assuming independent contributions from the carbon atoms in the cage. The correlations of those models show that charge transfer processes can be understood by individual contributions screened by a global factor that reduces the electron transfer.

8

Summary, Conclusions and Perspectives

> A good scientist is a person with original ideas. A good engineer is a person who makes a design that works with as few original ideas as possible. There are no prima donnas in engineering.
>
> Freeman Dyson

Time-dependent density functional theory is an interesting method to describe exactly (in principle) the evolution of atomic particles in collision. The electronic density offers an elegant alternative to the explicit solution of a many-body quantum system. All the many-body effects are included in the theory through the exchange-correlation potential. This exchange-correlation potential, even if exact in its formulation, needs to be approximated. For time-dependent problems considered in this thesis, this approximation is local in both, time and space.

The main objective of this thesis was to explore the limits of the approximations done in TDDFT to describe charge transfer processes in fast atomic collisions. In particular, the focus of the thesis was in the kind of problems that are beyond the present capabilities of atomic physics wavefunction based methods.

In chapter 2, we have presented some applications that motivate the study of atoms impacting molecules, clusters or surfaces. It shows the relevance for going beyond the atomic physics methods for dealing with such problems.

In chapter 3, a brief account of the methods was presented. We explored some methods to describe the electronic structure and how to couple that with the movement of atoms. Some attention was dedicated to the method of choice for this work, time-dependent density functional theory.

There are several methods in the literature to account for charges in a system. Those methods are not always well suited for dynamical processes. The chapter 4 explores some of those methods, describing their limitations in

atomic collisions.

In chapter 5, the first application was shown; the collision of a proton with a Helium atom. The results show good agreement with several experiments done for such systems.

When the static ground state of a system is used as the initial condition for propagation in TDDFT, some artifacts appear. The chapter 6 presents the velocity phase factor to correctly prepare the ground state of a moving particle once the static ground state was computed. The method is exact only for local potentials. The effect of the non-locality of the pseudopotentials is discussed and the limits of our approach are presented.

In chapter 7.5, a more challenging problem was addressed; the impact of a 2 MeV $Li^+$with a molecule of C_{60}. The challenge comes from the large number of atoms involved, and the large space of configurations of this system. The results show that the collisions where the projectile enters in the C_{60} cage can be modeled by charge transfer contributions from all the atoms in the target, weighted by a factor specific for the system and dependent of the orientation of the target.

Apart from the applications shown in the last two chapters, we are exploring the use of TDDFT on another challenging system.

8.1 Work in Progress

The big practical advantage of a collision at 2 MeV is that the speed of the projectile is fast enough to produce results in a reasonable amount of computational time. There is, however, a large gap between the kind of collisions that could be considered in the adiabatic regime and those fast collisions in the MeV range.

One application in the intermediate regime is the perpendicular collision of a neutral He atom with a surface of graphene. Graphene is a remarkable material and its properties can be used in a whole new generation of nano electronics.

The idea is the study of a collision of light atoms with a layer of graphene. At 10 keV the projectile has enough energy to induce not only charge transfer but also create topological defects that could induce changes in the transport properties as was recently studied [Lherbier *et al.*, 2011, 2012].

To study the problem we consider a piece of graphene containing 72 carbon atoms. The figure 8.1 shows the atomic configuration of the piece of graphene. Hydrogen atoms are attached to the boundaries.

The big advantage of this system is the significant reduction in the configuration space. Experimentally, the graphene sample can be aligned to be perpendicular to the direction of impact. The internal symmetries of the graphene reduce the different initial conditions to the small triangle shown on 8.1. As the He is represented with one state, the velocity phase factor is used to correctly prepare the state that will be propagated.

There are two main limitations for this kind of systems: The computational time necessary for the propagation and the fact that the simulation is not done using periodic boundary conditions.

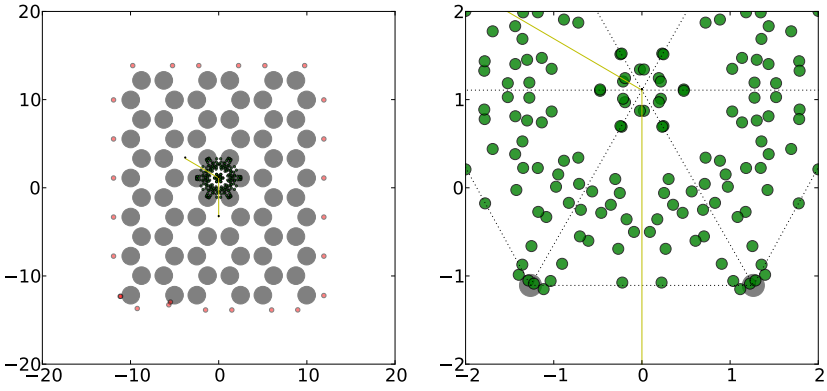

Figure 8.1: Initial atomic configuration to study the collision of a He atom with graphene. The gray circles represent the carbon atoms, the small red dots represent the hydrogen atoms used to close the boundaries of the graphene. The green circles represent the projections of the initial conditions for the He atom.

8.2 Perspectives

This work opens several opportunities and challenges for further investigation.

At the most fundamental level, time-dependent density functional theory will be always limited by the quality of the exchange-correlation potential. Fast atomic collisions induce rapid changes in the density with time, and also with important gradients of the density. The adiabatic LDA is used far beyond its theoretical justification and the fact that it is able to show reasonable results is remarkable. Further exploration, with better exchange-correlation potentials could in principle provide better quantitative results in the future.

At the practical level, the use of real space mesh presents advantages compared with localized basis sets, in particular the possibility to describe non-bounded states that are poorly described with localize basis sets. However, the size of the simulation box is a big limitation for the scalability of this kind of simulations. Also the spacing of the mesh is particularly critical during the collision. In the future this kind of simulation could be done more efficiently using dynamical meshes or submeshes that move with the moving particles. Also the use of non-uniform time steps can be better adapted during the close interaction between projectile and target.

Appendices

A

Implementation of Velocity Phase Factor in Octopus

The velocity phase factor (VPF) was implemented inside the routine `td.F90` before the loop of the time-dependent propagation. At present, it only supports the VPF for a purely local Hamiltonian. This condition is not checked and remains for the user to be aware of such limitation. Also the moving particles should be separated enough between them and the parameters that limits the application of the phase should no overlap. This condition also is not checked and it is for the final user to enforce such condition.

From the user point of view, three variables control the operation of the velocity phase factor:

- `VPF_VelocityPhaseFactor`
- `VPF_Radius`
- `VPF_Slope`

The variable `VPF_VelocityPhaseFactor` controls if the VPF is used and how it should operate. Its value is an integer from 0 to 3. The default value 0 means that the VPF is not applied. Identical effect is produced if the value is different from 0 but the atoms described in the input file has not initial velocity.

A value equal to 1 means that a radial sigmoid is used. In this case the other variables `VPF_Radius` and `VPF_Slope` are used to determine the extension and sharpness of the sigmoid. This option implements the following expression

$$\Phi(\mathbf{r})_v = \Phi(\mathbf{r})_0 \prod_{\tau=1}^{M} e^{i\mathbf{v}_\tau\cdot(\mathbf{r}-\mathbf{r}_\tau)\ S(\mathbf{r}-\mathbf{r}_\tau)}, \tag{A.1}$$

where $S(\mathbf{r}-\mathbf{r}_\tau)$ is the sigmoid

$$S(\mathbf{r}-\mathbf{r}_\tau) = 1-(1+e^{-\alpha(|\mathbf{r}-\mathbf{r}_\tau|-r_{cut})})^{-1}. \tag{A.2}$$

The value of r_{cut} is given by `VPF_Radius` and the value of α by `VPF_Slope`.

A value of `VPF_VelocityPhaseFactor` equal to 2 means a planar Heaviside function.

$$\begin{aligned}\Phi(\mathbf{r})_v &= \Phi(\mathbf{r})_0 \prod_{\tau=1}^{M} \exp\left[i\mathbf{v}_\tau \cdot (\mathbf{r}-\mathbf{r}_\tau)\,(1 - H(\hat{v}\cdot(\mathbf{r}-\mathbf{r}_\tau) - r_{cut})\right) \\ &\quad + i|\mathbf{v}_\tau| r_{cut}\, H(\hat{v}\cdot(\mathbf{r}-\mathbf{r}_\tau) - r_{cut})] \end{aligned} \tag{A.3}$$

where the $H(\hat{v}\cdot(\mathbf{r}-\mathbf{r}_\tau) - r_{cut})$ is the Heaviside step function

$$H(x) = \int_{-\infty}^{x} \delta(s)\,\mathrm{d}s \tag{A.4}$$

In this case only `VPF_Radius` is used to set r_{cut}

The final value is 3, a planar sigmoid in the forward direction to the propagation, where $H(\hat{v}\cdot(\mathbf{r}-\mathbf{r}_\tau) - r_{cut})$ is replaced by the sigmoid $S(\hat{v}\cdot(\mathbf{r}-\mathbf{r}_\tau) - r_{cut})$. Again, the value of r_{cut} is given by `VPF_Radius` and the value of α by `VPF_Slope`.

Bibliography

Alfeld, P. (1984), *"A trivariate clough—tocher scheme for tetrahedral data,"* Computer Aided Geometric Design **1** (2), 169 .

Allen, M. P., and D. J. Tildesley (1989), *Computer simulation of liquids* (Oxford university press).

Amaldi, U., and S. Braccini (2011), *"Present challenges in hadrontherapy techniques,"* Euro. Phys. J. Plus **126** (7), 1.

Anders, E., and M. Ebihara (1982), *"Solar-system abundances of the elements,"* Geochimica et Cosmochimica Acta **46** (11), 2363 .

Andrade, X., A. Castro, D. Zueco, J. L. Alonso, P. Echenique, F. Falceto, and A. Rubio (2008), *"A modified Ehrenfest formalism for efficient large-scale ab initio molecular dynamics,"* ArXiv .

Andrade, X., A. Castro, D. Zueco, J. L. Alonso, P. Echenique, F. Falceto, and Á. Rubio (2009), *"Modified Ehrenfest Formalism for Efficient Large-Scale ab initio Molecular Dynamics,"* Journal of Chemical Theory and Computation **5** (4), 728.

Aumayr, F., and H. Winter (1985), *"Total single-electron-capture cross sections for impact of* H^+*,* H_2*,* He^+*, and* Ne^+ *(2 ˘ 20 keV) on Li,"* Phys. Rev. A **31**, 67.

Avendaño-Franco, G., B. Piraux, M. Grüning, and X. Gonze (2012), *"Time-dependent density functional theory study of charge transfer in collisions,"* Theo. Chem. Acc. **131** (11), 1.

Bader, R. F. W. (1990), *"Atoms in Molecules: A Quantum Theory, International Series of Monographs on Chemistry 22,"* .

Bakry, R., R. M. Vallant, M. Najam-ul Haq, M. Rainer, Z. Szabo, C. W. Huck, and G. K. Bonn (2007), *"Medicinal applications of fullerenes,"* International journal of nanomedicine **2** (4), 639.

Barnett, C. F., and H. K. Reynolds (1958), *"Charge Exchange Cross Sections of Hydrogen Particles in Gases at High Energies,"* Phys. Rev. **109**, 355.

Basir, Y., and S. L. Anderson (1997), *"Collisions of rare gas ions with* C_{60}*: Endohedral formation, energy transfer, and scattering dynamics,"* J. Chem. Phys. **107** (20), 8370.

Belkić, D. c. v. (1978), *"A quantum theory of ionisation in fast collisions between ions and atomic systems,"* J. Phys. B-At Mol. Opt. **11** (20), 3529.

Belkić, D. c. v. (2010), *"Review of theories on ionization in fast ion-atom collisions with prospects for applications to hadron therapy,"* Journal of Mathematical Chemistry **47** (4), 1366.

Belkić, D. c. v., R. Gayet, and A. Salin (1979), *"Electron capture in high-energy ion-atom collisions,"* Physics Reports **56** (6), 279.

Belkić, D. c. v., Mancev, Ivan, and J. Hanssen (2008), *"Four-body methods for high-energy ion-atom collisions,"* Rev. Mod. Phys. **80**, 249.

Berne, B. J., G. Cicootti, and D. F. Coker (1998), *Classical and quantum dynamics in condensed phase simulations* (World Scientific).

Berne, O., G. Mulas, and C. Joblin (2012), *"Interstellar C60+,"* arXiv:1211.7252 , 0.

Berrondo, M., and O. Goscinski (1975), *"Energy as a functional of the density matrix,"* Int J. Quantum Chem. **9** (S9), 67.

Björström, C. M., A. Bernasik, J. Rysz, A. Budkowski, S. Nilsson, M. Svensson, M. R. Andersson, K. O. Magnusson, and E. Moons (2005), *"Multilayer formation in spin-coated thin films of low-bandgap polyfluorene:PCBM blends,"* Journal of Physics: Condensed Matter **17** (50), L529.

Bocquillon, G., C. Bogicevic, C. Fabre, and A. Rassat (1993), *"C60 fullerene as carbon source for diamond synthesis,"* The Journal of Physical Chemistry **97** (49), 12924.

Born, M., and R. Oppenheimer (1927), *"Zur Quantentheorie der Molekeln,"* Annalen der Physik **84**, 457.

Bragg, W. H., and R. Kleeman (1905), *"XXXIX. On the particles of radium, and their loss of range in passing through various atoms and molecules,"* Philosophical Magazine Series 6 **10** (57), 318.

Bransden, B., and C. Joachain (2003), *Physics of Atoms and Molecules*, Pearson Education (Prentice Hall).

Bransden, B., and R. McDowell (1992), *Charge Exchange and the Theory of Ion-atom Collisions*, International series of monographs on physics (Oxford University Press, Incorporated).

Brunger, M. J., and S. J. Buckman (2002), *"Electron-molecule scattering cross-sections. I. Experimental techniques and data for diatomic molecules,"* Physics Reports **357** (3 - 5), 215.

Buffa, F. (2009), in *Radiotherapy and Brachytherapy*, NATO Science for Peace and Security Series B: Physics and Biophysics, edited by Y. Lemoigne and A. Caner (Springer Netherlands) pp. 3–9.

Burke, P. (1993), *"Electron-atom scattering theory and Calculations,"* Adv. Atom. Mol. Opt. Phy. **32**, 39.

Caldwell, K. A., D. E. Giblin, and M. L. Gross (1992), *"High-energy collisions of fullerene radical cations with target gases: capture of the target gas and charge stripping of C_{60}^+, C_{70}^+, and C_{84}^+,"* Journal of the American Chemical Society **114** (10), 3743.

Cameron, A. (1973), *"Abundances of the elements in the solar system,"* Space Science Reviews **15** (1), 121.

Cameron, A. E., and J. D. F. Eggers (1948), *"An Ion "Velocitron","* Review of Scientific Instruments **19** (9), 605.

Cami, J. (2012), *"Fullerenes in circumstellar and interstellar environments,"* arXiv , 0.

Cami, J., J. Bernard-Salas, E. Peeters, and S. E. Malek (2010), *"Detection of C60 and C70 in a Young Planetary Nebula,"* Science **329** (5996), 1180.

Campbell, E. (2003), *Fullerene collision reactions*, Vol. 5 (Kluwer Academic Pub).

Car, R., and M. Parrinello (1985), *"Unified Approach for Molecular Dynamics and Density-Functional Theory,"* Phys. Rev. Lett. **55**, 2471.

Castro, A., M. A. L. Marques, and A. Rubio (2004), *"Propagators for the time-dependent Kohn–Sham equations,"* J. Chem. Phys. **121** (8), 3425.

Chen, L., S. Martin, J. Bernard, and R. Brédy (2007), *"Direct Measurement of Internal Energy of Fragmented C60,"* Phys Rev Lett **98**, 193401.

Currell, F. J. (2003), *The Physics of Multiply and Highly Charged Ions: Volume 1: Sources, Applications and Fundamental Processes* (Springer).

Dalgarno, A. (1967), *"Atom-Atom Collision Processes in Astrophysics: Theoretical Studies,"* Rev. Mod. Phys. **39**, 850.

Dalgarno, A. (2006), *"The galactic cosmic ray ionization rate,"* P. Natl. Acad. Sci. USA **103** (33), 12269.

De Giovannini, U., D. Varsano, M. A. L. Marques, H. Appel, E. K. U. Gross, and A. Rubio (2012), *"Ab initio angle- and energy-resolved photoelectron spectroscopy with time-dependent density-functional theory,"* Phys. Rev. A **85**, 062515.

Delcorte, A., J. Bour, F. Aubriet, J.-F. Muller, and P. Bertrand (2003), *"Sample Metallization for Performance Improvement in Desorption/Ionization of Kilodalton Molecules: Quantitative Evaluation, Imaging Secondary Ion MS, and Laser Ablation,"* Analytical Chemistry **75** (24), 6875.

Delcorte, A., S. Yunus, N. Wehbe, N. Nieuwjaer, C. Poleunis, A. Felten, L. Houssiau, J.-J. Pireaux, and P. Bertrand (2007), *"Metal-Assisted Secondary Ion Mass Spectrometry Using Atomic (Ga+, In+) and Fullerene Projectiles,"* Analytical Chemistry **79** (10), 3673.

Dirac, P. A. M. (1930), *"Note on Exchange Phenomena in the Thomas Atom,"* Math. Proc. Cambridge **26**, 376.

Dreuw, A., and M. Head-Gordon (2004), *"Failure of Time-Dependent Density Functional Theory for Long-Range Charge-Transfer Excited States: The ZincbacteriochlorinBacteriochlorin and BacteriochlorophyllSpheroidene Complexes,"* Journal of the American Chemical Society **126** (12), 4007.

Dreuw, A., J. L. Weisman, and M. Head-Gordon (2003), *"Long-range charge-transfer excited states in time-dependent density functional theory require non-local exchange,"* J. Chem. Phys. **119** (6), 2943.

Drukker, K. (1999), *"Basics of Surface Hopping in Mixed Quantum/Classical Simulations,"* Journal of Computational Physics **153** (2), 225 .

DuBois, R. D. (1985), *"Charge transfer and ionization of lithium by protons and helium ions,"* Phys. Rev. A **32**, 3319.

DuBois, R. D., and L. H. Toburen (1985), *"Electron capture by protons and helium ions from lithium, sodium, and magnesium,"* Phys. Rev. A **31**, 3603.

Dutton, G. J., W. Jin, J. E. Reutt-Robey, and S. W. Robey (2010), *"Ultrafast charge-transfer processes at an oriented phthalocyanine/C_{60} interface,"* Phys. Rev. B **82**, 073407.

Ehrenfreund, P., and B. Foing (1995), *"Search for fullerenes and PAHs in the diffuse interstellar medium,"* Planetary and Space Science **43** (10-11), 1183 .

Eichler, J. (1990), *"Theory of relativistic ion-atom collisions,"* Physics Reports **193** (4–5), 165 .

Engel, E., R. M. Dreizler, E. Engel, and R. M. Dreizler (2011), in *Density Functional Theory*, Theoretical and Mathematical Physics (Springer Berlin Heidelberg) pp. 307–349, 10.1007/978-3-642-14090-7.

Esposito, S. (2005), *"Again on Majorana and the Thomas-Fermi model: a comment to physics/0511222,"* arXiv:physics/0512259 .

Fainstein, P. D., V. H. Ponce, and R. D. Rivarola (1988), *"A theoretical model for ionisation in ion-atom collisions. Application for the impact of multicharged projectiles on helium,"* J. Phys. B-At Mol. Opt. **21** (2), 287.

Fendrich, M., T. Wagner, M. Stöhr, and R. Möller (2006), *"Hindered rotation of a copper phthalocyanine molecule on* C_{60}*: Experiments and molecular mechanics calculations,"* Phys. Rev. B **73**, 115433.

Fermi, E. (1927), *"Un Metodo Statistico per la Determinazione di alcune Prioprietà dell'Atomo,"* Rend. Accad. Naz. Lincei **6**, 602.

Field, G. B., D. W. Goldsmith, and H. J. Habing (1969), *"Cosmic-Ray Heating of the Interstellar Gas,"* Astrophys. J. Lett. **155**, L149.

Fock, V. (1930), *"Näherungsmethode zur Lösung des quantenmechanischen Mehrkörperproblems,"* Zeitschrift für Physik **61**, 126.

Foing, B. H., and P. Ehrenfreund (1994), *"Detection of two interstellar absorption bands coincident with spectral features of C60+,"* Nature **369** (6478), 296.

Fuchs, M., and M. Scheffler (1999), *"Ab initio pseudopotentials for electronic structure calculations of poly-atomic systems using density-functional theory,"* Computer Physics Communications **119** (1), 67 .

García-Hernández, D., and J. Díaz-Luis (2013), *"Diffuse interstellar bands in fullerene planetary nebulae: the fullerenes - diffuse interstellar bands connection,"* arXiv , 0.

García-Hernández, D. A., S. Iglesias-Groth, J. A. Acosta-Pulido, A. Manchado, P. García-Lario, L. Stanghellini, E. Villaver, R. A. Shaw, and F. Cataldo (2011), *"The Formation of Fullerenes: Clues from New C60, C70, and (Possible) Planar C24 Detections in Magellanic Cloud Planetary Nebulae,"* Astrophys. J. Lett. **737** (2), L30.

Gilbert, T. L. (1975), *"Hohenberg-Kohn theorem for nonlocal external potentials,"* Phys. Rev. B **12**, 2111.

Glauber, R., and G. Matthiae (1970), *"High-energy scattering of protons by nuclei,"* Nuclear Physics B **21** (2), 135 .

Glauber, R., *et al.* (1959), *Lectures in theoretical physics*, Vol. 1 (Interscience, New York).

Gonze, X., R. Stumpf, and M. Scheffler (1991), *"Analysis of separable potentials,"* Phys. Rev. B **44**, 8503.

Gross, E., and K. Burke (2006), in *Time-Dependent Density Functional Theory*, Lecture Notes in Physics, Vol. 706, edited by M. Marques, C. Ullrich, F. Nogueira, A. Rubio, K. Burke, and E. Gross (Springer Berlin / Heidelberg) pp. 1–13, 10.1007/3-540-35426-3.

Gross, J. H. (2011), *Mass Spectrometry - A Textbook* (Springer).

Guerra, C. F., J.-W. Handgraaf, E. J. Baerends, and F. M. Bickelhaupt (2004), *"Voronoi deformation density (VDD) charges: Assessment of the Mulliken, Bader, Hirshfeld, Weinhold, and VDD methods for charge analysis,"* J. Comput. Chem. **25** (2), 189.

Guerra, F., and N. Robotti (2005), *"A forgotten publication of Ettore Majorana on the improvement of the Thomas-Fermi statistical model,"* arXiv:physics/0511222 .

van Gunsteren, W. F., and H. J. Berendsen (1990), *"Computer simulation of molecular dynamics: Methodology, applications, and perspectives in chemistry,"* Angewandte Chemie International Edition in English **29** (9), 992.

Hartwigsen, C., S. Goedecker, and J. Hutter (1998), *"Relativistic separable dual-space Gaussian pseudopotentials from H to Rn,"* Phys. Rev. B **58**, 3641.

Hasan, A., B. Tooke, M. Zapukhlyak, T. Kirchner, and M. Schulz (2006), *"Kinematically complete experiment on transfer excitation in intermediate-energy p + He collisions,"* Phys. Rev. A **74**, 032703.

Hedén, M., K. Hansen, and E. E. B. Campbell (2005), *"Molecular fusion of $(C_{60})_N$ clusters in the gas phase after femtosecond laser irradiation,"* Phys. Rev. A **71**, 055201.

Heine, V. (1970), in *Solid State Physics*, Vol. 24, edited by F. S. Henry Ehrenreich and D. Turnbull (Academic Press) pp. 1 – 36.

Henkelman, G., A. Arnaldsson, and H. Jãnsson (2006), *"A fast and robust algorithm for Bader decomposition of charge density,"* Comput. Phys. Commun. **36** (3), 354.

Hirai, H., K. ichi Kondo, N. Yoshizawa, and M. Shiraishi (1994), *"Amorphous diamond from C[sub 60] fullerene,"* Applied Physics Letters **64** (14), 1797.

Hirshfeld, F. (1977), *"Bonded-atom fragments for describing molecular charge densities,"* Theo. Chimica Acta **44**, 129.

Hohenberg, P., and W. Kohn (1964), *"Inhomogeneous Electron Gas,"* Phys. Rev. **136**, B864.

Hong, Z. R., B. Maennig, R. Lessmann, M. Pfeiffer, K. Leo, and P. Simon (2007), *"Improved efficiency of zinc phthalocyanine/C[sub 60] based photovoltaic cells via nanoscale interface modification,"* Applied Physics Letters **90** (20), 203505.

Huang, H., W. Chen, S. Chen, D. C. Qi, X. Y. Gao, and A. T. S. Wee (2009), *"Molecular orientation of CuPc thin films on C[sub 60]/Ag(111),"* Applied Physics Letters **94** (16), 163304.

Iglesias-Groth, S., A. Manchado, R. Rebolo, J. I. González Hernández, D. A. García-Hernández, and D. L. Lambert (2010), *"A search for interstellar anthracene towards the Perseus anomalous microwave emission region,"* Mon Not. R Astron. Soc. **407** (4), 2157.

Illescas, C., and A. Riera (1998), *"Classical Outlook on the Electron Translation Factor Problem,"* Phys. Rev. Lett. **80**, 3029.

Jamorski, C., J. B. Foresman, C. Thilgen, and H.-P. Lüthi (2002), *"Assessment of time-dependent density-functional theory for the calculation of critical features in the absorption spectra of a series of aromatic donor–acceptor systems,"* J. Chem. Phys. **116** (20), 8761.

Jensen, A. W., S. R. Wilson, and D. I. Schuster (1996), *"Biological applications of fullerenes,"* Bioorganic and Medicinal Chemistry **4** (6), 767 .

Jensen, F. (2007), *Introduction to computational chemistry* (Wiley).

Jones, J. E. (1924), *"On the Determination of Molecular Fields. II. From the Equation of State of a Gas,"* P. Roy. Soc. A-Math. Phy. **106** (738), 463.

Kabat, D. N. (1992), *"Validity of the Eikonal approximation,"* Comments Nucl.Part.Phys. **20**, 325.

Keim, M., A. Achenbach, H. J. Lüdde, and T. Kirchner (2005), *"Time-dependent density functional theory calculations for collisions of bare ions with helium,"* Nucl. Instrum. Meth. B **233**, 240 243.

Kelkar, A. H., U. Kadhane, D. Misra, L. Gulyas, and L. C. Tribedi (2010), *"Single and multiple ionization of* C_{60} *fullerenes and collective effects in collisions with highly charged C, F, and Si ions with energy 3 MeV/u,"* Phys. Rev. A **82**, 043201.

Kerker, G. P. (1980), *"Non-singular atomic pseudopotentials for solid state applications,"* Journal of Physics C: Solid State Physics **13** (9), L189.

Kestner, N. R., and O. Sinanaglu (1962), *"Study of Electron Correlation in Helium-Like Systems Using an Exactly Soluble Model,"* Phys. Rev. **128**, 2687.

Kleinman, L., and D. M. Bylander (1982), *"Efficacious Form for Model Pseudopotentials,"* Phys. Rev. Lett. **48**, 1425.

Klerk, L. A., N. P. Lockyer, A. Kharchenko, L. MacAleese, P. Y. W. Dankers, J. C. Vickerman, and R. M. A. Heeren (2010), *"C60+ Secondary Ion Microscopy Using a Delay Line Detector,"* Analytical Chemistry **82** (3), 801.

Kohn, W., and L. J. Sham (1965), *"Self-Consistent Equations Including Exchange and Correlation Effects,"* Phys. Rev. **140**, A1133.

Kraft, G. (2000), *"Tumortherapy with ion beams,"* Nucl. Instrum. Meth. A **454** (1), 1.

Kresse, G., and J. Hafner (1993), *"Ab initio molecular dynamics for liquid metals,"* Phys. Rev. B **47**, 558.

Lamberti, W. (2005), in *Handbook of Microscopy for Nanotechnology*, edited by N. Yao and Z. Wang (Springer US) pp. 207–225.

Lawicki, A., A. I. S. Holm, P. Rousseau, M. Capron, R. Maisonny, S. Maclot, F. Seitz, H. A. B. Johansson, S. Rosén, H. T. Schmidt, H. Zettergren, B. Manil, L. Adoui, H. Cederquist, and B. A. Huber (2011), *"Multiple ionization and fragmentation of isolated pyrene and coronene molecules in collision with ions,"* Phys. Rev. A **83** (2), 022704.

Leach, S. (1995), *"Laboratory studies of polycyclic aromatic hydrocarbons, fullerenes and linear carbon chains in an astrophysical context,"* Planetary and Space Science **43** (10-11), 1153 .

van Leeuwen, R., and E. J. Baerends (1994), *"Exchange-correlation potential with correct asymptotic behavior,"* Phys. Rev. A **49**, 2421.

Levine, I. N. (2000), *Quantum chemistry*, Vol. 5 (Prentice Hall Upper Saddle River, NJ).

Lévy, M., and J. Sucher (1969), *"Eikonal Approximation in Quantum Field Theory,"* Phys. Rev. **186**, 1656.

Lévy-Leblond, J.-M. (1967), *"Nonrelativistic particles and wave equations,"* Communications in Mathematical Physics **6** (4), 286.

Lherbier, A., S. M.-M. Dubois, X. Declerck, Y.-M. Niquet, S. Roche, and J.-C. Charlier (2012), *"Transport properties of graphene containing structural defects,"* Phys. Rev. B **86**, 075402.

Lherbier, A., S. M.-M. Dubois, X. Declerck, S. Roche, Y.-M. Niquet, and J.-C. Charlier (2011), *"Two-Dimensional Graphene with Structural Defects: Elastic Mean Free Path, Minimum Conductivity, and Anderson Transition,"* Phys. Rev. Lett. **106**, 046803.

Lodders, K. (2003), *"Solar System Abundances and Condensation Temperatures of the Elements,"* Astrophys. J. **591**, 1220.

Maciel, W. J., *et al.* (2013), *Astrophysics of the Interstellar Medium* (Springer).

Mada, S., K.-n. Hida, M. Kimura, L. c. v. Pichl, H.-P. Liebermann, Y. Li, and R. J. Buenker (2007), *"Charge transfer and electronic excitation in collisions of protons with water molecules below* 10 keV*,"* Phys. Rev. A **75**, 022706.

Majima, T., A. Yogo, F. Obata, H. Tsuchida, Y. Nakai, and A. Itoh (2002), *"The role of nuclear stopping power in fast heavy ion collision with {C60},"* Nucl. Instrum. Meth. B **193** (1–4), 209 .

Martin, R. (2004), *Electronic structure: basic theory and practical methods* (Cambridge Univ Pr).

Martin, S., L. Chen, A. Salmoun, B. Li, J. Bernard, and R. Brédy (2008), *"Fragmentation patterns of multicharged C_{60}^{r+} (r=3-5) studied with well-controlled internal excitation energy,"* Phys. Rev. A **77**, 43201.

Marx, D., and J. Hutter (2000), *"Ab initio molecular dynamics: Theory and implementation,"* Modern methods and algorithms of quantum chemistry **1**, 301.

Marx, D., and J. Hutter (2009), *Ab Initio Molecular Dynamics* (Cambridge University Press).

McKee, C. F., and J. P. Ostriker (1977), *"A theory of the interstellar medium - Three components regulated by supernova explosions in an inhomogeneous substrate,"* Astrophys. J. **218**, 148.

Meister, J., and W. H. E. Schwarz (1994), *"Principal Components of Ionicity,"* J. Phys. Chem-US **98** (33), 8245.

Mergel, V., R. Dörner, M. Achler, K. Khayyat, S. Lencinas, J. Euler, O. Jagutzki, S. Nüttgens, M. Unverzagt, L. Spielberger, W. Wu, R. Ali, J. Ullrich, H. Cederquist, A. Salin, C. J. Wood, R. E. Olson, D. c. v. Belkić, C. L. Cocke, and H. Schmidt-Böcking (1997), *"Intra-atomic Electron-Electron Scattering in p-He Collisions (Thomas Process) Investigated by Cold Target Recoil Ion Momentum Spectroscopy,"* Phys. Rev. Lett. **79**, 387.

Micha, D. A., and K. Runge (1994), *"Time-dependent many-electron approach to slow ion-atom collisions: The coupling of electronic and nuclear motions,"* Phys. Rev. A **50**, 322.

Milani, C. (1996), *"The valence of small fullerenes,"* Chem Phys Lett **258**, 554.

Moliére, G. (1947), *"Theorie der streuung schneller geladener teilchen I. einzelstreuung am abgeschirmten Coulomb-Feld,"* Zeitschrift Naturforschung Teil A **2**, 133.

Morrison, M. A. (1983), *"The physics of low-energy electron-molecule collisions: a guide for the perplexed and the uninitiated,"* Aust. J. Phys. **36** (3), 239.

Mroz, P., G. P. Tegos, H. Gali, T. Wharton, T. Sarna, and M. R. Hamblin (2007), *"Photodynamic therapy with fullerenes,"* Photochemical & Photobiological Sciences **6** (11), 1139.

Mulliken, R. S. (1955a), *"Electronic Population Analysis on LCAO-MO Molecular Wave Functions. III. Effects of Hybridization on Overlap and Gross AO Populations,"* J. Chem. Phys. **23** (12), 2338.

Mulliken, R. S. (1955b), *"Electronic Population Analysis on LCAO-MO Molecular Wave Functions. IV. Bonding and Antibonding in LCAO and Valence-Bond Theories,"* J. Chem. Phys. **23** (12), 2343.

Mulliken, R. S. (1955c), *"Electronic Population Analysis on LCAO[Single Bond]MO Molecular Wave Functions. I,"* J. Chem. Phys. **23** (10), 1833.

Mulliken, R. S. (1955d), *"Electronic Population Analysis on LCAO[Single Bond]MO Molecular Wave Functions. II. Overlap Populations, Bond Orders, and Covalent Bond Energies,"* J. Chem. Phys. **23** (10), 1841.

Nakatsukasa, T., and K. Yabana (2001), *"Photoabsorption spectra in the continuum of molecules and atomic clusters,"* The Journal of Chemical Physics **114** (6), 2550.

Neuhasuer, D., and M. Baer (1989), *"The time-dependent Schr[o-umlaut]dinger equation: Application of absorbing boundary conditions,"* The Journal of Chemical Physics **90** (8), 4351.

Oliveira, R. M., M. Ueda, and L. A. Berni (2004), *"First results on the fast neutral lithium beam diagnostics probing the edge plasma of the ETE tokamak,"* Brazilian Journal of Physics **34**, 1655 .

Osawa, E., H. Kroto, P. Fowler, and E. Wasserman (1993), *"The Evolution of the Football Structure for the C _{60} Molecule: A Retrospective [and Discussion],"* Philosophical Transactions of the Royal Society of London. Series A: Physical and Engineering Sciences **343** (1667), 1.

Ossenkopf, V., H. S. P. Müller, D. C. Lis, P. Schilke, T. A. Bell, S. Bruderer, E. Bergin, C. Ceccarelli, C. Comito, J. Stutzki, A. Bacman, A. Baudry, A. O. Benz, M. Benedettini, O. Berne, G. Blake, A. Boogert, S. Bottinelli, F. Boulanger, S. Cabrit, P. Caselli, E. Caux, J. Cernicharo, C. Codella, A. Coutens, N. Crimier, N. R. Crockett, F. Daniel, K. Demyk, P. Dieleman, C. Dominik, M. L. Dubernet, M. Emprechtinger, P. Encrenaz, E. Falgarone, K. France, A. Fuente, M. Gerin, T. F. Giesen, A. M. di Giorgio, J. R. Goicoechea, P. F. Goldsmith, R. Güsten, A. Harris, F. Helmich, E. Herbst, P. Hily-Blant, K. Jacobs, T. Jacq, C. Joblin, D. Johnstone, C. Kahane, M. Kama, T. Klein, A. Klotz, C. Kramer, W. Langer, B. Lefloch, C. Leinz, A. Lorenzani, S. D. Lord, S. Maret, P. G. Martin, J. Martin-Pintado, C. McCoey, M. Melchior, G. J. Melnick, K. M. Menten, B. Mookerjea, P. Morris, J. A. Murphy, D. A. Neufeld, B. Nisini, S. Pacheco, L. Pagani, B. Parise, J. C. Pearson, M. Pérault, T. G. Phillips, R. Plume, S.-L. Quin, R. Rizzo, M. Röllig, M. Salez, P. Saraceno, S. Schlemmer, R. Simon, K. Schuster, F. F. S. van der Tak, A. G. G. M. Tielens, D. Teyssier, N. Trappe, C. Vastel, S. Viti, V. Wakelam, A. Walters, S. Wang, N. Whyborn, M. van der Wiel, H. W. Yorke, S. Yu, and J. Zmuidzinas (2010), *"Detection of interstellar oxidaniumyl: Abundant H_2O^+ towards the star-forming regions DR21, Sgr B2, and NGC6334,"* Astron. Astrophys. **518**, L111.

Palancher, H., N. Wieschalla, P. Martin, R. Tucoulou, C. Sabathier, W. Petry, J.-F. Berar, C. Valot, and S. Dubois (2009), *"Uraniummolybdenum nuclear fuel plates behaviour under heavy ion irradiation: An X-ray diffraction analysis,"* Journal of Nuclear Materials **385** (2), 449 .

Perdew, J. P., S. Kurth, A. Zupan, and P. Blaha (1999), *"Accurate Density Functional with Correct Formal Properties: A Step Beyond the Generalized Gradient Approximation,"* Phys. Rev. Lett. **82**, 2544.

Perdew, J. P., and Y. Wang (1992), *"Accurate and simple analytic representation of the electron-gas correlation energy,"* Phys. Rev. B **45**, 13244.

Pohl, A., P.-G. Reinhard, and E. Suraud (2000), *"Towards Single-Particle Spectroscopy of Small Metal Clusters,"* Phys. Rev. Lett. **84**, 5090.

Pople, J. A., and R. K. Nesbet (1954), *"Self-Consistent Orbitals for Radicals,"* J. Chem. Phys. **22** (3), 571.

Ren, J., S. Meng, and E. Kaxiras (2012), *"Theoretical investigation of the C60/copper phthalocyanine organic photovoltaic heterojunction,"* Nano Research **5** (4), 248.

Rentenier, A. (2004), *Fragmentation de la molécule C60 par impact d'ions légers étudiée en multicorrélation.Sections efficaces, spectroscopie d'électrons*, Ph.D. thesis (Université Paul Sabatier - Toulouse III).

Restrepo, O., A. Prabhakaran, K. Hamraoui, N. Wehbe, S. Yunus, P. Bertrand, and A. Delcorte (2010), *"Mechanisms of metal-assisted secondary ion mass spectrometry: a mixed theoretical and experimental study,"* Surface and Interface Analysis **42** (6-7), 1030.

Restrepo, O. A., and A. Delcorte (2011), *"Molecular dynamics study of metal-organic samples bombarded by kiloelectronvolt projectiles,"* Surface and Interface Analysis **43** (1-2), 70.

Rohmund, F., E. E. B. Campbell, O. Knospe, G. Seifert, and R. Schmidt (1996), *"Collision Energy Dependence of Molecular Fusion and Fragmentation in* C_{60}^{+} + C_{60} *Collisions,"* Phys. Rev. Lett. **76**, 3289.

Roothaan, C. C. J. (1960), *"Self-Consistent Field Theory for Open Shells of Electronic Systems,"* Rev. Mod. Phys. **32**, 179.

Rozsályi, E., E. Bene, G. J. Halász, Á. Vibók, and M. C. Bacchus-Montabonel (2010), *"Theoretical treatment of charge transfer in collisions of* C^{2+} *ions with HF: Anisotropic and vibrational effect,"* Phys. Rev. A **81**, 062711.

Rozsályi, E., E. Bene, G. J. Halász, Á. Vibók, and M. C. Bacchus-Montabonel (2011), *"Ab initio study of charge-transfer dynamics in collisions of* C^{2+} *ions with hydrogen chloride,"* Phys. Rev. A **83**, 052713.

Rozsályi, E., L. F. Errea, L. Méndez, and I. Rabadán (2012), *"Ab initio calculation of charge transfer in proton collisions with* N_2*,"* Phys. Rev. A **85**, 042701.

Rudd, M. E., R. D. DuBois, L. H. Toburen, C. A. Ratcliffe, and T. V. Goffe (1983), *"Cross sections for ionization of gases by 5-4000-keV protons and for electron capture by 5-150-keV protons,"* Phys. Rev. A **28**, 3244.

Rudd, M. E., Y. K. Kim, D. H. Madison, and J. W. Gallagher (1985), *"Electron production in proton collisions: total cross sections,"* Rev. Mod. Phys. **57**, 965.

Runge, E., and E. K. U. Gross (1984), *"Density-Functional Theory for Time-Dependent Systems,"* Phys. Rev. Lett. **52**, 997.

Rutherford, E. (1911), *"The scattering of alpha and beta particles by matter and the structure of the atom,"* Philosophical Magazine **21**, 669 .

San-Miguel, A., and P. Toulemonde (2005), *"High-pressure properties of group IV clathrates,"* High Pressure Research **25** (3), 159.

Sanville, E., S. D. Kenny, R. Smith, and G. Henkelman (2007), *"Improved grid-based algorithm for Bader charge allocation,"* J. Comput. Chem. **28** (5), 899.

Schardt, D., T. Elsässer, and D. Schulz-Ertner (2010), *"Heavy-ion tumor therapy: Physical and radiobiological benefits,"* Rev. Mod. Phys. **82**, 383.

Schrödinger, E. (1926), *"An Undulatory Theory of the Mechanics of Atoms and Molecules,"* Phys. Rev. **28**, 1049.

Schwab, M. (2012), in *Encyclopedia of Cancer*, edited by M. Schwab (Springer Berlin Heidelberg) pp. 3144–3144.

Sellgren, K. (2001), *"Aromatic hydrocarbons, diamonds, and fullerenes in interstellar space: puzzles to be solved by laboratory and theoretical astrochemistry,"* Spectrochim Acta A **57** (4), 627 .

Shen, H., P. Hvelplund, D. Mathur, A. Bárány, H. Cederquist, N. Selberg, and D. C. Lorents (1995), *"Fullerene-fullerene collisions: Fragmentation and electron capture,"* Phys. Rev. A **52**, 3847.

Slater, J. (2012), in *Ion Beam Therapy*, Biological and Medical Physics, Biomedical Engineering, Vol. 320, edited by U. Linz (Springer Berlin Heidelberg) pp. 3–16.

Slater, J. C. (1951), *"A Simplification of the Hartree-Fock Method,"* Phys. Rev. **81**, 385.

Smalley, R., H. Kroto, and J. Heath (1985), *"C60: Buckminsterfullerene,"* Nature **318**, 162.

Smith, D. F., E. W. Robinson, A. V. Tolmachev, R. M. A. Heeren, and L. Pasa-Tolić (2011), *"C60 Secondary Ion Fourier Transform Ion Cyclotron Resonance Mass Spectrometry,"* Analytical Chemistry **83** (24), 9552.

Solomko, V., A. Delcorte, B. Garrison, and P. Bertrand (2004), *"Sputtering of a polycyclic hydrocarbon molecule: TOF-SIMS experiments and molecular dynamic simulations,"* Appl Surf Sci **231**, 48.

Solomko, V., M. Verstraete, A. Delcorte, B. J. Garrison, X. Gonze, and P. Bertrand (2006), *"Modeling the dissociation and ionization of a sputtered organic molecule,"* Appl Surf Sci **252** (19), 6459.

Stahl, F., P. von Ragué Schleyer, H. F. Bettinger, R. I. Kaiser, Y. T. Lee, and H. F. Schaefer (2001), *"Reaction of the ethynyl radical, C2H, with methylacetylene, CH3CCH, under single collision conditions: Implications for astrochemistry,"* J. Chem. Phys. **114** (8), 3476.

Stier, P. M., and C. F. Barnett (1956), *"Charge Exchange Cross Sections of Hydrogen Ions in Gases,"* Phys. Rev. **103**, 896.

Tang, W., E. Sanville, and G. Henkelman (2009), *"A grid-based Bader analysis algorithm without lattice bias,"* Journal of Physics: Condensed Matter **21** (8), 084204.

Teter, M. (1993), *"Additional condition for transferability in pseudopotentials,"* Phys. Rev. B **48**, 5031.

Thomas, L. H. (1927), *"The calculation of atomic fields,"* Math. Proc. Cambridge **23**, 542.

Thompson, D. L. (1998), *Modern Methods for Multidimensional Dynamics Computations in Chemistry: Editor, Donald L. Thompson* (World Scientific Publishing Company).

Thorson, W. R., and J. B. Delos (1978), *"Theory of near-adiabatic collisions. I. Electron translation factor method,"* Phys. Rev. A **18**, 117.

Troullier, N., and J. L. Martins (1991a), *"Efficient pseudopotentials for plane-wave calculations,"* Phys. Rev. B **43**, 1993.

Troullier, N., and J. L. Martins (1991b), *"Efficient pseudopotentials for plane-wave calculations,"* Phys. Rev. B **43**, 1993.

Tully, J. C. (1990), *"Molecular dynamics with electronic transitions,"* The Journal of Chemical Physics **93** (2), 1061.

Wang, F., X. Hong, J. Wang, B. Gou, and J. Wang (2012), *"Comparison of three methods for calculation of electron transfer probability in H+ + Ne,"* Physics Letters A **376** (4), 469.

Wang, F., X. Xu, X. Hong, J. Wang, and B. Gou (2011), *"A theoretical model for electron transfer in ion-atom collisions: Calculations for the collision of a proton with an argon atom,"* Physics Letters A **375** (37), 3290.

Was, G. (2007), *Fundamentals of Radiation Materials Science: Metals and Alloys* (Springer-Verlag Berlin Heidelberg).

Was, G., J. Busby, T. Allen, E. Kenik, A. Jensson, S. Bruemmer, J. Gan, A. Edwards, P. Scott, and P. Andreson (2002), *"Emulation of neutron irradiation effects with protons: validation of principle,"* Journal of Nuclear Materials **300** (23), 198 .

Weibel, D., S. Wong, N. Lockyer, P. Blenkinsopp, R. Hill, and J. C. Vickerman (2003), *"A C60 Primary Ion Beam System for Time of Flight Secondary Ion Mass Spectrometry: Its Development and Secondary Ion Yield Characteristics,"* Analytical Chemistry **75** (7), 1754.

Welsh, L. M., K. H. Berkner, S. N. Kaplan, and R. V. Pyle (1967), *"Cross Sections for Electron Capture by Fast Protons in* H_2*, He,* N_2*, and Ar,"* Phys. Rev. **158**, 85.

Wiberg, K. B., and P. R. Rablen (1993), *"Comparison of atomic charges derived via different procedures,"* J. Comput. Chem. **14** (12), 1504.

Williams, J. F. (1967), *"Measurement of Charge-Transfer Cross Sections for 0.25- to 2.5-MeV Protons and Hydrogen Atoms Incident upon Hydrogen and Helium Gases,"* Phys. Rev. **157**, 97.

Wilson, R. R. (1946), *"Radiological Use of Fast Protons,"* Radiology **47** (5), 487.

Winnewisser, G. (2011), *Interstellar Molecules: Their Laboratory and Interstellar Habitat*, Vol. 241 (Springer).

Wyrowski, F., K. M. Menten, R. Güsten, and A. Belloche (2010), *"First interstellar detection of* OH^+*,"* Astron. Astrophys. **518**, A26.

Yajnik, S. (2013), in *Proton Beam Therapy* (Springer New York) pp. 1–11.

Zettergren, H., H. A. B. Johansson, H. T. Schmidt, J. Jensen, P. Hvelplund, S. Tomita, Y. Wang, F. Martín, M. Alcamí, B. Manil, L. Maunoury, B. A. Huber, and H. Cederquist (2010), *"Magic and hot giant fullerenes formed inside ion irradiated weakly bound C60 clusters,"* J. Chem. Phys. **133**, 4301.

Zheng, C. (2007), *"A perfectly matched layer approach to the nonlinear Schrdinger wave equations,"* Journal of Computational Physics **227** (1), 537 .

Ziurys, L. M. (2006), *"The chemistry in circumstellar envelopes of evolved stars: Following the origin of the elements to the origin of life,"* P. Natl. Acad. Sci. USA **103** (33), 12274.

Aknowledgements

Write a thesis is a battle, an individual battle against our own fears and weaknesses. Fortunately, there are people around us encouraging us to go forward, to enter in combat and succeed.

At this point, writing these lines, I remember all the people that direct my path until this very instant. All the people who encourage me to pursue a PhD and even those who discourage me many years ago. I would like to thank for their advises, their guidance and their words.

The good fortune allow me to enumerate my personal acknowledgments geographically and avoid the task even harder to enumerate hierarchically, a task, not only hard but even pointless. Each individual contribute in a unique way to shape my present, impossible to measure their impact on me as a scientist, as an intellectual and as human being.

From Belgium, I would like to start to thank my promoter Prof. Xavier Gonze. He shape my vision of a perfect mach between physics and engineering, transferring his clear vision of this wide subject that is electronic structure. His outstanding organizational qualities, his leadership, and his serenity of spirit are an inspiration for me. I have no enough lines to describe how grateful I am with him for all the support he has shown me over the course of my PhD.

I would like also to thank the members of my jury, for reading my text, for their numerous remarks, corrections and suggestions, if you read a decent text is in big part due to them. Their comments and fruitful discussions allowed me to improve the quality of this thesis : Prof. Pierre Defrance, Prof. Arnaud Delcorte, Prof. Miguel Marques, Prof. Bernard Piraux and Prof. Matthieu Verstraete.

I would like to thank all my colleagues that share with me this nice building in the forest: Annette, Sadia, Jean-Michel, Alain, you were always very kind with me. To my colleagues in the office: Anna, I enjoy our discussions, sharing of ideas, your friendship will never be forgotten. Olga, you make me feel useful, I enjoy the discussions walking back to home, your memories about Russia,

your experience and vitality, were an inspiration for me. Martin, you are such a good scientist, it is a pity that you leave us, but I understand that it was for good. David, you are a very good engineer, organize, proactive, I have a lot to learn from people like you. Geoffroy, you bring a fresh air to the group, your motivation will bring new horizons in the group. Also I have to thanks Fabiana Dapieve for make feel useful, for invite me to participate of her projects and ideas. I will be glad if our collaborations could expand in the long term.

Jean-Christophe, Gian-Marco you create a very active community around you and your ideas, it was a pleasure to share that spirit all those years. I would like to extend my acknowledges to my sense of gratitude to all my colleagues in the building SC17: Andrés, Aurélien, Bruno, Matteo, Nicolas, Samuel, Simon, Xavier, I have many things in my memory remembering all those years in the group.

En Colombia, tengo tanto que agradecer a mis padres: Martha Lucia y Angel Guillermo, ellos se sacrificaron de mil maneras por darnos a mi hermano y a mi la mejor educación que pudieron. Nos dieron las alas y abrieron la jaula, fueron otras tierras las nos vieron volar. Mi patria es ahora un lugar distante, pero sus paisajes, sus aromas y sus montañas estan siempre cercanas en mi memoria. Ahora, solo el hogar me da un lugar común, un referente, un faro al cual me anclo antes de partir, una vez mas, a nuevas y lejanas tierras. Se necesita alma de gaviota para emprender la aventura de ser cientifico. Gracias mamá, gracias papá por su empeño en que aprendiera a volar. Espero que os sintais orgullosos de mi, como yo de ustedes. Un agradecimiento especial a mis tias por apoyarme desde que estaba pequeño.

Durante el tiempo que viví en Europa tuve la oportunidad de visitar a mi familia viviendo en el continente. Un agradecimiento especial a mis primas Sandra, Claudia y Carolina, por acojerme en sus hogares. Agradecimiento extendido a sus familias por hacerme sentir un poco mas cerca de mi hogar.

A mi hermano Marcelo, escribo estas lineas desde tu apartamento en Puerto España. Miro por la ventana como el sol baña las montañas de la isla, Como a esas montañas, tu luz ha brillado para mi cuando mas lo necesitaba. Tu me has apoyado tanto estos anos, me has tendido la mano en los momentos mas difíciles. Esta tesis no hubiese sido posible, literalmente sin tu apoyo.

Deseo también extender mi agradecimiento a mis maestros y compañeros en la Universidad donde me formé, tanto aquellos que me estimularon a no quedarme en Colombia, como aquellos que me advertían sobre lo que iría encontrar en Europa, los escuche a todos y seguí algunos. A unos y otros espero encontrarlos de nuevo un da en este misterioso laberinto que es la vida. Un agradecimiento especial a mi profesor Manuel Páez, mucho le debo a el por estar ahora yo aquí.

Un agradecimiento tambien especial a Aldo, por escucharme por largo rato, aquel 20 de agosto cuando no deseaba que nadie se enterara que ese dia cumplia años. Gracias por escucharme aquel dia, y gracias por los nuevos horizontes que has abierto para mi, lo aprecio de corazón.

Yo no estaria aqui hoy si no fuese por Oscar Restrepo, mi gratitud hacia el y a Natalia por todo su apoyo y ayuda todos estos años vividos en Belgica. Grat-

itud extendida a todas las personas buenas que encontre en este pais, James Ortiz, Victor Baldovino, Raquel Matheos, Paula Liliana Alvarez, Alejandro Karelovic, Florencia Alvez, Sandra Rufino, Sandrine Fleith, Abla Safadi.

No Brasil, um abraço aos meus amigos e colegas no Brasil, Carlos Bonilla, Jefferson Morais, Rodrigo Turcati, Denis Cocuroci. Se o mar da vida nos leva de novo na mesma praia, será um prazer e um honra trabalhar de novo com vocês.

A minha vida na Bélgica não tivesse tido a mesma cor sino fose pela presencia da minha família. A minha amada Viviane, por compartir esta aventura que fue sempre mas minha que tua, por tua paciência todos estes anos, por teu carinho e compreensão. A meu pequenino Théo, tua vinda ao mundo fez me aprimorar muito meu francês. Lembrarei sempre caminhar juntos a ver o trenzinho, as caminhadas ao lago, as tardes em Louvain-la-plage. Tu pagaste o preço mais alto da minha aventura, minha ausência na tua vida estos meses todos. Teu pai foi só uma fotinho no Skype, é agora a mim recuperar a presencia na tua vida e o teu amor. Nossa distância deixo um dolor gigante na minha alma. So meu coração sabe as dificuldades que eu tive em escrever cada linha da tese quando a única palavra que saia dos meus dedos era “saudades”.

Port of Spain
Trinidad and Tobago
28 of July 2013

Curriculum Vitæ

Personal data:

Name:	Guillermo Avendaño Franco
Birth date:	20.08.1978
Birth place:	Manizales (Colombia)
Mother:	Martha Lucia Franco Mejía
Father:	Angel Guillermo Avendaño Cardona
Nationality:	Colombian

Training:

1995	"Liceo Arquidiocesano de Nuestra Señora"
1996-2003	"Fisico" Universidad de Antioquia
Dec. 2008	Starts "Doctorat en Sciences de l'Ingénieur" under direction of Prof. Xavier Gonze

Publications

- *Time-dependent density functional theory study of charge transfer in collisions*
  G. Avendaño-Franco, B. Piraux, M. Grüning, X. Gonze
  Theoretical Chemistry Accounts **131:11** 1–10 (2012)

- *Velocity phase factor in non-adiabatic collisions using Time-dependent density functional theory*
  G. Avendaño-Franco, X. Gonze
  In preparation

- *Charge transfer processes in a collision of 2 MeV Li^+ with C_{60} using Time-dependent density functional theory*
  G. Avendaño-Franco, X. Gonze
  In preparation

- *Charge transfer processes in a collision of 10 keV He with graphene using Time-dependent density functional theory*
  G. Avendaño-Franco, X. Gonze
  In preparation